Influence of Unsteady Losses and Deviations on Compression System Stability with Inlet Distortion

by

Eric James Strang

Bachelor of Science in Aerospace Engineering
The Pennsylvania State University (1989)

Submitted to the Department of Aeronautics and Astronautics in Partial Fulfillment of the Requirements for the Degree of

Master of Science in Aeronautics and Astronautics

at the

Massachusetts Institute of Technology

June 1991

© Massachusetts Institute of Technology, 1991, All Rights Reserved

Signature of Author _____
Department of Aeronautics and Astronautics
June 1, 1991

Certified by _____
Dr. C.S. Tan
Thesis Supervisor

Approved by _____
Professor Harold Y. Wachman
Chairman, Department Graduate Committee

MASSACHUSETTS INSTITUTE
OF TECHNOLOGY

JUN 12 1991

LIBRARIES

Aero

Influence of Unsteady Losses and Deviations on Compression System Stability with Inlet Distortion

by

Eric J. Strang

Submitted to the Department of Aeronautics and Astronautics
on June 1991 in partial fulfillment of the
requirements for the Degree of Master of Science in
Aeronautics and Astronautics

Abstract

Calculations have been carried out to quantify the effects of unsteady losses and unsteady deviations on compression system stability with an inlet distortion. Several computations were implemented for a range of compressor (axisymmetric) characteristics and a range of parameters (inertia parameters, magnitude of distortions, etc.) of practical interest. Compressor instability is prevented generally to a lower flow coefficient and correspondingly a higher distorted pressure rise. In addition, if the inlet distortion is single-lobed, unsteady blade effects (losses/deviations) stabilize modes of higher harmonic content than the first harmonic. Unsteady losses and unsteady deviations in effect increase the compressor inertia by as much as 50% (unsteady lag parameter, $\tau \sim 0.5$) for a compressor with axisymmetric performance that has high curvature. A simpler effective inertia model was proposed for both unsteady losses and unsteady deviations which accurately predicts stability for small τ.

Analysis has also been implemented to ascertain the significance of compressor swirl sensitivity. Mean flow calculations indicate that this effect causes an increase in rotor turning and a significant increase in total pressure loss (on the order of one mean dynamic head) through the IGVs in the region of negative swirl. It is shown that this sensitivity to swirl has a destabilizing influence on compression system stability. Inclusion of unsteady losses and unsteady deviations has a greater impact on the stability margin for compressors which are sensitive to swirl.

Furthermore, the extent to which inter blade row flow redistribution affects compressor performance and stability margin has been examined. The inclusion of this flow feature in the compression system model has been determined to have minimal (less than 1%) effect on compressor performance and stability margin.

Thesis Supervisor: Dr. Choon S. Tan
Title: Principal Research Engineer

Acknowledgements

The author wishes to extend his appreciation to everyone who has made the completion of this project possible, in particular:

Dr. Choon S. Tan for his endless concern, guidance, encouragement and friendliness. Thank you.

Professor Edward M. Greitzer for his support and helpful advice.

Dr. John P. Longley for his guidance, encouragement and patience.

Bob Haimes for his assistance with the computer facilities at the GTL.

Knox (girlie-boy) Millsaps for teaching me how to relax on the weekends.
Peter (the silkworm) Silkowski who makes me feel as if I have nothing to worry about. Go festival.
Dan (tubs) Gysling for showing it is alright to let your stomach stick out further than your chest. Yeah, you can hit it with a sledge hammer and shoot it with a shotgun.
S.J. (mo-mess-j) Song for proving to me that it is not possible to be quiet 24 hours straight. Hey, nothing broke.
Laurent (la-la-larry love) for proving that GTL men can meet women.
Chris (the howler) Howell for his endless stories (I like the burning couch story).
Aaron (the baron) Gleixner for just being a clown. The **VIOLATOR** with unflinching conscience.
Martin (stir fry) Graf for laughing loud, proving to me someone was having fun. You want some of this!
David (go tribe) Tew who I have yet to fully understand a complete sentence. It's called Sim City, let me show you. Uno's?
Taras (tear-butt / shimstock) Palczynski for displaying the latest football uniforms. If you are in Florida, don't miss Gatorland.
Norm (I survived the storm) Sun for realizing U of M is done with the entrance of PSU to the Big 10. Hey, dudemar.
Mark (chief) Campbell for being the only true sports fan I've met here.
Yew-poh (skipdog) Mak for not having a clue. OK, where is his leash.
Yi-lung (yeaster) Yang for being a good guy.
Earl (the squirrel) Renaud for no discrimination of fact and fiction.
Victor (victorsky) Filipenco for building(?) the fastest model hydroplane.
Dilip (blip) Prasad for raising the lab dress code to a respectable level.
Ted (are you really that young?) Valkov for existing. Just give me another ice tea.
Scott (the rocket won't go) Barton who must be a clown (he went to ND).
Jon (JJJJooonnnyyy) Simon for his nerd humor.
Ted (let's play football again) Manning
Yuan (GQ) Qiu
Fred (the gas turbine) Newman
Tonghuo (shangster) Shang
Frank (franco) Kolczak
Scott () Sandler for removing the letter "r" from the alphabet.

Most special thanks go to my parents and my brother for their love and support.
Thanks Mom, Dad and Chris

The author would also like to thank his great friends from home who have kept me in line throughout.
Steve (the big kahuna) Lakus
Frank (frankton plankton) Socash
Gil (red squirrel) Scott
Chris (the dunzo factor) Dunn
Mike (kovester-kovester) Kowaleski
Chris (benny) Benson
Lisa (fornster) Fournier

And thank you too, HERMAN.

The project was conducted at the Gas Turbine Laboratory under a grant from the NASA Lewis Research Center (grant no. NAG3-953), Dr. Colin Drummond, program manager. Financial support for the author was provided by the Air Force Research in Aero Propulsion Technology (AFRAPT) program.

Thesis Contents

List of Figures

Nomenclature

a	=	speed of sound
a_n	=	Fourier coefficients of axial velocity perturbation at compressor face
A	=	flow through area
b	=	zeroth harmonic Fourier coefficient of plenum perturbation
b_x	=	axial chord
B	=	Greitzer non-dimensional stability parameter
c_n	=	Fourier coefficients of compressor characteristic slope
C_x	=	axial velocity
d_n	=	Fourier coefficients of steady state rotor loss slope
e_n	=	Fourier coefficients of steady state stator loss slope
L_{inlet}	=	length of ducting upstream of compressor
L_{exit}	=	length of ducting downstream of compressor
L_r	=	instantaneous rotor loss
L_s	=	instantaneous stator loss
n	=	harmonic number
N	=	number of stages
Ps	=	static pressure
Pt	=	total pressure
ΔP	=	blade row pressure rise
r	=	mean radius
s	=	blade pitch
t	=	time

T = non-dimensional throttle parameter

U = blade speed

w = relative velocity

x = axial coordinate

$\delta()$ = perturbation quantity

α = swirl angle

Γ = blade inertia parameter

θ = non-dimensional circumferential coordinate

λ = unsteady blade response parameter (rotor inertia)

μ = unsteady blade response parameter (rotor+stator inertia)

ρ = density

τ = blade row unsteady parameter

τ_r = rotor unsteady parameter

τ_s = stator unsteady parameter

ϕ = axial flow coefficient = C_x/U

υ = non-dimensional tangential velocity

ψ = non-dimensional compressor pressure rise = $(Ps_{exit}-Pt_{inlet})/\rho U^2$

ζ = stagger angle

ω = radian frequency of perturbation

ϖ = non-dimensional radian frequency = $\omega r/U$

Subscripts and superscripts:

abs = absolute frame

exit = compressor exit

inlet = compressor inlet

rel = relative frame

ss = steady state

r = rotor

s = stator

$(\bar{})$ = time and annulus averaged quantity

Chapter 1
Introduction

1.1 Description of Problem - Inlet Distortion

1.1.1 Background

Aero-compressors often encounter distorted inlet flowfields which generally result in a loss of compressor performance and stability margin. These distortions may be generated by inlet separation due to aircraft maneuvers at high angles of attack, strong crosswind induced inlet separation, shock induced separation in supersonic intakes, complex intake geometries, etc. Loss in compressor performance and stability margin have a strong impact on overall engine performance. Thus, it is a problem that requires much attention during the design phase of engine development. Considerable efforts have been directed towards the development of methods for prediction of engine response to inlet distortions. However, there are empiricisms associated with many of these methods and they are deemed inadequate. Furthermore, they do not include many of the physical effects that could have a potential influence on the compressor response to inlet distortion. The research work to be presented constitutes an effort at removing these empiricisms as well as the inclusion of those various physical effects not considered hitherto.

1.1.2 Inlet Distortion

The inlet distortion encountered by the aero-compressor can be of various forms. The distortion can be a non-uniformity in total pressure due to flow separation at the intake leading edge, a non-uniformity in static pressure if there exists a bend in the intake ahead of the compressor, or a non-uniformity in total temperature due to re-ingestion of hot exhaust gas (prevalent in VSTOL aircraft). The most common distortion encountered by aero-engines is a total pressure non-uniformity at the inlet; this may extend circumferentially and/or radially. Reid (1) showed that circumferential total pressure distortions have a far more adverse impact on aero-compressor performance than do radial total pressure distortions. The surge pressure ratio as a function of distortion type (circumferential/radial extent) is shown in figure 1.1, taken from reference 2. It is seen that the largest loss in performance is for the situation where the extent of a circumferential distortion covers a 90° segment. The static pressure far upstream is uniform so that associated with the total pressure non-uniformity there is a circumferential non-uniformity in velocity. For distortions of the square wave type shown in figure 1.2.a, there exists an interaction between the compressor and the incoming flow distortion; this interaction results in the redistribution of the incoming flow through the establishment of a static pressure field (due to the presence of the compressor). For this case, the respective flow quantities at the compressor inlet face are as shown in figure 1.2.b. The actual local performance of the compressor would be expected to vary circumferentially with this circumferential distortion in velocity. As alluded to in the above, the development of a flow model and prediction technique for assessing the response of multistage compressors to inlet distortion will be of primary interest here.

1.2 Previous Modelling Techniques

There are many methods for determining the compressor performance in distorted flow each with varying degree of empiricisms. In this section two techniques are reviewed: the parallel compressor model and the inertia models.

1.2.1 Parallel Compressor Theory

A method for predicting compressor performance in the presence of inlet distortion is the parallel compressor theory (2,3). Parallel compressor theory predicts the distorted performance of a compressor by averaging the inlet performance of two similar compressors operating in parallel with different inlet total pressure and the same exit static pressure as shown in figure 1.3 (taken from reference 4). Parallel compressor theory predicts compressor stability margin for distortions of circumferential extent greater than 60°. The model is less accurate in predicting compressor performance for distortions less than 60° (as unsteady effects may become important). When the distortion sector covers a circumferential extent greater than 60°, the time required for the blade to pass through the spoiled sector is several orders of magnitude greater than the blade convection time scale (whereas for less than 60°, these two time scales become nearly of the same order). Figure 1.4 shows the surge margin for a compressor with and without a distortion. It can thus be seen that the parallel compressor theory gives a reasonable prediction of the compressor surge line. The parallel compressor model was further expanded by Mazzawy (4) to an improved model that uses multiple parallel segments to define the distorted flowfield. Each segment is of constant circumferential extent and accounts for a fraction of the total mass flow through the compression system. This method extends parallel compressor

theory to include unsteady and 2-D flow effects on the blade row performance. The result was an improved prediction of distortion attenuation and circumferential description of flow quantities.

1.2.2 Inertia Models

A significant improvement in the development of a theoretical model for predicting compressor performance in rotating stall follow from the work of Moore (5). In his work, he introduced an inertia model for the response of the blade row to the flowfield; the model involves the addition of an inertia correction to the axisymmetric performance of a compressor that accounts for the acceleration and deceleration of fluid in the blade passage (see chapter 2).

In 1987, Hynes-Greitzer (6,7) applied the inertia model (proposed by Moore) to the development of a method for predicting the performance and stability of multistage compressors operating in the presence of inlet distortion. As in classical hydrodynamic stability analysis, Hynes-Greitzer derived a stability criteria by determining the growth rate of a general unsteady disturbance about a steady non-uniform flow through the compressor. The computed results of figures 1.5.a and 1.5.b (taken from reference 6) from the Hynes-Greitzer theoretical model indicate that the predicted compressor pressure rise at instability agrees with the experimental data of figures 1.6.a and 1.6.b (taken from reference 2).

Other methods for assessing the problem of stability include the use of time marching schemes to solve the unsteady flow equations; an example is that provided by the work of Adamczyk (8) who investigated the unsteady response of an isolated rotor to a circumferential distortion.

Additional theoretical and experimental work has been performed by Longley (9,10,11) to demonstrate the usefulness of the Hynes-Greitzer model for predicting compressor performance in the presence of inlet distortions. Results from experimental measurements appear to show that the essential fluid dynamical features have been modelled correctly.

1.3 Present Investigations

The key fluid dynamical features associated with a distorted flow through the multistage compressor have been predicted in the Hynes-Greitzer model. It nevertheless has simplifying assumptions on various physical effects such as unsteady loss, unsteady deviations, etc. The results of reference 9 have demonstrated the usefulness of such an approach for determining the response of multistage compressors to inlet distortion. It is therefore of importance to examine the consequences of these assumptions and the influence of these physical effects assumed negligible hitherto on compressor performance and stability margin in distorted flows.

The current effort involves extending the flow model to include the effects of unsteady losses and unsteady deviations on distorted compressor performance. The response of the relative exit air angle and the blade loss to changes in incidence has been modelled quasi-steadily in the work of references (6,7,9). However, experimental data has shown that when the compressor is subjected to an inlet distortion, the instantaneous flow quantity (loss/deviation) lags the steady state due to a delayed boundary layer response to changes in incidence. The time it takes for the boundary layer to respond scales with the time it takes for a fluid particle to traverse through the blade passage (i.e. the convection time scale). Mazzawy (4) and Nagano et al (12) suggested the use of a lag law to model the unsteady losses and unsteady

deviations which displays this hysteresis effect. The lag law reasonably predicts the unsteady blade response to incidence as shown in figures (1.7.a,1.7.b). Consequently, a fluid dynamic model has been developed to describe these small length scale effects (small length scale effects are on the order of a blade pitch whereas large length scale effects are on the order of compressor circumference).

The influence of two additional physical aspects of the flowfield on compressor performance and stability margin will also be investigated. These are: (i) the degree of sensitivity of inlet guide vanes (IGVs) to a variation in incidence; and (ii) the inclusion of inter blade row gaps in a multistage compressor. A theoretical model has been developed to include these effects in the determination of compressor stability margin.

In summary, the present theoretical model is capable of predicting compression system stability with an inlet distortion in which the following fluid dynamic effects are included:

(i) unsteady correction for acceleration/deceleration of fluid within blade passage.

(ii) flow redistribution upstream of compressor inlet face.

(iii) unsteady losses.

(iv) unsteady deviations.

(v) swirl sensitivity.

(vi) non-uniform compressor exit static pressure field (steady, distorted flow).

(vii) inter-blade row flow redistribution.

Chapter 2

Flow Models for Aero-engine Compression Systems

2.1 Compression System Model

The analysis is based on a flow model through an aero-engine compression system consisting of an upstream duct, a compressor, a downstream duct, a plenum and a throttle. A schematic of the compression system is shown in figure 2.1 The ducts, and to a certain extent the compressor blade passages, can be thought to constitute the inertance of the system. The plenum essentially gives the system compliance, or mass storage capability, and the throttle can be viewed as the resistance of the system. The following sections describe the governing flow equations for each component and the respective coupling among the various components.

2.2 Flow Model

The flow model and the accompanying assumptions for each component in the compression system are described next. In particular, we note the following simplifying assumptions:

A.) Upstream/downstream duct flowfield models

(1) 2-D, linearised, Euler equations of motion

(2) Axial mean flow upstream

B.) Compressor model

(1) Low speed (incompressible)

(2) High hub-to-tip ratio (two dimensional flowfield in x,θ)

C.) Plenum

(1) Isentropic

(2) Spatially uniform pressure

D.) Throttle

(1) Parabolic characteristic

(2) Throttle exits the flow to ambient conditions

In the work of Moore, Hynes, Greitzer, and Longley, the following additional simplifying assumptions were made: (i) the blade rows respond quasi-steadily to changes in incidence (inclusion of unsteady losses and unsteady deviations are neglected); (ii) the IGVs are 'perfect' (which suggests that the exit air angle is independent of incidence); (iii) the static pressure at compressor exit is circumferentially uniform in a steady distorted flow; and (iv) no inter blade row gaps (hence, no flow redistribution between blade rows). Here, we wish to relax all of the above assumptions.

2.2.1 Upstream Duct

The upstream duct flowfield is modelled as a two dimensional (x,θ), incompressible and inviscid flow. Thus, the flowfield in the upstream duct is governed

by the Euler equations. An analytic solution is obtainable through linearisation of the equations. As is shown by Hynes-Greitzer (6), the linearisation used adequately models the flowfield.

The solution consists of a potential part and a vortical part (due to the presence of the total pressure non-uniformity). The linearisation adopted for the upstream flow model implies that the total pressure distortion far upstream of the compressor simply advects downstream with the axial mean flow to the compressor inlet face. Thus, we have

$$P_t(\theta)_{inlet} = P_t(\theta)_{-\infty} \tag{2.1}$$

where the subscript "inlet" refers to the compressor inlet face and the subscript "$-\infty$" refers to a far upstream location at the duct entrance.

However, there is flow redistribution at the compressor face as a result of the compressor coupling with the incoming distorted flow; i.e., the compressor sets up a static pressure field which redistributes the flow as shown in figure 2.2. Thus, the flow coefficient at the compressor face consists of the corresponding distorted profile far upstream and a correction due to circumferential flow redistribution. Therefore, the upstream duct must be at least 2-3 compressor radii in length in order that the compressor has no potential effect on the inlet distortion far upstream.

The solution technique for the Euler equations linearised about the mean axial flow has been described elegantly in the work of Longley (9). The solution has been used to establish the definition of the flow quantities at the compressor inlet face. Fourier representation was used to exactly describe the structure of these flow quantities (see chapter 3), thus taking advantage of the periodicity in the flow through the compressor. For completeness, the analytical solutions are presented in the following description.

The tangential velocity (non-dimensionalised by rotor speed) at the inlet face of the compressor is given by

$$(\delta\upsilon)_{n=0} = 0 \tag{2.2.a}$$

$$(\delta\upsilon)_{n\neq0} = \left(\frac{i|n|}{n}\right)(\delta\phi)_{n\neq0} \tag{2.2.b}$$

where all perturbations are described in spectral space and consequently the subscript n denotes the harmonic number.

The static pressure perturbation at the inlet face to the compressor is then given by

$$\left(\frac{\delta P_s}{\rho U^2}\right)_{n=0} = -i\bar{\omega}\eta_{inlet}(\delta\phi)_{n=0} \tag{2.3.a}$$

$$\left(\frac{\delta P_s}{\rho U^2}\right)_{n\neq0} = -\left(\frac{i\bar{\omega}}{|n|} + \bar{\phi}\right)(\delta\phi)_{n\neq0} \tag{2.3.b}$$

2.2.2 Compressor Model

The performance of a compressor blade row in a non-uniform and unsteady flow field will not be locally the same as that in uniform flow. Possible causes for this change in performance are: (a) fluid inertia correction accounting for acceleration/deceleration of the fluid within the blade passages (proposed by Moore, employed by Hynes, Greitzer and Longley), (b) unsteady losses, (c) unsteady deviations, and (d) other variations that are on the same scale as the blade pitch. Description of each influence is given in the following sections.

The distorted pressure rise for a blade row at a fixed point in the absolute frame can be written as

$$\left.\frac{Ps_{exit} - Ps_{inlet}}{\rho U^2}\right|_{distorted} = \left.\frac{Ps_{exit} - Ps_{inlet}}{\rho U^2}\right|_{steady} + \left.\frac{Ps_{exit} - Ps_{inlet}}{\rho U^2}\right|_{unsteady} \quad (2.4)$$

The steady portion represents the local uniform flow pressure rise whereas the respective unsteady portion represents the aforementioned unsteady effects. The blade rows are modelled as semi-actuator disks. Figure 2.3 presents a geometrical representation of the blade passage. Conservation of mass and momentum, applied to a blade passage control volume, gives

$$\left.\frac{Ps_{exit} - Ps_{inlet}}{\rho U^2}\right|_{steady} = \frac{1}{2}\phi^2(\sec^2\alpha_{rel_{inlet}} - \sec^2\alpha_{rel_{exit}}) - L \quad (2.5)$$

where ϕ is the flow coefficient (C_x/U), α is the relative inlet/exit blade angle and L is the relative total pressure loss (See Appendix I for further detail concerning the definition of the steady state compressor pressure rise).

2.2.3 Fluid Inertia Correction

It is assumed that for an unsteady distorted flow, the distorted static pressure difference is given by the sum of the static pressure difference for a steady flow and an unsteady pressure correction as shown in equation (2.4). This correction accounts for the acceleration/deceleration of fluid within the blade passage as described here. The unsteady pressure rise for a blade passage is then derived as follows:

$$\text{Force} = \left(\frac{Ps_{exit} - Ps_{inlet}}{\rho U^2}\right)A = -\frac{d(mw)}{dt} = -m\frac{dw}{dt} = (\text{mass}) \text{ X } (\text{acceleration}) \quad (2.6)$$

with the flow area, A, defined as

$$A = s\cos\zeta$$

where s is the blade pitch, ζ is the blade stagger angle and w is the relative velocity of the fluid in the blade passage (fluid traversing through the blade passage at an angle, with respect to the axial direction, equivalent to the stagger angle). Therefore, the relative velocity is given by

$$w = C_x\cos\zeta \quad (2.7)$$

where C_x is the axial velocity.

The above expression for the unsteady pressure correction relative to the blade can be rewritten as follows

$$\left.\frac{Ps_{exit} - Ps_{inlet}}{\rho U^2}\right|_{\text{unsteady}} = -\Gamma\frac{r}{U}\left.\frac{\partial\phi}{\partial t}\right|_{\text{relative to blade}} \quad (2.8)$$

where

$$\Gamma = \frac{b_x\sec^2\zeta}{r}$$

with b_x being the axial chord length. In the relative frame for a rotor blade passage as described in the schematic presented in figure 2.4

$$\left.\frac{\partial\phi}{\partial t}\right|_{\text{relative to blade}} = \frac{\partial\phi}{\partial t} + \frac{U\partial\phi}{r\,\partial\theta} \quad (2.9)$$

Therefore, the unsteady static pressure rise across a rotor blade row is given by

$$\left.\frac{Ps_{exit} - Ps_{inlet}}{\rho U^2}\right|_{\text{unsteady, rotor}} = -\Gamma_r\frac{r}{U}\left(\frac{\partial\phi}{\partial t} + \frac{U\,\partial\phi}{r\,\partial\theta}\right) \quad (2.10)$$

And for a stator blade passage, the unsteady static pressure rise is as follows

$$\left.\frac{Ps_{exit} - Ps_{inlet}}{\rho U^2}\right|_{unsteady,\ stator} = -\Gamma_s \frac{r}{U}\left(\frac{\partial \phi}{\partial t}\right) \qquad (2.11)$$

In the above, the subscripts "r" and "s" refer to rotor and stator, respectively.

2.2.4 Unsteady Loss

The steady state blade relative total pressure loss through a blade passage is determined using an empirical correlation provided by Howell (13). Experimental data was obtained for cascades relating the relative blade loss coefficient to the blade incidence as shown in figure 2.5 (taken from reference 13). The use of such a correlation in the model assumes that the loss changes instantaneously with incidence. The following description relaxes this assumption.

Mazzawy (4) experimentally observed an additional viscous unsteady flow effect which occurs within the blade passage. Due to a delayed boundary layer response to changes in blade incidence, the relative total pressure loss does not change instantly with changes in incidence but rather lags the quasi-steady loss. This flow effect has been referred to as unsteady loss. As shown in the experimental data of figure 1.7.a, there is a hysteresis in the loss versus blade incidence. Hence, a good approximation of the experimental data is given by

$$\tau \frac{r}{U}\left.\frac{\partial L}{\partial t}\right|_{relative\ to\ blade} = L_{ss} - L \qquad (2.12)$$

where L represents the blade relative total pressure loss and the subscript "ss" refers to steady state. The time constant, τ, is defined as

$$\tau = \frac{b_x U}{C_x r} \sim 0.1 - 0.3 \quad (\sim\text{blade passage convection time})$$

Inclusion of unsteady losses in equation (2.5) gives then for the rotor static pressure rise and the stator static pressure rise, respectively

$$\frac{\Delta Ps}{\rho U^2} = \frac{1}{2}\phi^2(\sec^2\alpha_{rel_{inlet}} - \sec^2\alpha_{rel_{exit}}) - L_{r_{ss}} + \tau_r \frac{r}{U}\left(\frac{\partial L_r}{\partial t} + \frac{U}{r}\frac{\partial L_r}{\partial \theta}\right) - \Gamma_r \frac{r}{U}\left(\frac{\partial \phi}{\partial t} + \frac{r}{U}\frac{\partial \phi}{\partial \theta}\right) \quad (2.13)$$

$$\frac{\Delta Ps}{\rho U^2} = \frac{1}{2}\phi^2(\sec^2\alpha_{abs_{inlet}} - \sec^2\alpha_{abs_{exit}}) - L_{sss} + \tau_s \frac{r}{U}\frac{\partial L_s}{\partial t} - \Gamma_s \frac{r}{U}\frac{\partial \phi}{\partial t} \quad (2.14)$$

2.2.5 Unsteady Deviation

The ideal blade row static pressure rise (steady, inviscid) is shown in equation (2.5) to be a function of the flow coefficient, the relative inlet air angle and the relative exit air angle. Ideally, the flow of air leaves at an angle equal to that of the design exit blade angle; however, this is only an approximation at best. In general, the flow angle at blade row exit is different from the blade metal angle; this difference is termed the deviation. As before, an empirical correlation is required to determine the steady state blade deviation. The work of Howell on experimental data for cascades (figure 2.5 taken from reference 13) provides a base for relating the blade deviation to the incidence. Similarly, as was found in the investigation of unsteady losses, this correlation assumes the blade deviation responds instantaneously with changes in incidence.

As shown in figure 1.7.b, Mazzawy showed that there also exists a hysteresis in the blade deviation as a function of the incidence. The deviation lags the quasi-steady deviation because of a time lagging effect in the boundary layer response to changes in incidence. Consequently, the same approximation used before proves to be valid. The deviation lag law is given by

$$\tau \frac{r}{U} \frac{\partial \alpha}{\partial t}\bigg|_{\text{relative to blade}} = \alpha_{ss} - \alpha \qquad (2.15)$$

where α represents the relative exit air angle and the subscript "ss" refers to steady state. Similarly, the time constant, τ, is defined as

$$\tau = \frac{b_x}{r}\frac{U}{C_x} \quad (\sim\text{blade passage convection time})$$

For compressors, the typical value of τ is about 0.1 - 0.3. Therefore, the unsteady distorted pressure rise for a blade passage, associated with the inclusion of unsteady losses, unsteady deviations, and an unsteady correction for the fluid inertia, is given as:

rotor

$$\frac{\Delta Ps}{\rho U^2} = \frac{1}{2}\phi^2(\sec^2\alpha_{rel_{inlet}} - \sec^2\alpha_{rel_{exit}}) - L_{r_{ss}} + \tau_r \frac{r}{U}\left(\frac{\partial L_r}{\partial t} + \frac{U\partial L_r}{r\,\partial\theta}\right) - \Gamma_r \frac{r}{U}\left(\frac{\partial \phi}{\partial t} + \frac{r\,\partial\phi}{U\partial\theta}\right) \qquad (2.16)$$

$$\alpha_{rel_{exit}} = \alpha_{rel_{exit,ss}} - \tau_r \frac{r}{U}\left(\frac{\partial \alpha_{rel_{exit}}}{\partial t} + \frac{U\partial \alpha_{rel_{exit}}}{r\,\partial\theta}\right)$$

stator

$$\frac{\Delta Ps}{\rho U^2} = \frac{1}{2}\phi^2(\sec^2\alpha_{abs_{inlet}} - \sec^2\alpha_{abs_{exit}}) - L_{s_{ss}} + \tau_s \frac{r}{U}\frac{\partial L_s}{\partial t} - \Gamma_s \frac{r}{U}\frac{\partial \phi}{\partial t} \qquad (2.17)$$

$$\alpha_{abs_{exit}} = \alpha_{abs_{exit,ss}} - \tau_s \frac{r}{U}\left(\frac{\partial \alpha_{abs_{exit}}}{\partial t}\right)$$

Summing up the contributions of each blade row gives then for an n-stage compressor

$$\frac{\Delta Pt\text{-}s}{\rho U^2} = \psi\big(\phi(\theta)\big) - L_{rss} - L_{sss} + \tau_r \frac{r}{U}\left(\frac{\partial L_r}{\partial t} + \frac{U \partial L_r}{r\,\partial \theta}\right) + \tau_s \frac{r\,\partial L_s}{U\,\partial t} - \mu \frac{r\,\partial \phi}{U \partial t} - \lambda \frac{\partial \phi}{\partial \theta} \quad (2.18)$$

where the inertia parameters are defined by

$$\lambda = \sum_{i=1}^{n} (\Gamma_r)_i \quad \text{and} \quad \mu = \sum_{i=1}^{n} (\Gamma_r + \Gamma_s + \Gamma_{igv})_i$$

The inclusion of unsteady deviations is accounted for within the first term on the left hand side of equation (2.18).

2.2.6 Inter Blade Row Gaps

Up until now, flow redistribution between blade rows has been excluded from the analysis. It has been assumed that the flow quantities at the exit of a blade row are equivalent to those entering the next blade row. This is no longer true when there exists some finite distance, or gap, between blade rows. These gaps have been modelled as two dimensional incompressible Euler flowfields where bulk swirl can exist. The governing equations have been derived in Appendix II. Within the gap region, a vortical mode, a potential decaying mode and a potential growing mode will be present. The total pressure non-uniformity advects with the mean flow. For a steady distorted flow, the zeroth harmonic remains unchanged between blade rows.

However, this is not true for an unsteady distorted flow. The description of the unsteady perturbations for the zeroth harmonic are given by

$$\delta\phi_{\text{gap exit}} = \delta\phi_{\text{gap inlet}} \tag{2.19.a}$$

$$\delta\upsilon_{\text{gap exit}} = \left(\frac{-i\varpi\eta_{\text{gap}}}{\bar{\phi}} + 1\right)\delta\upsilon_{\text{gap inlet}} \tag{2.19.b}$$

$$\left(\frac{\delta Ps}{\rho U^2}\right)_{\text{gap exit}} = \left(\frac{i\varpi\eta_{\text{gap}}}{\bar{\phi}} + 1\right)\left(\frac{\delta Ps}{\rho U^2}\right)_{\text{gap inlet}} \tag{2.19.c}$$

When tracking the n^{th} harmonic variation within the gap, the following expression relates the inlet flow quantities of the downstream blade row to the exit flow quantities of the upstream blade row.

$$\underline{\chi}_{\text{inlet}} = \underline{\underline{A}}_{\text{inlet}}\,\underline{\underline{A}}^{-1}_{\text{exit}}\,\underline{\chi}_{\text{exit}} \tag{2.20}$$

where

$$\chi = \begin{bmatrix} \phi \\ v \\ \dfrac{P_s}{\rho U^2} \end{bmatrix}$$

the matrix A_{exit} is defined by

$$\begin{bmatrix} 1 & 1 & 1 \\ \beta_n & -i\dfrac{|n|}{n} & i\dfrac{|n|}{n} \\ 0 & \bar{\phi}(i\dfrac{|n|}{n}\beta_n - 1) & \bar{\phi}(-i\dfrac{|n|}{n}\beta_n - 1) \end{bmatrix}$$

and the matrix A_{inlet} is defined as

$$\begin{bmatrix} e^{-in\eta_{gap}\beta_n} & e^{-iln\eta_{gap}} & e^{iln\eta_{gap}} \\ \beta_n e^{-in\eta_{gap}\beta_n} & -i\frac{ln}{n}e^{-iln\eta_{gap}} & i\frac{ln}{n}e^{iln\eta_{gap}} \\ 0 & \bar{\phi}(i\frac{ln}{n}\beta_n - 1)\, e^{-iln\eta_{gap}} & \bar{\phi}(-i\frac{ln}{n}\beta_n - 1)\, e^{iln\eta_{gap}} \end{bmatrix}$$

where

$$\beta_n = \tan\bar{\alpha} + \frac{r\omega}{n\bar{u}}$$

Suppression of the time dependence in the above defined matrices relates the flow quantities at gap inlet to gap exit for a steady distorted flow.

2.2.7 Downstream Duct

The following section formulates the governing equations which describe the downstream duct flowfield. The downstream duct flow is assumed to be two dimensional (x,θ), incompressible and inviscid , and can therefore be represented by the two dimensional Euler equations (as in the upstream duct flowfield). In constrast with the upstream duct flow, bulk swirl can exist downstream from the compressor.

Hynes-Greitzer assumed the flow leaving the compressor to be axial. Furthermore, it was assumed that the static pressure (for a steady distorted flow) is circumferentially uniform in θ since the streamlines are parallel (i.e. the relative exit air angle is circumferentially uniform in θ). This assumption does not correctly model the flowfield downstream from the compressor and has therefore been deemed inappropriate. It is relieved here by allowing for the inclusion of unsteady deviations in the model (described in a previous section). Therefore, the static pressure at the compressor exit is circumferentially non-uniform in θ. Furthermore, the circumferentially mean flow at compressor exit is no longer assumed to leave axially as was done in the previous work of Hynes, Greitzer and Longley.

A linearisation of the two dimensional Euler equations allows for determining an analytic solution to the downstream duct flowfield. Appendix II formally presents the governing flow equations, the linearisation of these equations and the method of obtaining a solution to the desired flow quantities (axial velocity, tangential velocity and static pressure). The form of the solution to these flow quantities both in space and time is given at the end of the appendix. Again, Fourier representation was used to describe the structure of these flow quantities as was done in (9) (see chapter 3 for further description of the spectral representation). The solution to the Euler equations shows the existence of three possible modes: a vortical mode (A_n's), a decaying potential mode (B_n's) and a growing potential mode (C_n,s).

Therefore, using the solution presented in Appendix II, a relationship between the flow quantities at the compressor exit and the plenum can be established. The static pressure perturbation for the zeroth harmonic (spatially integrated mean in θ direction) is as follows

$$\frac{\delta Ps_{plenum} - \delta Ps_{exit}}{\rho U^2} = i\tilde{\omega}\eta_{duct}\,\delta\phi_{exit} \qquad (2.21)$$

where η_{duct} is the non-dimensional downstream duct length (non-dimensionalised by the mean compressor radius). The nth harmonic components (which describe the spatial non-uniformity) of the flow coefficient, tangential velocity (non-dimensional form, n) and static pressure must have the following form in the downstream duct.

$$\delta\phi(x,\theta,t) = \sum_{\substack{n=-\infty \\ n\neq 0}}^{\infty} \left(A_n e^{-i\beta_n \frac{nx}{r}} + B_n e^{-|n|\frac{x}{r}} + C_n e^{|n|\frac{x}{r}} \right) e^{in\theta + i\omega t} \qquad (2.22.a)$$

$$\delta\upsilon(x,\theta,t) = \sum_{\substack{n=-\infty \\ n\neq 0}}^{\infty} \left(\beta_n A_n e^{-i\beta_n \frac{nx}{r}} - i\frac{|n|}{n} B_n e^{-|n|\frac{x}{r}} + i\frac{|n|}{n} C_n e^{|n|\frac{x}{r}}\right) e^{in\theta+i\omega t} \quad (2.22.b)$$

$$\frac{\delta P_s}{\rho U^2}(x,\theta,t) = \bar{\phi} \sum_{\substack{n=-\infty \\ n\neq 0}}^{\infty} \left(\left(-1 + i\frac{n}{|n|}\beta_n\right) B_n e^{-|n|\frac{x}{r}} + \left(-1 - i\frac{n}{|n|}\beta_n\right) C_n e^{|n|\frac{x}{r}}\right) e^{in\theta+i\omega t} \quad (2.22.c)$$

The downstream duct is defined to be long enough such that there is purely axisymmetric coupling between the plenum and the compressor/downstream duct flowfield. Thus, a growing potential mode can not physically exist (C_n's = 0). This reduces equations (2.22) to the following expressions (where for convenience, the summation sign has been ignored).

$$(\delta\phi)_n = A_n + B_n \quad (2.23.a)$$

$$(\delta\upsilon)_n = \beta_n A_n - i\frac{|n|}{n} B_n \quad (2.23.b)$$

$$\left(\frac{\delta P_s}{\rho U^2}\right)_n = \bar{\phi}\left(-1 + i\frac{n}{|n|}\beta_n\right) B_n \quad (2.23.c)$$

Upon manipulating the above equations, it can be shown that the compressor exit static pressure spatial non-uniformity can alternatively be written as

$$\left(\frac{\delta P_s}{\rho U^2}\right)_n = i\bar{\phi}\frac{n}{|n|}\left(\beta_n(\delta\phi)_n - (\delta\upsilon)_n\right) \quad (2.24)$$

where

$$\beta_n = \tan\bar{\alpha} + \frac{\bar{\omega}}{n}$$

The unsteady pressure perturbations at the compressor exit must satisfy the equations presented in (2.21,2.24).

The set of equations governing a steady distorted flow are simply obtained by suppressing the time dependence in equations (2.22). Hence, the compressor exit static pressure (spatially integrated mean in θ) is equivalent to the plenum static pressure.

$$Ps_{exit} = Ps_{plenum} \tag{2.25}$$

And, for the n^{th} harmonic

$$\phi(x,\theta) - \bar{\phi} = \sum_{\substack{n=-\infty \\ n\neq 0}}^{\infty} A_n e^{in\theta - in\tan\bar{\alpha}\frac{x}{r}} + B_n e^{in\theta - |n|\frac{x}{r}} + C_n e^{in\theta + |n|\frac{x}{r}} \tag{2.26.a}$$

$$\upsilon(x,\theta) - \bar{\upsilon} = \sum_{\substack{n=-\infty \\ n\neq 0}}^{\infty} \tan\bar{\alpha}\, A_n e^{in\theta - in\tan\bar{\alpha}\frac{x}{r}} - i\frac{|n|}{n} B_n e^{in\theta - |n|\frac{x}{r}} + i\frac{|n|}{n} C_n e^{in\theta + |n|\frac{x}{r}} \tag{2.26.b}$$

$$\frac{P_s}{\rho U^2}(x,\theta) - \frac{\bar{P}_s}{\rho U^2} = \bar{\phi} \sum_{\substack{n=-\infty \\ n\neq 0}}^{\infty} \left(-1 + i\frac{n}{|n|}\tan\bar{\alpha}\right) B_n e^{in\theta - |n|\frac{x}{r}} + \left(-1 - i\frac{n}{|n|}\tan\bar{\alpha}\right) C_n e^{in\theta + |n|\frac{x}{r}}$$

(2.26.c)

Similarly, as before

$$\left(\frac{P_s}{\rho U^2}\right)_n = i\bar{\phi}\frac{n}{|n|}\left(\tan\bar{\alpha}(\phi)_n - (\upsilon)_n\right) \tag{2.27}$$

The compressor exit static pressure must satisfy these conditions. In summary, for a steady distorted flow the boundary conditions are such that the spatially mean static pressure must be equivalent to the plenum pressure and the pressure spatial non-uniformity must have the form described in equation (2.27).

2.2.8 Plenum Dynamics / Throttle

The performance of the exit throttle in a steady distorted flow is assumed to follow a parabolic pressure characteristic. The plenum static pressure is then related to the throttle static pressure by the following expression

$$\frac{Ps_{plenum} - Ps_{throttle}}{\rho U^2} = \frac{1}{2} T\bar{\phi}^2 \tag{2.28}$$

where T simply specifies the throttle setting. Linearisation about the steady distorted flow gives

$$\frac{\delta Ps_{plenum}}{\rho U^2} = T\bar{\phi}\delta\phi_{throttle} \tag{2.29}$$

where the throttle is assumed to exit the flow to ambient conditions. Mass conservation for the plenum / throttle system requires

$$\rho A_{duct}\left(\bar{C}_{x_{exit}} - C_{x_{throttle}}\right) = V_{plenum}\frac{d\rho}{dt} \tag{2.30}$$

where A is the downstream duct cross-sectional area, Cx is the axial velocity (with the overscore denoting circumferentially integrated mean), and V is the plenum volume. Linearising the mass conservation constraint gives

$$\rho A_{duct} U\left(\bar{\delta\phi}_{exit} - \delta\phi_{throttle}\right) = V_{plenum}\frac{d(\delta\rho)}{dt} \tag{2.31}$$

Since the plenum is isentropic, the following perturbation relation is obtained

$$\frac{\delta Ps_{plenum}}{\rho U^2} = \frac{a^2}{U^2}\frac{\delta\rho}{\rho} \tag{2.32}$$

Combining equations (2.29,2.31,2.32) gives the unsteady plenum dynamics relation

$$\left(4B^2\frac{L_{tot}}{r}\frac{r\,d}{U dt} + \frac{1}{T\bar{\phi}}\right)\frac{\delta Ps_{plenum}}{\rho U^2} = \delta\bar{\phi}_{exit} \tag{2.33}$$

The B parameter, due to Greitzer (15), is defined as follows

$$B = \frac{U}{2a}\sqrt{\frac{V_{plenum}}{A_{duct}L_{tot}}}$$

where a is the speed of sound and the effective total compression system length is

$$\frac{L_{tot}}{r} = \mu + \frac{L_{inlet}}{r} + \frac{L_{exit}}{r}$$

The subscripts "inlet" and "exit" refer to the inlet duct (upstream of compressor) and exit duct (downstream of compressor) lengths. The B parameter, which consists of various geometrical and physical quantities, indicates the mode of instability that may occur. There exists a critical B parameter below which rotating stall occurs and above which surge oscillations occur.

2.3 Steady State Distorted Compressor Performance

Suppression of the time dependence in the governing equations (that describe the flow throughout the compression system) results in a set of equations for a steady distorted flow which are given by

$$\frac{\Delta Pt\text{-}s}{\rho U^2} = \psi_{id} - L_{r,ss} - L_{s,ss} - \lambda \frac{\partial \phi}{\partial \theta} \tag{2.34}$$

$$\frac{Ps_{plenum} - Ps_{throttle}}{\rho U^2} = \frac{1}{2} T\bar{\phi}^2$$

; the two loss terms in equation (2.34) are the steady state rotor and stator loss, respectively. The above expression is solved to determine the mean flow and corresponding compressor performance for a given distortion generated far upstream at the inlet.

2.4 Linear Stability Analysis

2.4.1 Introduction

The determination of compression system stability essentially involves a linear stability analysis similar to the usual hydrodynamic stability analysis. A general unsteady perturbation is added to the known (calculated) mean flow and the resulting growth of unsteady disturbances is examined. By expressing the unsteady disturbances as a harmonic series in time, the time dependent governing equations yield a dispersion relation in terms of flow distortion, steady state compressor performance characteristics, the geometry, and the growth rate. This dispersion relation can then be

solved for the growth rate. If the perturbation grows with time, then the compressor is operating with a flowfield instability present, otherwise it is stable. The approach taken essentially constitutes an eigenvalue problem for the determination of the disturbance eigenmode and the corresponding eigenvectors.

The time dependent governing equations are linearised and the form of the equation for the perturbation terms is given by

$$\frac{\Delta Pt\text{-}s}{\rho U^2} = \left.\frac{d\psi_{id}}{d\phi}\right|_{\phi(\theta)} \delta\phi - \delta L_r - \delta L_s - \mu\frac{r}{U}\frac{\partial(\delta\phi)}{\partial t} - \lambda\frac{\partial(\delta\phi)}{\partial\theta} \qquad (2.35)$$

From the unsteady plenum dynamics (equation)

$$\left(4B^2\frac{L_{tot}}{r}\frac{r\,d}{U dt} + \frac{1}{T\phi}\right)\frac{\delta Ps_{plenum}}{\rho U^2} = \delta\phi_{exit}$$

The instantaneous loss perturbations (unsteady losses) are

for a rotor $$\delta L_r|_n = \frac{\delta L_{rss}|_n}{1+i\tau_r(\bar{\omega}+n)} \qquad (2.36.a)$$

and for a stator $$\delta L_s|_n = \frac{\delta L_{sss}|_n}{1+i\tau_s\bar{\omega}} \qquad (2.36.b)$$

The instantaneous deviation perturbations (unsteady deviations) are

for a rotor $$\delta\alpha_r|_n = \frac{\delta\alpha_{rss}|_n}{1+i\tau_r(\bar{\omega}+n)} \qquad (2.37.a)$$

and for a stator $$\delta\alpha_s|_n = \frac{\delta\alpha_{sss}|_n}{1+i\tau_s\bar{\omega}} \qquad (2.37.b)$$

The inclusion of unsteady deviations complicates the problem. The time dependent governing equations can no longer be manipulated into a standard eigenvalue problem as was done in the past (see Appendix III). Even if this was possible, it would be computationally inefficient since it would mean expanding the matrix, A, by a factor equivalent to the number of blade rows within the compressor. Typical matrix operations are of order N^3 (where N is the order of the matrix); then, for example, doubling the size of the matrix results in increasing the execution time by a factor of 2^3 (or 8). A different approach was then needed to determine the system stability. The essence of the technique is as follows. For a given $\tilde{\omega}$, a general unsteady perturbation is defined at the compressor inlet face. This perturbation is tracked through the compressor from inlet to exit. At the compressor exit, the unsteady downstream duct flow model and the unsteady plenum dynamics apply the respective matching conditions on the pressure perturbations as described in the previous section. The resultant set of equations representing the harmonic structure of the flow perturbation can be written as the following matrix equation

$$\underline{\underline{A}}\,\underline{x} = 0 \tag{2.38}$$

where the matrix A is a function of the mean distorted flow and the eigenvalues, $\tilde{\omega}$. The eigenvalues of the compression system are defined by those values of $\tilde{\omega}$ for which there exists a flow coefficient perturbation of the flowfield which satisfies equation (2.38). In order that there be such a solution, the matrix A must be singular which suggests that the determinant be zero. Hence, values of $\tilde{\omega}$ are determined from

$$\det\left(\underline{\underline{A}}\right) = f(\tilde{\omega}) = 0 \tag{2.39}$$

Since any eigenvalue with a negative imaginary part implies an unstable mode, it is only necessary to determine the number of solutions to equation (2.39) that lie in the negative half of the complex eigenvalue plane (9). The method used here is the Nyquist Criterion, or the Principle of the Argument (see reference 15). The application of the method will be discussed in greater detail in the following chapter.

2.4.2 Stability Assessment Method

The following analysis describes how the flow perturbations are tracked through the compressor. Unsteady perturbations in flow coefficient, tangential velocity and static pressure are known at the compressor inlet from solving the time dependent Euler flow equations governing the upstream duct flowfield. The flow coefficient perturbation can be represented by the Fourier series

$$\delta\phi = \sum_{n=-\infty}^{\infty} a_n e^{in\theta + i\omega t} \tag{2.40}$$

The tangential velocity perturbation (non-dimensionalised by rotor speed) at the inlet face of the compressor is given by

$$(\delta\upsilon)_{n=0} = 0$$

$$(\delta\upsilon)_{n\neq 0} = \left(\frac{i|n|}{n}\right)(\delta\phi)_{n\neq 0}$$

And, the static pressure perturbation at the inlet face to the compressor is then given by

$$\left(\frac{\delta P_s}{\rho U^2}\right)_{n=0} = -i\varpi\eta_{inlet}\left(\delta\phi\right)_{n=0}$$

$$\left(\frac{\delta P_s}{\rho U^2}\right)_{n\neq 0} = -\left(\frac{i\varpi}{|n|} + \bar{\phi}\right)\left(\delta\phi\right)_{n\neq 0}$$

These perturbed quantities are all known at the inlet for a given eigenvalue, ϖ. Clearly, the inlet flow coefficient perturbation is equivalent to the exit flow coefficient perturbation by the conservation of mass. Upon linearisation of the compressor model equation (2.16) for static-to-static pressure rise across a blade row, an expression relating the perturbed inlet flow variables to the respective exit perturbed flow variables can be obtained as follows:

$$\left(\frac{\delta\Delta P_s}{\rho U^2}\right)_m = \left(\upsilon^{rel}_{inlet}(\theta)\right)_{mn}\left(\delta\upsilon^{rel}_{inlet}\right)_n - \left(\upsilon^{rel}_{exit}(\theta)\right)_{mn}\left(\delta\upsilon^{rel}_{exit}\right)_n - (\delta L)_m - \Lambda\left(i\varpi + iU_j\delta_{mn}\right)_{mn}\left(\delta\phi\right)_n \tag{2.42}$$

where the subscript "j" refers to the blade row (i.e.; the non-dimensional blade speed, U, equals one for rotors and zero for stators). Likewise, we have the definition of the tangential velocity perturbation as

$$\left(\delta\upsilon^{rel}\right)_m = \left(\upsilon^{rel}(\theta)\tan(\alpha^{rel}(\theta)) + \phi(\theta)\right)_{mn}\left(\delta\alpha^{rel}\right)_n + \left(\tan(\alpha^{rel}(\theta))\right)_{mn}\left(\delta\phi\right)_n \tag{2.43}$$

Equation (2.43) thus relates the known inlet flow perturbations to the perturbation in the relative inlet air angle. The exit relative air angle perturbation has been assumed to

depend on the inlet relative air angle perturbation only. Therefore, it can be simply determined from

$$\left(\delta\alpha_{exit}^{rel}\right)_m = \left(\frac{d\alpha_{inlet}^{rel}}{d\alpha_{exit}^{rel}}\right)_{mn} \left(\delta\alpha_{inlet}^{rel}\right)_n \tag{2.44}$$

The perturbation in the exit tangential velocity is now simply calculated by equation (2.43). The third term in equation (2.42) represents the blade row loss perturbation. The total pressure loss is a function of the flow coefficient and the relative inlet air angle. Hence, it is described as

$$(\delta L)_m = \left(\frac{dL}{d\alpha_{inlet}^{rel}}\right)_{mn} \left(\delta\alpha_{inlet}^{rel}\right)_n + \left(\frac{dL}{d\phi}\right)_{mn} (\delta\phi)_n \tag{2.45}$$

The derivative terms in equations (2.44) and (2.45) are defined locally for a steady distorted flow. The remaining term in the blade row pressure rise perturbation is the unsteady correction accounting for the acceleration/deceleration of fluid within the blade passage. Since inter blade row gaps have yet to be considered, this analysis is repeated until the unsteady flow perturbations are determined at the compressor exit. Inclusion of unsteady losses and unsteady deviations in the analysis is simply done by linearising the lag law defined in section 2.2. The instantaneous flow perturbation is related to the steady state flow perturbation by the following expression

$$(\delta Q)_m = \frac{(\delta Q_{ss})_m}{1 + i\tau_j(\varpi + U_j m)} \tag{2.46}$$

where Q indicates the respective flow quantity (loss / deviation). The flow coefficient, tangential velocity and static pressure perturbations are all known at the compressor exit face. Hence, the unsteady downstream flowfield and the unsteady plenum dynamics must be considered. Equations (2.21,2.24,2.33) from section 2.2 enforce the matching conditions on the compressor exit pressure perturbation. The resultant set of equations is expressed in equation (2.38).

2.5 Summary

This chapter has been devoted to providing description of the underlying modelling assumptions, the governing equations for each individual component within the compression system and the associated boundary conditions (or component matching conditions). The following chapter will present the computational implementation of this compression system model.

Chapter 3

Computational Description

3.1 Introduction

The computational implementation of the present compression system model primarily follows the work of Longley (9). A computational tool has been developed to solve the described flowfields making up the compression system in order to predict both the steady distorted compressor performance and the compression system stability. The calculation consists of two parts. The first part solves the governing equations for a steady distorted flow. Then, the second part adds a most general unsteady perturbation to the known solution of the mean flow and then examines whether or not the perturbation grows or decays with time, thus indicating the stability of the compression system. The following sections will discuss the means by which each part of the calculation is carried out.

3.2 Meanflow Calculation

3.2.1 Overall Description of the Procedure

The meanflow calculation solves the steady distorted flow equations given both the inlet total pressure distortion defined far upstream of the compressor inlet and the

throttle setting, or operating point. These two quantities uniquely determine the compression system flowfield. In addition, the calculation requires specification of the steady state clean flow performance of the compressor (see Appendix I for further description of the steady state clean flow performance).

As was done in chapter 2, the time dependence in the governing equations is suppressed and the resultant set of equations describes the steady distorted flowfield (meanflow). A pseudo-spectral method was used to obtain the desired solution. Discrete Fourier series representation of the flow quantities was chosen in order to take advantage of the periodicity of the flow circumferentially. Therefore, the flow quantities can be defined by

$$\phi = \sum_{k=-K}^{K+1} A_k(t)\, e^{ik\theta} \tag{3.1}$$

The flow quantities are defined at 2K+1 circumferential locations in physical space. FFT's are used to transform the circumferentially defined flow profiles to spectral space.

3.2.2 Newton-Rhapson Iterative Scheme

The compressor model equation (2.34) is a nonlinear ordinary differential equation. Therefore, the iterative scheme used to find a solution is based on the Newton-Rhapson method (see reference 16), which gives quadratic convergence. Consider the governing steady distorted flow equation (2.34) expressed in spectral space.

$$\left(\frac{Ps_{exit}(\theta)}{\rho U^2}\right)_n - \left(\frac{Pt_{inlet}(\theta)}{\rho U^2}\right)_n = \left(\psi_{id}(\phi(\theta))\right)_n - \left(L_r(\phi(\theta))\right)_n - \left(L_s(\phi(\theta))\right)_n - \left(in\lambda\phi(\theta)\right)_n \tag{3.2}$$

where n denotes the harmonic number. Assume for the sake of simplicity, the compressor exit static pressure is circumferentially uniform, the IGVs are 'perfect', and unsteady losses and deviations are neglected. Then, the exit static pressure is defined by the throttle equation (2.28). If the distortion is steady, then the total pressure at the compressor inlet is equivalent to the inlet total pressure distortion defined upstream. The ideal pressure rise, rotor loss and stator loss are defined as a function of the local value of the flow coefficient. And, clearly, the final term on the right hand side of the equation is a function of the flow coefficient. Therefore, an initial guess is made for the flow coefficient profile and as will be shown, Newton-Rhapson iteration is used to determine the flow coefficient profile which satisfies the steady state distorted flow equation. Hence, for a flow coefficient profile which does not necessarily satisfy equation (3.2).

$$(\text{ERROR})_n = \left(\psi_{id}(\phi(\theta))\right)_n + \left(\frac{Pt_{inlet}(\theta)}{\rho U^2}\right)_n - \frac{1}{2} T \bar{\phi}^2 - (L_r(\phi(\theta)))_n - (L_s(\phi(\theta)))_n - \left(in\lambda\phi(\theta)\right)_n \tag{3.3}$$

For convenience, rewrite equation (3.3) as

$$(\text{ERROR}) = f\left(\phi^{old}(\theta)\right) \tag{3.4}$$

Expand equation (3.4) in a Taylor series in order to determine a new flow coefficient which satisfies the governing equations. This gives

$$f\left(\phi^{new}(\theta)\right) = f\left(\phi^{old}(\theta)\right) + \frac{df}{d\phi}\delta\phi + O(\delta\phi^2) \tag{3.5}$$

From equation (3.4), the function evaluated at the old flow coefficient is equivalent to the 'ERROR' and for the function evaluated at the new flow coefficient, it is necessary that the 'ERROR' go to zero. Therefore, the following expression is obtained

$$\text{ERROR} = \underline{\underline{A}}\,(\delta\phi) \tag{3.6}$$

where the matrix A (which represents the change in the function, f, with ϕ) is defined by

$$-\frac{d\psi_{id}}{d\phi} + \frac{dL_r}{d\phi} + \frac{dL_s}{d\phi} + in\lambda + \left(T\tilde{\phi}\cos\alpha + \frac{1}{2}\tilde{\phi}^2\sin\alpha\right)_{n=0}$$

The angle α is defined to be 0 or 90 degrees dependent upon whether one iterates along a constant throttle line or a constant mass flow line. The matrix A is a banded matrix with the zeroth harmonic represented on the diagonal. Then, by simply expanding about the old value of the change in flow coefficient, the classic form of Newton-Rhapson iteration is obtained

$$\underline{\underline{A}}\,(\Delta\delta\phi) = \text{ERROR} - \underline{\underline{A}}\,(\delta\phi^{old}) \tag{3.7}$$

This iterative technique originally developed by Longley has proven to be effective in reaching a converged solution to the governing steady distorted flow equations. Inclusion of unsteady losses and unsteady deviations required some modifications to the iterative technique; however, the general form is still the same.

3.3 Stability Calculation

3.3.1 Spectral Method

For the stability assessment of the compression system, a general unsteady flow perturbation is added to the previously calculated meanflow solution. If any such perturbation grows in time then the system is unstable, otherwise it is stable. Similarly, Fourier series representation of the perturbations was used. Hence, the structure of the perturbation has the form

$$\delta(\,) = \sum_{k} A_k \, e^{ik\theta + i\omega t} \tag{3.7}$$

In physical terms, the unsteady perturbations to the flow may be viewed as incipient stall cells when they propagate around the annulus and as small amplitude, surge-like system transients when they are predominantly one-dimensional in character (6).

3.3.2 Nyquist Criterion

The stability analysis could originally be written in the form of a standard eigenvalue problem. As discussed earlier, this was no longer possible when other complicating flow features (i.e., unsteady deviations, inter blade row gaps) are included. The method used in this case is Nyquist Criterion or the Principle of the Argument (see reference 15) which amounts to the solution of the following equation:

$$\frac{1}{2\pi i} \oint_{C} \frac{f'(\tilde{\omega})}{f(\tilde{\omega})} \, d\tilde{\omega} = N_{zeros} - N_{poles} \tag{3.8}$$

The function, $f(\tilde{\omega})$, is differentiable and has no singularities. The right hand side of equation (3.8) is the difference in the number of zeros, N_{zeros}, and the number of poles, N_{poles}, which exist within the defined contour, C. Since the function is analytic within the specified contour C, no poles exist in the lower half of the $\tilde{\omega}$ - plane. Therefore, equation (3.8) reduces to

$$\frac{1}{2\pi}\Delta_C \, ARG\big(f(\tilde{\omega})\big) = N_{zeros} \tag{3.9}$$

where the change in the argument of the function around the contour C is given by $2\pi N_{zeros}$. The contour C to be used is defined in figure 3.1. The calculation then consists of evaluating $f(\tilde{\omega})$ for each value of $\tilde{\omega}$ around the contour. The contour defined in the $\tilde{\omega}$-plane is then transformed into the $f(\tilde{\omega})$-plane as shown in figure 3.2. The number of times the $f(\tilde{\omega})$ contour winds around the origin indicates the number of zeros which lie in the contour C ($\tilde{\omega}$-plane). Hence, the winding number indicates the number of unstable modes.

3.4 Typical Calculation

A typical calculation involves both performing the mean flow calculation and the stability calculation. This requires specification of the following: (i) inlet total pressure distortion, (ii) the operating point (temporal/spatial mean flow coefficient or throttle setting), (iii) the necessary quantities in defining the compressor axisymmetric performance, (iv) the inertia parameters (λ,μ,η,τ_r,τ_s) and (v) the B parameter (defines the plenum size; see chapter 2).

Evaluation of the axisymmetric performance requires the specification of the design relative blade inlet and exit air angles, the design blade loss coefficient and the steady

state blade model. Figure 3.3 gives an example of the axisymmetric performance for a 3-stage compressor (where the total-to-static pressure rise normalised by ρU^2 is plotted against the flow coefficient,ϕ). Figure 3.4 is an example of the specification of a 0.1 magnitude, 120 degree square wave total pressure distortion at the inlet (the oscillations are due to the use of truncated Fourier series). The solution to the meanflow is entirely defined by the flow coefficient profile at the inlet face of the compressor. All flow quantities of interest may be determined from this profile. Shown in figure 3.5 are the flow coefficient pofiles at neutral stability predicted by the original inertia model and the improved unsteady loss model. The solution to the stability calculation are the eigenmodes presented in figure 3.6. These are the eigenmodes predicted by the improved unsteady loss model at neutral stability (note the first harmonic lies on the real axis indicating neutral stability). In summary, the results to be presented within the next several chapters were calculated in the aforementioned manner.

Chapter 4

Investigation into Unsteady Losses and Deviations on Compressor Performance and Stability Margin

4.1 Introduction

The objective of these investigations is to assess the effect of various fluid dynamic features, not accounted for in previous models, on compressor performance and stability margin. These features are as follows: (i) unsteady losses, (ii) unsteady deviations, (iii) IGV swirl sensitivity, (iv) circumferentially non-uniform compressor exit static pressure, and (v) inter blade row gaps. This chapter is devoted to studying the effects of unsteady losses, unsteady deviations and a circumferentially non-uniform compressor exit static pressure field. Each flow feature will be investigated individually.

4.2 Parameter Study

In each calculation, three models were considered: (i.) original inertia model (neglecting unsteady losses and unsteady deviations), (ii.) improved inertia model (inclusion of unsteady losses and/or unsteady deviations), and (iii.) an effective inertia model. A comparative study of the results from these computed cases will enable us to

determine the importance of unsteady losses/deviations and the applicability of a simpler effective inertia model.

4.2.1 Assumptions

For all calculations within the parameter study (unless otherwise specified), the following assumptions require further elaboration.

A.) The effective length of the compression system was chosen to be a value which remains within the bounds of the model. The effect of the compressor on the upstream duct flow (flow redistribution) extends about two to three compressor radii as shown in figure 4.1 (taken from reference 2). Similarly, it is assumed that a downstream duct length of two compressor radii is enough to uphold the assumption that there be only purely axisymmetric coupling between the plenum and the compressor/downstream flowfield. Therefore, the overall effective length (non-dimensionalised by mean compressor radii) of the compression system, including the compressor length (μr), should be a minimum of 6.0.

B.) The rotor inertia, λ, was defined to be approximately 0.25 per stage and the compressor inertia, μ, was defined to be 0.50 per stage since these are common values for a compressor. These inertia parameters are defined purely by blade geometry. There is no need to investigate the effect of compressor inertia on stability margin since it has been examined in references (6,7,9).

C.) The B parameter (see chapter 2 for definition) was chosen to be 1.0 in order to avoid resonant conditions. The resonant B parameter indicates when the natural system surge frequency matches the frequency of axisymmetric pressure perturbations due to disturbances travelling around the annulus passing in and out of the circumferentially spoiled sector (see reference 7).

4.2.2 Parameters of Investigation

The computations were established to assess the extent to which the following parameters of interest have on the compressor stability margin.

$$\text{unsteady effects} = F\{\text{axisymmetric performance, distortion magnitude}, B, \tau_r, \tau_s\}$$

where the subscripts "r" and "s" denote that which pertains to the rotor and the stator, respectively. The description here justifies the selection of the parameters to be investigated.

Calculations were made for a wide range of compressor characteristics to determine the effects of design reaction, design flow coefficient and the number of stages. These studies were conducted for a single stage compressor and a four stage compressor (which indicates whether the effects of unsteady losses and unsteady deviations on compressor performance and stability margin scale with the number of stages) given the design conditions: i.) low reaction, low flow coefficient; ii.) low reaction, high flow coefficient; iii.) high reaction, low flow coefficient; iv.) high reaction, high flow coefficient. This selection spans a wide range of compressor blade design parameters and determines the type of compressor (axisymmetric characteristic) where the unsteady effects considered are most important. The respective axisymmetric characteristics are presented in figure 4.2.

A series of calculations were made for both a flat characteristic and a steep characteristic where all parameters were held constant except the unsteady lag parameter, τ. The value for τ varied from 0.1 to 0.5 which covers a realistic range of values. The purpose here is to determine the effect of axial chord length on compressor performance and stability margin.

Inlet distortion was found to have a more adverse effect on compressors which have a steep axisymmetric characteristic. Therefore, a high curvature characteristic was used to determine the effect of the B parameter (for $\tau = 0.2$ and 0.5). This will indicate whether the type of system instability (stall or surge) has a large impact on the distorted pressure rise and stability margin.

Calculations were made using the high curvature characteristic for a range of distortion magnitudes in order to determine if the loss in compressor performance scales with the magnitude of the distortion. Each calculation was made for a single-lobed square wave distortion of 120 degrees extent (this was believed to be far from the critical sector angle). This type of distortion is of practical interest.

The parameter study considers all of the relevant parameters and has provided the grounds for quantitative insight into determining the effect of unsteady losses and unsteady deviations on stability prediction.

4.3 Unsteady Losses

4.3.1 Effective Lambda

It is apparent that an effective inertia model, as will be described here, can be devised for both unsteady losses and unsteady deviations. In chapter 2, we discussed the physical approximation used to estimate the lag of the instantaneous loss behind the steady state value. If the term on the left hand side of equation (2.12) is small, then the expression can be rewritten for a rotor in a steady, distorted flow

$$L_r = L_{r_{ss}} - \tau_r \frac{dL_{r_{ss}}}{d\phi} \frac{d\phi}{d\theta} \tag{4.1}$$

Upon substitution, we arrived at

$$\frac{\Delta Pt\text{-}s}{\rho U^2} = \psi_{id} - L_{r\,ss} - L_{sss} - \lambda_{eff}\frac{\partial \phi}{\partial \theta} \qquad (4.2)$$

where

$$\lambda_{eff} = \lambda - \tau_r \frac{dL_{rss}}{d\phi} \qquad (4.3)$$

Unsteady losses can effectively be modelled by adjusting the rotor inertia as defined above. As we shall see in the computed results, the effective inertia model is a useful one for small values of τ, typically not more than 0.2.

4.3.2 Clean Flow Stability Margin

For the original inertia model, it can be shown that the n^{th} harmonic modes become unstable at the peak of the characteristic for a compressor operating in a clean flow. On the negative sloped side of the performance characteristic, the compression system is in stable operation (9). Whereas, on the positive sloped side of the performance characteristic, the compression system is in unstable operation. The inclusion of unsteady losses have a small positive effect on clean flow compression system stability. The extent to which these effects delay instabilities to occur at a lower flow coefficient is dependent on the magnitude of the unsteady lag parameter, τ. For example, figure 4.3 presents the clean flow neutral stability points (τ=0.0 and τ=1.0) for the 3-stage c106 compressor (see reference 9 for further details concerning this compressor). Clearly, neutral stability moves to the left of the peak with increasing unsteady lag parameter. Therefore, it can be deduced that unsteady losses have the effect of

increasing the compressor inertia. For this reason, neutral stability occurs slightly to the left of the peak (positive slope). In essence, the lagging effects balance the destabilizing effect of a positive slope at this point. However, the impact on clean flow stability margin is nearly negligible for low speed compressors.

4.3.3 Distorted Flow Stability Margin

a.) Effect on Stability Prediction

The effect of unsteady losses on stability prediction for compressors of various design is illustrated in figures 4.4.a and 4.4.b. Presented in the figures is a measure in loss of performance (measured as the difference between the axisymmetric peak pressure rise and the distorted pressure rise at neutral stability normalised by the distortion magnitude) for eight different compressors (see figure 4.2) in a distorted flowfield (0.1 in magnitude covering a circumferential extent of 120°). In most cases, the unsteady loss model predicts the neutral stability to occur at a lower flow coefficient and a correspondingly higher distorted pressure rise (in comparison to the case where unsteady losses are neglected). In addition, these results tend to show that the inclusion of unsteady losses has a greater impact on performance for compressors of high design reaction (rotors are more highly loaded). These computed results also indicate the applicability of the use of an effective inertia model for the unsteady loss (see equation 4.3).

b.) Effect of Unsteady Loss Parameter

The effect of unsteady losses on stability predicion for compressors of various clean flow performance is shown in figure 4.5. Presented in the figure is a measure of loss in performance for two compressors, one with a steep clean flow characteristic and

the other with a rather flat characteristic. Unsteady losses have a stabilizing effect on system stability resulting in a lower loss in performance. Compressor instability occurs at a lower flow coefficient and a correspondingly higher distorted pressure rise. For a single-lobed distortion, unsteady losses stabilize the higher harmonic modes and hence, it is the first harmonic which dictates the system stability.

Further analysis of these results has indicated that under certain circumstances, a simpler unsteady loss model can be used, resulting in computational efficiency. For small unsteady loss parameter, τ, the effect on compressor performance can be simply modelled by an effective λ where λ represents the inertia of fluid in the rotors (based on geometry). Given in figure 4.5 is the prediction of loss in performance using an effective λ and clearly it accurately predicts stability for small τ. More importantly, the value of λ_{eff} appears to be increasing linearly with increasing τ (where the geometrical λ is 0.75), and shown is the linear correlation for each respective compressor. In summary, compression system stability can be predicted quite efficiently, with inclusion of unsteady losses, given the geometrical definition of the rotor inertia and the unsteady loss lag parameter, τ.

c.) Magnitude of Unsteady Lagging Effects in Rotor vs. Stator

The calculations presented here determine where in the compressor the inclusion of unsteady losses has a greater impact on compressor performance and stability margin. Figures 4.6.a and 4.6.b quantitatively show the effects of varying τ_r while holding τ_s constant and vice versa. Each figure contains the same information at two realistic ends of the B parameter spectrum, 0.1 (near resonance) and 1.0 (away from resonance). The horizontal curves in each figure illustrate no visible change in the pressure rise loss

parameter for a varying τ_s (0.1 - 0.5). On the contrary, a distinguishable change in pressure rise loss performance, similar to that of changing $\tau=\tau_r=\tau_s$, is observed. The degree of unsteady lagging in loss is largest in the rotors which is due to the spatial unsteadiness the rotor sees when passing through the distortion.

d.) Effect of Plenum Size

The influence of plenum size on stability prediction can be investigated by varying the B parameter. Shown in Figure 4.7 are the predictions of neutral stability made by the three models for the high curvature characteristic. For small τ, good agreement is achieved between the improved unsteady loss model and the simpler effective inertia model. On the contrary, for $\tau = 0.5$, the difference in modelling techniques is a mean value of 2% which is not nearly as good an agreement as for smaller values of τ. Also, it is evident that the variation of the B parameter over the range from 0.1 to 1.0 has little effect on distorted compressor performance (with and without the inclusion of unsteady losses in the flow model). Note, for each model, resonance between the compressor, distortion and plenum/duct occurs at the same point, $B_{res} \sim 0.3$.

e.) Effect of Distortion Magnitude

Figure 4.8 shows the effect of distortion magnitude on loss in performance (range of distortion magnitudes from 0.1 to 0.25) for the high curvature characteristic. The main effect is that, for a given set of inertia parameters, the difference in pressure rise loss parameters between the full unsteady loss model and the original inertia model remains nearly constant with varying distortion magnitude as long as τ is small. Again,

there is good agreement between the full unsteady loss model and the effective inertia model.

f.) Eigenmodes at Neutral Stability

If unsteady losses are neglected as in the original inertia model, all modes become unstable at neutral stability. Unsteady losses stabilize those modes of strongest harmonic content greater than the first. In other words, the first harmonic modes go unstable at neutral stability and at some lower flow coefficient the second harmonic modes become unstable followed by the third and so on. Figure 4.9 presents the eigenmodes at neutral stability where those indicated are predicted by the full unsteady loss model and the eigenmodes predicted by the original inertia model lie on the real axis. Simplifying the calculation by using the effective lambda approach predicts the mean flow performance similarly but does not predict the same eigenmodes at neutral stability. Now, these predictions hold for a single lobed distortion. On the contrary, if the distortion is two lobed, the second harmonic controls stability.

4.4 Unsteady Deviations

4.4.1 Effective Inertia

Similarly for unsteady deviations, it has become apparent that an effective inertia model can be derived to accurately predict the effects of unsteady deviations. If the term on the left hand side of equation (2.15) is small, then the expression can be rewritten for a rotor in a steady, distorted flow

$$\alpha_r = \alpha_{r_{ss}} - \tau_r \frac{d\alpha_{r_{ss}}}{d\phi} \frac{d\phi}{d\theta} \tag{4.4}$$

where α is the relative exit rotor angle. Therefore, for each rotor the effective inertia becomes

$$\lambda_{eff} = \lambda_{rotor} - \tau_r \frac{d\alpha_{r_{ss}}}{d\phi} \tan\bar{\alpha} \left(\bar{\phi}^2 + \bar{v}^2\right) \tag{4.5}$$

where the flow quantities are defined in the relative frame. Modelling unsteady deviations simply by increasing the inertia will result in computational efficiency. As will be shown later, this is an accurate approximation for values of τ typically lower than 0.3.

4.4.2 Clean Flow Stability Margin

The inclusion of unsteady deviations has a similar effect on clean flow stability as do the inclusion of unsteady losses. Neutral stability occurs to the left of the peak of the characteristic (positive slope). Therefore, unsteady deviations increase compressor clean flow stability margin.

4.4.3 Distorted Flow Stability Margin

a.) Effect on Stability Prediction

As in the case of unsteady losses, a similar parameter study was conducted with unsteady deviations (excluding unsteady losses) in order to isolate their effect on stability margin. The effect of unsteady deviations on stability prediction for compressors of various design conditions is shown in figures 4.10.a and 4.10.b. Clearly, unsteady deviations have a stabilizing effect on compression system stability and therefore a lower loss in distorted performance. As was seen with the inclusion of unsteady losses, compressor instability generally occurs at a lower flow coefficient and

corresponding higher pressure rise. Furthermore, the same effect on the system eigenmodes is observed as in figure 4.9. The same trends were observed for variation of B parameter, distortion magnitude, axisymmetric performance and unsteady lag parameter.

b.) Unsteady Losses versus Unsteady Deviations

Subsequently, calculations were carried out to quantitatively assess the difference that unsteady losses and unsteady deviations have on distorted compressor performance. Figure 4.11 presents a measure in loss of performance (of the 3-stage c106 subjected to a 0.1,120 degree circumferential distortion; see references 9, 10 and 11) as predicted by the inertia model with inclusion of (i) unsteady losses, (ii) unsteady deviations, and (iii) unsteady losses and unsteady deviations. Unsteady losses have a slightly greater positive impact on loss in performance with increasing unsteady lag parameter. More importantly, the effects of unsteady losses and unsteady deviations are additive. For example, given τ=0.6, the decrease of loss in performance for the three models is approximately 15%, 12% and 23%, respectively.

c.) Stability Prediction Using Effective Inertia to Account for Unsteady Deviations

Figure 4.12 illustrates the applicability of a simpler effective inertia model. For τ less than 0.5 the aggreement is very good. Similarly, as before, the effective rotor inertia increases linearly with increasing τ ($\lambda_{eff} = \{0.87\tau+1\}\lambda$). Consequently, for small τ (less than 0.5), a simple effective inertia model can be used to determine distorted compressor performance and stability margin accurately for both the inclusion of unsteady losses and unsteady deviations.

4.5 Circumferentially Non-uniform Compressor Exit Static Pressure Field

In the work of Hynes, Greitzer and Longley, it was assumed that the flow leaving the compressor exit stator was parallel and axial for a steady distorted flow. As a result of a circumferentially uniform exit flow angle, it follows that the static pressure is also circumferentially uniform. The current effort relaxes this assumption by allowing for a circumferentially non-uniform compressor exit static pressure field and the existence of mean bulk swirl in the downstream duct. Calculations were conducted to determine to what extent this assumption affects compressor performance and stability margin.

The performance at neutral stability of the c106 3-stage low-speed compressor (see references 9, 10 and 11) when subjected to a 0.1 magnitude 120° circumferential extent distortion was evaluated. It was determined that relieving the aforementioned assumption has negligible effect on compressor performance and stability margin. The difference in prediction was less than 1% in both distorted pressure rise and stability margin. The compressor exit flow angle showed a circumferential varition of as much as 5° and the static pressure variation about the mean was approximately 0.02 (static pressure non-dimensionalised by ρU^2). As a result, the assumption made in the work of Hynes, Greitzer and Longley is valid, and more importantly, reduces the complexity of the downstream duct model.

4.6 Summary of Results/Conclusions

4.6.1 An Explanation

The inclusion of unsteady losses and deviations results in the introduction of a temporal and a spatial unsteady correction for the rotor blades, and a temporal unsteady correction for the stator blades. It has been shown that the spatial unsteady correction

for the rotor blades is clearly the dominant effect. Therefore, in a steady distorted flow, the length scale which characterizes the distortion is the spoiled sector width (which is of the order of the mean compressor radii), and the corresponding time scale is of the order of the ratio of the mean compressor radii to the blade speed (r/U). Originally, it was assumed that the blade exit flow quantities (loss, deviation) respond instantaneously to changes in incidence. Large changes in incidence occur during the time characterized by r/U. Therefore, the blade exit and hence the downstream blade rows 'see' the entire extent of the spoiled sector (low flow region of the inlet disturbance). Inclusion of unsteady losses and deviations account for the time-lagging behavior of the blade boundary layer. These effects introduce a new time scale (of order convection time, $\frac{b_x}{c_x}$). The adoption of this time scale in the flow model causes a delay in the compressor response (which occurs in reality) to large changes in incidence and thus, for a blade row, the blade exit quantities only 'see' a certain reduced extent of the incoming flow disturbance. Obviously, as the convection time scale is increased (by increasing τ) towards the order of r/U, the extent to which the incoming flow disturbance adversely affects blade performance is reduced. Therefore, unsteady losses and deviations enhance compressor performance and stability margin.

4.6.2 Summary

Effects of Unsteady Losses and Unsteady Deviations on Compressor Performance and Stability Margin

(i) Compressor instabilities generally occur at a higher distorted pressure rise and corresponding lower flow coefficient.

(ii) Unsteady losses and deviations stabilize eigenmodes of strongest harmonic content greater than the first harmonic. Therefore, when subjected to a single-lobed distortion, the first harmonic goes unstable first, followed by the second, the third, etc.

(iii) The inclusion of unsteady losses and deviations has the effect of increasing compressor inertia. Subsequently, an effective rotor inertia can be defined for both unsteady losses and deviations. For small τ, the effective inertia model accurately predicts instability and the respective distorted performance when compared to the predictions made by the full unsteady loss/deviation model.

(iv) The individual effects of unsteady losses and deviations on compressor performance and stability margin are additive.

Effect of Circumferentially Non-uniform Compressor Exit Static Pressure Field on Compressor Performance and Stability Margin

(i) The non-uniformity in static pressure at compressor exit has a negligible effect on distorted pressure rise near the onset of system instability (< 1%).

(ii) Likewise, its influence on stability margin (measured in terms of flow coefficient) is negligible (< 1%)

Chapter 5

Swirl Sensitive Compressors

5.1 Introduction

In the previous models developed by Hynes, Greitzer and Longley, the IGVs were modelled as 'perfect' (i.e. exit flow angle of IGVs is independent of incidence). However, the magnitude and circumferential extent of a total pressure distortion can create large variations in the swirl angle at the inlet to the IGVs. As a result, the blade incidence may be quite high, hence, possibly resulting in flow separation. This physical effect may have a serious impact on compressor performance and stability margin.

The purpose of this chapter is to assess the general effects of variations of inlet swirl on compressor performance and stability margin; we will refer to this as a swirl sensitivity study. Swirl sensitivity is simply accounted for by modelling the IGV blade passage in a similar fashion as was done for the stators. Howell's correlations for blade deflection and loss coefficient were used to define the respective steady state flow quantities as a function of incidence. The following section presents the effect of swirl sensitivity on mean flow quantities and the justification for the model and the flow

phenomena observed. Computed results will be shown to elucidate its effect on stability.

5.2 C106 3-Stage Compressor

5.2.1 Effect of Swirl Sensitivity on Mean Flow Quantities

Calculations were performed using the c106 3-stage compressor since it was convenient for comparison purposes. Flowfield measurements of the c106 3-stage compressor subjected to a 0.2 magnitude, 120 degree circumferential total pressure distortion were made by Longley (9,11). The calculations to be presented here pertain to the c106 compressor when subjected to a 0.1 magnitude, 120 degree circumferential total pressure distortion. Shown in figure 5.1 is the axisymmetric characteristic predicted by theory when compared to measured data by Longley. The flow coefficient profile at the compressor inlet face is given in figure 5.2. The low flow region (circumferential location of 250°) indicates separated IGVs. Furthermore, there is very good agreement between that which is predicted and the flow data measured by Longley (presented within the caption). Figure 5.3 presents the relative IGV inlet and exit flow angles. Clearly, the inlet swirl variations range from -20 to 15 degrees. Due to the extremely high incidence on the IGVs at approximately the 230 degree circumferential location, there is a large change in the IGV exit flow angle which for the most part is constant elsewhere (similarly, there is good agreement between theory and measurement). Figure 5.4 illustrates the fundamental difference between the swirl sensitive IGV model and the 'perfect' IGV model predictions of the loss. The loss is constant circumferentially for the 'perfect' IGV model. On the other hand, within the region of negative swirl, the total pressure loss through the (swirl sensitive) IGVs is of order of one mean dynamic head as shown in figure 5.4. For the same variation in inlet

swirl, this magnitude in blade loss was also observed in the experimental measurements. In figure 5.5, the static pressure profiles at IGV inlet and exit as well as at the remaining stator exit reflect the presence of the large loss spike through the IGVs. The incidence on the IGVs is high enough to cause flow separation, hence, accounting for the large loss. The large variations in IGV pressure loss and exit blade deviation suggests that the c106 compressor is swirl sensitive. The relative air angle of the flow at the inlet plane of the first rotor blade row is shown in figure 5.6. As before, higher flow incidence is observed at a circumferential location where large losses are predicted. This leads to higher rotor blade loading; and hence greater rotor turning as illustrated in figure 5.7. Overall, it was observed that compressor with swirl sensitivity degrades performance. Although there is a greater ideal pressure rise due to increased turning, it is outweighed by the significant increase in total pressure loss. For the c106 3-stage compressor, inclusion of swirl sensitivity in the model predicitons causes a decrease in performance (distorted pressure rise) of 1.1% and a decrease in stability margin of 6.4%.

The correspondence between theory and experiment (measurements by Longley, see reference 9) is extremely good besides the difference in distortion magnitude (factor of two). This might possibly be a result of the exclusion of unsteady losses, unsteady deviations and inter blade row gaps. The key point is that the IGV model responds to variations in inlet swirl and flow coefficient in identically the same fashion as in experiment.

In summary, the results from mean flow calculations have shown that inclusion of swirl sensitivity causes an increase in rotor turning and a significant increase in total pressure loss through the inlet guide vanes in the region of negative swirl (negative sign convention arises from measuring angle in direction opposite rotor direction). More

importantly the model accurately captures the fundamental fluid dynamic effects associated with the response of a blade row to inlet swirl variations.

5.2.2 Stability of Swirl Sensitive Compressors

Calculations have also been performed to assess the significance of compressor swirl sensitivity on stability margin. These predictions indicate that inlet swirl sensitivity has a destabilizing influence on compressor performance. The results presented in figures 5.8 and 5.9 show the effects of unsteady deviations on the stability of a compressor which is swirl sensitive. The results shown in figures 5.8 and 5.9 correspond to B parameter values of 1.0 (away from resonance) and 0.1 (near resonance), respectively. Shown in each figure is a measure of increase in stability margin (difference between the mean flow coefficient corresponding to modelling without inclusion of unsteady deviations and the mean flow coefficient corresponding to the modelling with the inclusion of unsteady deviations normalized by the flow coefficient, $\bar{\phi}(\tau=0)$, i.e. $\frac{\bar{\phi}(\tau=0) - \bar{\phi}(\tau)}{\bar{\phi}(\tau=0)}$). For an unsteady lag parameter τ greater than 0.6 (IGVs are modelled as swirl sensitive), an increase in stability margin of 4% is observed for the case with B=0.1 and an increase in stability margin of 6% in the case with B=1.0. On the contrary, only about a 1% to 2.5% increase in stability margin is noted for a compressor with 'perfect' IGVs. Hence, inclusion of unsteady deviations appears to have a greater impact on stability margin of swirl sensitive compressors.

This is more apparent when considering the circumferential gradients in the flow quantities involved. For example, figure 5.10 presents the steady state relative total pressure loss profile (steady distorted flow) for the 3-stage c106 compressor when subjected to a 0.1 magnitude, 120 degree square wave distortion (the steady state

relative total pressure was the flow quantity chosen because the large loss spike, as well as the associated large circumferential gradient in loss, in the region of negative swirl has been shown previously to be responsible for the observed degradation in performance and stability margin). The two profiles correspond to the 'perfect' IGV and swirl sensitive IGV modelling techniques. Clearly, the peak total pressure loss for the compressor with swirl sensitive IGVs is nearly double that of the compressor modelled with 'perfect' IGVs. The region of negative swirl (high blade incidence) occurs over the circumferential extent from about 220 to about 250 degrees. Within this region, the maximum gradient of the steady state loss, $\left(\frac{\Delta L}{\Delta \theta}\right)$, for the compressor with swirl sensitive IGVs is approximately five times greater than that for the compressor with 'perfect' IGVs. As the rotor passes through this region of high incidence, the lag in the response of the blade exit flow quantities to the changes at the blade inlet will mitigate the subsequent large increase in blade loss due to the flowfield in the high incidence region. Therefore, in these situations, unsteady lagging effects will be expected to have a greater impact on the stability margin.

5.3 Summary of Results

The following key points have resulted from the inclusion of swirl sensitivity in the flow modelling for compressors:

(i) For swirl sensitive IGVs, an increase in rotor turning occurs and a large loss spike of order one mean dynamic head is observed due to flow separation at where the blade incidence is high (region of negative inlet swirl).

(ii) Swirl sensitivity has a destabilizing effect on compression system stability.

(iii) Inclusion of unsteady deviations (as well as unsteady losses) appear to have a greater impact on the stability margin of compressors which are sensitive to swirl.

Chapter 6

Compressor Flow Model with Finite Blade Row Gaps

6.1 Introduction

The investigations undertaken here concern the inclusion of inter blade row gaps within the compressor model (see chapter 2). In the work of Hynes, Greitzer and Longley, the gap between successive blade rows is assumed to be negligible (i.e., flow quantities leaving a blade row are exactly equivalent to the flow quantities entering the following blade row). This assumption is relieved here in order to assess the importance of including this effect within the flow model. Specifically, it is of interest to determine the effect of the presence of blade row gaps on the flowfield redistribution of incoming distorted flow within the compressor, as well as on compression system performance / stability.

6.2 Computational Complexity

The difficulty encountered during computation is simply that the matrix that relates the flow quantities across the gap becomes ill-conditioned (refer to chapter 2).

Exponential terms are involved (e^n, e^{-n}) and for high harmonic numbers, one column goes to infinity and another goes to zero (i.e., for n=4, matrix column elements differ by three orders in magnitude). Two methods have been employed to get around this problem. The first of which was to reduce the harmonic content used in describing the meanflow quantities. The second method involves expanding the exponential terms in Taylor series and dropping the terms of second order and higher in gap size. However, these approaches would compromise the accuracy of the solution to a certain extent. Therefore, it is important to point out that our primary interest is to establish the general trends associated with the inclusion of gaps. The effort has been directed at arriving at a general statement concerning the effect of the presence of inter blade row gaps on distorted compressor performance and stability margin.

6.3 Inter Blade Row Gaps

6.3.1 Effect of the Presence of Gaps on Flowfield Redistribution of Incoming Flow Disturbance Upstream of Compressor

The extent to which the presence of inter blade row gaps affect the redistribution of flow upstream of the compressor is first considered. Calculations were carried out for a single stage compressor (identical to the 1st stage of the c106 3-stage compressor). The compressor stage is subjected to a 0.025 magnitude, 120° circumferential extent total pressure distortion far upstream at the duct inlet. The temporally mean flowfield is calculated for an operating point near neutral stability. The two cases considered are: (i) a single stage with no inter blade row gaps, and (ii) a single stage with 15% inter blade row gaps (non-dimensionalised by compressor mean radius). As shown in figure 6.1, the flow coefficient profiles at the inlet face to the compressor (IGV inlet) appear to indicate further flow redistribution upstream of the compressor. The low flow region is

accelerated to a greater extent by approximately 1-2%; the corresponding static pressure fields established by the compressor at the compressor inlet face is shown in figure 6.2. The static pressure and flow coefficient appear to be consistent with one another. The total pressure distortion at the compressor inlet face is the same for both cases.

6.3.2 Flowfield Redistribution Between Blade Rows

Due to the presence of the inter blade row gap, there exists the possibility for further redistribution of the flow coefficient non-uniformity between the blade rows. It is of interest to establish the amount of flowfield redistribution which takes place between blade rows and to determine whether there is an overall attenuation or growth of the flow non-uniformity through the compressor. The following will attempt to address these issues.

Meanflow calculations were performed for the first stage of the c106 3-stage compressor (see reference 9). The response of this single stage (with 15% mean compressor radius gaps) to the same distortion as before (0.025 magnitude 120° circumferential extent distortion) at an operating point near the onset of instability was examined. Figure 6.3 shows the evolution of the flow coefficient profile through the compressor. There is a slight adjustment in the flow; however, this appears to be minimal. The flow tends to decelerate in the low flow region (circumferential location of 250°) and accelerate in the high flow region (circumferential location of 120°). The modal amplitudes (1st and 2nd harmonics) of the flow coefficient tend to grow upon entering the rotor and decay upon entering the stator. This redistribution of the flow coefficient is consistent with the respective variations (circumferential and axial) in static pressure as shown in figures 6.4.a and 6.4.b. The flow redistribution is a result of the fluid resistance which the flow encounters when entering the downstream blade

row. Figure 6.5 presents the total pressure profile at IGV exit and rotor inlet. The total pressure non-uniformity simply advects with the mean flow which agrees with the gap flow model (see chapter 2).

Further calculations indicated that the trends in the flow redistribution are the same for the single stage compressor and three stage c106 compressor and therefore is believed to depend weakly upon the number of stages.

6.4 Effect of Gaps on Compressor Performance and Stability Margin

As a result of the effect of the presence of the inter blade row gaps on the redistribution of the incoming flow disturbance, there is an increase in the distorted pressure rise near neutral stability. For various gap lengths (axial distance between blade rows non-dimensionalised by mean compressor radius), the change in the flow coefficient at neutral stability is negligible. The following table presents the respective percentage increase in distorted pressure rise for a c106 single stage compressor and a c106 3-stage compressor.

% Increase in Distorted Pressure Rise Near Neutral Stability

GAP LENGTH (% mean compressor radius)	1-stage compressor	3-stage compressor
0%	0.0%	0.0%
10%	0.3%	0.4%
15%	0.4%	0.4%

The percentage increase in distorted pressure rise is essentially negligible. Furthermore, the effect of gaps on distorted pressure rise appears not to be cummulative with the number of stages. In conclusion, the presence of inter blade row gaps has an extremely small effect on compressor performance and stability margin. Therefore, inclusion of gaps in low speed, high hub-to-tip ratio compressors can be ignored within the flow model for purposes of simplification.

6.5 Summary of the Effects of Inter Blade Row Gaps on Compressor Performance and Stability Margin

(i) The redistribution of the flow non-uniformity upstream of the compressor and between blade rows is negligible.

(ii) The presence of gaps increases the distorted pressure rise by less than 1% at an operating point near neutral stability.

Chapter 7

Conclusions

7.1 Summary

A theoretical model has been developed which correctly accounts for the following fluid dynamic effects intrinsic to compression system flowfields: unsteady losses, unsteady deviations, swirl sensitivity, non-uniform compressor exit static pressure field, and inter blade row flow redistribution. Computational implementation of this model has allowed for the individual investigation of the effect of these phenomena on compressor performance and stability margin. As a result, a more thorough appreciation of the two dimensional aspects of the problem has been established.

7.2 Conclusions

The following conclusions can be deduced from the computed results based on the present flow model:

I) *Unsteady losses and unsteady deviations.*

(i) Compressor instabilities generally occur at a higher distorted pressure rise and corresponding lower flow coefficient.

(ii) Unsteady losses and deviations stabilize eigenmodes of strongest harmonic content greater than the first harmonic. Therefore, when subjected to a single-lobed distortion, the first harmonic goes unstable first, followed by the second, the third, etc.

(iii) The inclusion of unsteady losses and unsteady deviations has the effect of increasing compressor inertia. Subsequently, an effective rotor inertia can be defined for both unsteady losses and deviations. For small τ, the effective inertia model accurately predicts instability and the respective distorted performance when compared to the predictions made by the full unsteady loss/deviation model.

(iv) The individual effects of unsteady losses and deviations on compressor performance and stability margin are additive.

II) *Non-uniform compressor exit static pressure field*

(i) The non-uniformity in compressor exit static pressure has a negligible effect on compressor performance and stability margin.

III) *Swirl sensitivity*

(i) For swirl sensitive IGVs, an increase in rotor turning occurs and a large loss spike of order one mean dynamic head is observed due to flow separation where the blade incidence is high (region of negative inlet swirl).

(ii) Swirl sensitivity has a destabilizing effect on compression system stability.

(iii) Inclusion of unsteady deviations (as well as unsteady losses) appear to have a greater impact on the stability margin of compressors which are sensitive to swirl.

IV) *Inter blade row gaps*

(i) The presence of inter blade row gaps has negligible impact on the redistribution of flow both upstream of the compressor inlet and between blade rows.

(ii) Near neutral stability, inter blade row gaps slightly improve the performance of a compressor (less than 1%). The effect on stability margin is negligible.

7.3 Recommendations for Future Work

In recent years, there has been a revival of the interest in VSTOL aircraft development. In near-ground operation (takeoff/landing) the engines of VSTOL aircraft experience complex flowfield distortions, involving total pressure and total temperature non-uniformities. These distortions have large radial and circumferential extent, and hence are usually three dimensional. The source of the distorted flow is primarily due to the re-ingestion of hot exhaust gas due to the arrangement of engine intake and lift nozzles. The result of highly distorted inlet flowfields is loss in compressor stability as well as loss in engine performance.

Therefore, future work should consist of developing a model/computational technique for addressing the compressor's response to a three dimensional distorted flowfield at low Mach numbers. Due to the success of the current two dimensional modelling technique, it would be sensible to extend this model to three dimensions. This will require developing a blade model which includes flow effects which are intrinsically three dimensional (e.g. radial diffusion, stream surface twisting). Further attention must be directed towards determining the coupling of the blade row model and the other components of the compression system. Then, a method of stability assessment must be established. It should then be the purpose of the future work to provide the capability for predicting the performance, the stability and the transient response of a compressor when subjected to a three dimensional inlet distortion. The development of such a model/computational technique will constitute a major advancement in the evaluation of aero-compressor distortion tolerance.

References

1 Reid, C., "The Response of Axial Flow Compressors to Intake Flow Distortion," ASME Paper #69-GT-29, March (1969).

2 Greitzer, E. M. "Inlet Distortion in Axial Compressors," Gas Turbine Laboratory, MIT.

3 Stenning, A. H., "Inlet Distortion Effects in Axial Compressors," Chapter 14 in ASME Lecture Series on Fluid Mechanics of Turbomachinery, Iowa State Univ., August (1973).

4 Mazzawy, R. S., "Multiple Segment Parallel Compressor Model for Circumferential Flow Distortion," ASME Journal of Engineering for Power, Vol. 99, Apr. 1977, pp.228-246.

5 Moore, F. K., "A Theory of Rotating Stall of Multistage Compressors, Parts I-III," ASME Journal of Engineering for Gas Turbines and Power, Vol. 106, 1984, pp. 313-336.

6 Hynes, T. P. and Greitzer, E. M., "A Method for Assessing Effects of Inlet Flow Distortion on Compressor Stability," ASME Journal of Turbomachinery, Vol. 109, 1989, pp. 371-379.

7 Chue, R., T. P. Hynes, E. M. Greitzer, C. S. Tan, and J. P. Longley, "Calculations of Inlet Distortion Induced Compressor Flow Field Instability," International Journal of Heat and Fluid Flow, Vol. 10, No. 3, Sept. 1989, pp. 211-223.

8 Adamczyk, J. J., "Unsteady Fluid Dynamic Response of an Isolated Rotor with Distorted Inflow", AIAA Paper No. 74-49, AIAA 12th Aerospace Sciences Meeting, Washington, D.C.,January 30 - February 1, 1974.

9 Longley, J. P., "Inlet Distortion and Compressor Stability," Ph.D. Dissertation, Cambridge University Engineering Department, 1988.

10 Longley, J. P. and Hynes, T. P., "Stability of Flow Through Multistage Axial Compressors", ASME #89-GT-311.

11 Longley, J. P., "Measured and Predicted Effects of Inlet Distortion on Axial Compressors", ASME # 90-GT-214.

12 Nagano, S., Y. Machida, and H. Takata, "Dynamic Performance of Stalled Blade Rows," Japan Society of Mechanical Engineers Paper #JSME 11, presented at Tokyo Joint International Gas Turbine Conference, 1971, pp. 73-80.

13.Horlock, J.H., Axial Flow Compressors, Butterworths Scientific Publications, London, England, 1958.

14 Greitzer, E. M., "The Stability of Pumping Systems - The 1980 Freeman Scholar Lecture", Journal of Fluids Engineering, Vol. 103, June 1981, pp. 193-242.

15.Krall, N. A. and A. W. Trivelpiece, Principle of Plasma Physics, McGraw-Hill, Inc., 1973.

16 Dahlquist, Germund and Ake Bjorck, Numerical Methods, Prentice-Hall series in automatic computation, Englewood Cliffs, New Jersey, 1969.

Appendix I : Steady State Clean Flow Performance

The overall steady state clean flow performance for a compressor is simply determined by summing individual blade performance. Steady state individual blade performance is defined by the sum of the ideal pressure rise and the blade loss. It is assumed that the ideal pressure rise is a function of the flow coefficient, the relative inlet air angle and the relative exit air angle. The relative exit air angle is defined to be purely a function of incidence. Similarly, it is assumed that the blade loss is a function of the flow coefficient and incidence Therefore, given the blade incidence and the flow coefficient, it is necessary to use an empirical correlation to determine the steady state blade deflection (or relative exit air angle) and the steady state blade loss. Howell's deflection / loss correlations (13), presented in figure 2.5, are employed in order to account for steady state deviation and loss. This requires the specification of the design relative inlet and exit air angles for each blade row and the design blade loss coefficient.

The validity of this steady state clean flow performance model was evaluated by comparing it to measured axisymmetric characteristics. Design conditions were specified from the active control single stage compressor at MIT, Dr. J.P. Longley's C106 3-stage build, and Dr. I.J. Day's C106 4-stage build (the latter two compressors are at the Whittle Laboratory in Cambridge, England). The model compares reasonably well with these characteristics as shown in figure A1.1.

Appendix II : Analytic Solution to 2-D Incompressible Euler Flowfield (non-axial mean flow)

The upstream and downstream flowfields are modelled as 2-D inviscid incompressible flows. As in the Hynes-Greitzer model, the solution to the flowfield is obtained by linearising the Euler equations. The present derivation is similar to that of Longley but includes the existence of mean bulk swirl. Thus, a circumferentially unrolled piece of the flowfield is shown in the figure below:

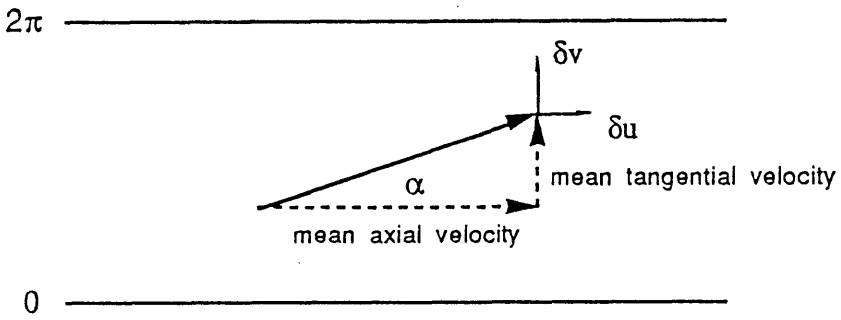

The governing equations in the analysis are

continuity: $$\frac{\partial u}{\partial x} + \frac{1}{r}\frac{\partial v}{\partial \theta} = 0 \qquad \text{(A2.1)}$$

momentum: $$\frac{\partial \hat{u}}{\partial t} + (\hat{u}\cdot\nabla)\hat{u} = -\frac{1}{\rho}\nabla P_s \qquad \text{(A2.2)}$$

identity: $$(\nabla x \hat{u}) x \hat{u} = (\hat{u}\cdot\nabla)\hat{u} - \nabla\left(\frac{1}{2}\,\hat{u}^2\right) \qquad \text{(A2.3)}$$

vorticity: $$\hat{\omega} = \nabla x \hat{u} \qquad \text{(A2.4)}$$

total pressure: $$P_t = P_s + \frac{1}{2}\rho V^2 \qquad \text{(A2.5)}$$

where $V^2=u^2 + v^2$.

Substitute equation (A2.3) into (A2.2). This gives

$$\frac{\partial \hat{u}}{\partial t} + (\nabla x \hat{u}) x \hat{u} + \nabla\left(\frac{1}{2}\,\hat{u}^2\right) = -\frac{1}{\rho}\nabla P_s \qquad \text{(A2.6)}$$

Using the definition of the total pressure and vorticity,

$$\frac{\partial \hat{u}}{\partial t} + \hat{\omega} x \hat{u} = -\frac{1}{\rho}\nabla P_t \qquad \text{(A2.7)}$$

Take the curl of equation (A2.7).

$$\frac{\partial \hat{\omega}}{\partial t} + \nabla x(\hat{\omega} x \hat{u}) = 0 \qquad \text{(A2.8)}$$

For a 2-D flowfield,

$$\hat{u} = (u,v,0)\ ,\ \hat{\omega} = (0,0,\xi)$$

Hence, in the radial direciton

$$\frac{\partial \xi}{\partial t} + \frac{\partial (u\xi)}{\partial x} + \frac{1}{r}\frac{\partial (v\xi)}{\partial \theta} = 0 \qquad \text{(A2.9)}$$

Define the stream function

$$u = \frac{1}{r}\frac{\partial \psi}{\partial \theta} \quad \text{and} \quad v = -\frac{\partial \psi}{\partial x} \tag{A2.10}$$

Then, by definition, this gives

$$\nabla^2 \psi = -\xi \tag{A2.11}$$

Substitute (A2.11) into (A2.9)

$$\frac{\partial}{\partial t}\left(\nabla^2 \psi\right) + u\frac{\partial}{\partial x}\left(\nabla^2 \psi\right) + \frac{v}{r}\frac{\partial}{\partial \theta}\left(\nabla^2 \psi\right) = 0 \tag{A2.12}$$

The stream function must have the form

$$\psi = r\bar{u}\theta - \bar{v}x$$

For small disturbances, $\psi = \bar{\psi} + \delta\psi$

$$\left(\frac{\partial}{\partial t} + \bar{u}\frac{\partial}{\partial x} + \frac{\bar{v}}{r}\frac{\partial}{\partial \theta}\right)\left(\nabla^2 \delta\psi\right) = 0 \tag{A2.13}$$

Clearly, from (A2.13), there exists a vortical mode which convects with the mean flow and two potential modes which describe the decay/growth of disturbances axially.

The solution has the form

$$\nabla^2 \delta\psi = f(t+kx\,,\,\theta) \tag{A2.14}$$

Using Fourier representation, the solution may be written as

$$\nabla^2\delta\psi = \sum_{n=-\infty}^{\infty} a_n e^{in\theta+kx+i\omega t} \qquad \text{(A2.15)}$$

where

$$i\omega+k\bar{u}+in\frac{\bar{v}}{r} = 0$$

Therefore,

$$k = -\frac{i}{r}\left(n\tan\bar{\alpha} + \frac{r\omega}{\bar{u}}\right)$$

The solution to (A2.13) is simply the sum of the homogeneous solution ($\nabla^2\delta\psi = 0$) and the particular solution determined by integrating (A2.15).

$$\delta\psi = \sum_{n=-\infty}^{\infty} -\frac{a_n}{\vartheta} e^{in\theta+i\beta_n x/r+i\omega t} \qquad \text{(A2.15)}$$

$$+ \sum_{\substack{n=-\infty \\ n\neq 0}}^{\infty} b_n e^{in\theta-|n|x/r+i\omega t}$$

$$+ \sum_{\substack{n=-\infty \\ n\neq 0}}^{\infty} c_n e^{in\theta+|n|x/r+i\omega t}$$

$$+\left(\zeta_1\theta + \zeta_2 x + \zeta_3 x\theta + \zeta_4\right) e^{i\omega t}$$

where

$$\vartheta = \beta_n{}^2+\frac{n^2}{r^2} \text{ and } \beta_n = \tan\bar{\alpha} + \frac{r\omega}{n\bar{u}}$$

The fourth term arises from the integration of (A2.15). The ζ_1 and ζ_2 terms represent the temporal decay/growth of the zeroth harmonic in the axial and circumferential directions. The ζ_3 may be ignored since it has no physical meaning. The constant, ζ_4, may be ignored since it does not affect the definition of the stream function.

Rewrite the Fourier coefficients to obtain a most general unsteady perturbation

$$\delta\psi = \sum_{\substack{n=-\infty \\ n\neq 0}}^{\infty} \frac{-ir\bar{u}}{n} A_n \, e^{in\theta + i\beta_n x/r + i\omega t}$$

$$+ \sum_{\substack{n=-\infty \\ n\neq 0}}^{\infty} \frac{-ir\bar{u}}{n} B_n e^{in\theta - |n|x/r + i\omega t}$$

$$+ \sum_{\substack{n=-\infty \\ n\neq 0}}^{\infty} \frac{-ir\bar{u}}{n} C_n e^{in\theta + |n|x/r + i\omega t}$$

$$+\left(r\bar{u}A_n \, e^{-i\omega x/u + i\omega t} + r\bar{u}\zeta_1'\theta - \bar{u}\zeta_2'x\right) e^{i\omega t} \qquad \text{(A2.16)}$$

Now, by linearising (A2.2, A2.5, A2.10), the perturbations in axial velocity, tangential velocity, static pressure and total pressure may be determined. These flow perturbations are then simply defined by

$$\begin{bmatrix} \frac{\delta u}{\bar{u}} \\ \frac{\delta v}{\bar{u}} \\ \frac{\delta P_s}{\rho \bar{u}^2} \end{bmatrix} = \begin{bmatrix} 0 & 1 & 0 \\ \frac{i\omega r}{\bar{u}} & 0 & 1 \\ 0 & -\frac{i\omega x}{\bar{u}} - 1 & 0 \end{bmatrix} \begin{bmatrix} A_0 \, e^{-i\omega x/\bar{u} + i\omega t} \\ B_0 \, e^{i\omega t} \\ C_0 \, e^{i\omega t} \end{bmatrix}$$

$$+ \sum_{\substack{n=-\infty \\ n\neq 0}}^{\infty} \begin{bmatrix} 1 & 1 & 1 \\ \beta_n & \frac{i|n|}{n} & \frac{i|n|}{n} \\ 0 & \frac{in}{|n|}\beta_n - 1 & -\frac{in}{|n|}\beta_n - 1 \end{bmatrix} \begin{bmatrix} A_n \, e^{in\theta - in\beta_n x/r + i\omega t} \\ B_n e^{in\theta - |n|x/r + i\omega t} \\ C_n e^{in\theta + |n|x/r + i\omega t} \end{bmatrix}$$

(A2.17)

Apendix III : Stability Calculation

The purpose of this appendix is to describe the method of stability assessment. The problem of stability assessment was addressed by Hynes, Greitzer, and Longley (6,7,9). The following presents the governing linearised set of equations which determine the compression system stability.

The flow model considered here is that of Hynes-Greitzer (6) with the inclusion of unsteady losses (which results in a differing set of equations when compered to the work presented by Longley (8)). Using the flow model as described in chapter 2, the following first order equations in $\tilde{\omega}$ are obtained (where b, a_n, c_n, d_n, e_n, f_n and g_n are the Fourier coefficients of the plenum static pressure perturbation, flow coefficient perturbation, ideal pressure rise slope, instantaneous rotor loss perturbation, instantaneous stator loss perturbation, the steady state rotor loss slope and the steady state stator loss slope, respectively).

'b' equation : plenum perturbation

$$\tilde{\omega} b = \frac{i}{4B^2 \eta T_\phi} - \frac{i}{4B^2 \eta} a_0 \qquad \text{(A3.1)}$$

'a' equations : flow perturbation

n=0 :
$$\tilde{\omega} a_0 = \frac{i}{\eta} b - \frac{i}{\eta} a_0 c_0 - \frac{i}{\eta} \sum_{\substack{s=-\infty \\ s\neq 0}}^{\infty} a_s c_{-s} + \frac{i}{\eta} d_0 + \frac{i}{\eta} e_0 \qquad \text{(A3.2)}$$

$n\neq 0$:

$$\tilde{\omega} a_n = -\frac{ic_0+n\lambda}{\left(\frac{2}{|n|}+\mu\right)} - \frac{i}{\left(\frac{2}{|n|}+\mu\right)} \sum_{\substack{s=-\infty \\ s\neq n}}^{\infty} a_s c_{n-s} + \frac{i}{\left(\frac{2}{|n|}+\mu\right)} (d_n+e_n) \qquad \text{(A3.3)}$$

'd' equations : rotor loss perturbation (steady state losses and unsteady losses)

$n=0$:

$$\tilde{\omega} d_0 = \frac{i}{\tau_r} d_0 - \frac{i}{\tau_r} a_0 f_0 - \frac{i}{\tau_r} \sum_{\substack{s=-\infty \\ s\neq 0}}^{\infty} a_s f_{-s} \qquad \text{(A3.4)}$$

$n\neq 0$:

$$\tilde{\omega} d_n = \frac{i}{\tau_r} (1+in\tau_r) d_n - \frac{i}{\tau_r} a_n f_0 - \frac{i}{\tau_r} \sum_{\substack{s=-\infty \\ s\neq n}}^{\infty} a_s f_{n-s} \qquad \text{(A3.5)}$$

'e' equations : stator loss perturbation (steady state losses and unsteady losses)

$n=0$:

$$\tilde{\omega} e_0 = \frac{i}{\tau_s} e_0 - \frac{i}{\tau_s} a_0 g_0 - \frac{i}{\tau_r} \sum_{\substack{s=-\infty \\ s\neq 0}}^{\infty} a_s g_{-s} \qquad \text{(A3.6)}$$

$n\neq 0$:

$$\tilde{\omega} e_n = \frac{i}{\tau_s} e_n - \frac{i}{\tau_s} a_n g_0 - \frac{i}{\tau_s} \sum_{\substack{s=-\infty \\ s\neq n}}^{\infty} a_s g_{n-s} \qquad \text{(A3.7)}$$

These equations can be written in the following form

$$\underline{\underline{A}}\, \underline{x} = \tilde{\omega}\, \underline{x} \qquad \text{(A3.8)}$$

This is a standard eigenvalue problem, therefore the eigenvalues can be easily obtained. The eigenvalues depict the growth rate of the unsteady perturbations within the system and hence determine stability. If the complex part of any eigenvalue is negative then the

compressor is unstable. Consequently, the solution to the eigenvalue problem is purely a fluid dynamic stability analysis.

Appendix IV : Description of Diagnostics

This appendix provides a brief description of some of the diagnostics used to determine the validity of the predictions made during a numerical calculation. Analytic expressions have been derived and evaluated to check the mean flow calculation and the stability calculation.

(a.) The first case is specifically for checking the mean flow calculation. Defining a linear ideal performance characteristic and a linear axisymmetric characteristic simplifies the compressor model equation because the respective characteristic slopes become constant. Therefore, for a given inlet distortion, the modal amplitudes of the flow coefficient profile at the inlet face to the compressor and their phase shifts relative to those of the total pressure distortion can be analytically determined. For a steady distorted flow, the total-to-static pressure rise is defined by

$$\frac{\Delta Pt\text{-}s}{\rho U^2} = \psi_{id} - L_r - L_s - \lambda \frac{\partial \phi}{\partial \theta} \qquad (A4.1)$$

This expression is considerably simplified by assuming the ideal and axisymmetric performance characteristics to be linear. For example, when including unsteady losses, the total-to-static pressure rise relation becomes

$$\frac{\Delta Pt\text{-}s}{\rho U^2} = (\bar{\psi}_{id} - \bar{L}_r - \bar{L}_s) + \frac{d\psi_{id}}{d\phi}(\phi-\bar{\phi}) - \frac{dL_r}{d\phi}(\phi-\bar{\phi}) - \frac{dL_s}{d\phi}(\phi-\bar{\phi}) - \lambda \frac{d\phi}{d\theta} \qquad (A4.2)$$

Using Fourier representation, the above relation becomes

n=0 :

$$\frac{1}{2}T\bar{\phi}^2 = \bar{\psi}_{id} - \bar{L}_r - \bar{L}_s = \bar{\psi}_A \qquad \text{(A4.3)}$$

For $n \neq 0$,

$$\sum_{\substack{n=-\infty \\ n\neq 0}}^{\infty} A_n e^{in\theta} = \sum_{\substack{n=-\infty \\ n\neq 0}}^{\infty} \left(\frac{d\psi_{id}}{d\phi} - \frac{dL_{rss}}{d\phi}\left(\frac{1}{1+in\tau_r}\right) - \frac{dL_{sss}}{d\phi} - in\lambda \right) B_n e^{in\theta} \qquad \text{(A4.4)}$$

where

A_n = Fourier coefficients of distortion

B_n = Fourier coefficients of flow coefficient

Therefore, for the n^{th} harmonic, equation (A4.4) can be rewritten as

$$B_n = \frac{A_n}{\left.\frac{d\psi_{id}}{d\phi}\right|_n - \left.\frac{dL_{rss}}{d\phi}\right|_n \left(\frac{1}{1+in\tau_r}\right) - \left.\frac{dL_{sss}}{d\phi}\right|_n - in\lambda} \qquad \text{(A4.5)}$$

The above equation was used to check the meanflow calculation when unsteady losses was considered. Similarly, this was done when unsteady deviations was considered.

(b.) A clean flow stability calculation can be performed analytically and used for comparison with the modes predicted by computation. Similar to the first case, the slopes of the ideal performance characteristic, the steady state rotor loss and the steady state stator loss are constant. In addition, the flow coefficient is obviously axisymmetric. Hence, for inclusion of unsteady losses, the eigenmodes are then defined by

'b' equation : plenum perturbation

$$\tilde{\omega} b = \frac{i}{4B^2\eta T\phi} - \frac{i}{4B^2\eta} a_0 \qquad \text{(A4.6)}$$

'a' equations: flow perturbation

n=0 : $$\tilde{\omega} a_0 = \frac{i}{\eta} b - \frac{i}{\eta} a_0 c_0 + \frac{i}{\eta} d_0 + \frac{i}{\eta} e_0 \qquad \text{(A4.7)}$$

n≠0 : $$\tilde{\omega} a_n = - \frac{ic_0 + n\lambda}{\left(\frac{2}{|n|} + \mu\right)} + \frac{i}{\left(\frac{2}{|n|} + \mu\right)} (d_n + e_n) \qquad \text{(A4.8)}$$

'd' equations : rotor loss perturbation (steady state losses and unsteady losses)

n=0 : $$\tilde{\omega} d_0 = \frac{i}{\tau_r} d_0 - \frac{i}{\tau_r} a_0 f_0 \qquad \text{(A4.9)}$$

n≠0 : $$\tilde{\omega} d_n = \frac{i}{\tau_r} (1 + in\tau_r) d_n - \frac{i}{\tau_r} a_n f_0 \qquad \text{(A4.10)}$$

'e' equations: stator loss perturbation (steady state losses and unsteady losses)

n=0 : $$\tilde{\omega} e_0 = \frac{i}{\tau_s} e_0 - \frac{i}{\tau_s} a_0 g_0 \qquad \text{(A4.11)}$$

n≠0 : $$\tilde{\omega} e_n = \frac{i}{\tau_s} e_n - \frac{i}{\tau_s} a_n g_0 \qquad \text{(A4.12)}$$

Therefore, four modes will be of the zeroth harmonic and there will be three modes per n^{th} harmonic.

For n=0,

$$a\,\tilde{\omega}^4 + b\,\tilde{\omega}^3 + c\,\tilde{\omega}^2 + d\,\tilde{\omega} + e = 0 \qquad \text{(A4.13)}$$

where

$$a = 4B^2\eta^2 T\phi\tau_r\tau_s$$

$$b = -\,i\eta\tau_r\tau_s - i4B^2\eta^2 T\phi(\tau_r+\tau_s) + ic_0 4B^2\eta T\phi\tau_r\tau_s$$

$$c = -\,\eta(\tau_r+\tau_s) - 4B^2\eta^2 T\phi - T\phi\tau_r\tau_s + c_0\tau_r\tau_s + 4B^2\eta T\phi((\tau_r+\tau_s)c_0 - \tau_s f_0 - \tau_r g_0)$$

$$d = i\eta + T\phi(\tau_r+\tau_s) - i(\tau_r+\tau_s)c_0 - i4B^2\eta T\phi(c_0 - f_0 - g_0) - T\phi\tau_r\tau_s + if_0\tau_s + ig_0\tau_r$$

$$e = T\phi - c_0 + f_0 + g_0$$

For $n \neq 0$,

$$a\,\tilde{\omega}^3 + b\,\tilde{\omega}^2 + c\,\tilde{\omega} + d = 0 \qquad \text{(A4.14)}$$

where

$$a = \left(\frac{2}{|n|} + \mu\right)\tau_r\tau_s$$

$$b = -\left(\frac{2}{|n|} + \mu\right)\eta\tau_r\tau_s - \eta\lambda\tau_r\tau_s + i\left(\frac{2}{|n|} + \mu\right)(\tau_r+\tau_s) - i\tau_r\tau_s c_0$$

$$c = \left(\frac{2}{|n|} + \mu\right) - (\tau_r+\tau_s)c_0 - \eta\lambda^2\tau_r\tau_s + f_0\tau_s + g_0\tau_r + i\left(\frac{2}{|n|} + \mu\right)n\tau_r - inc_0\tau_r\tau_s + in\lambda\tau_s + in\lambda\tau_r$$

$$d = -n\tau_r c_0 - n\lambda + n\tau_r g_0 + in^2\lambda\tau_r + ic_0 - if_0 - ig_0$$

Solving these 3rd and 4th order equations gives the eigenmodes for a clean flow through a compressor.

(c.) The mean flow calculation and stability calculation can be checked by the following means. Assume a single-lobed distortion of given magnitude ($\Delta Pt/\rho U^2$) has a spoiled sector of θ degrees circumferential extent. The total-to-static pressure rise for an unsteady distorted flow is given by equation (2.13). Now, for an m-lobed distortion of equivalent magnitude

$$\theta' = \frac{\theta}{m} \tag{A4.15}$$

the corresponding total-to-static pressure rise

$$\frac{\Delta Pt\text{-}s}{\rho U^2} = \psi_{id}(\phi(\frac{\theta}{m})) - L_{r_{ss}}(\phi(\frac{\theta}{m})) - L_{s_{ss}}(\phi(\frac{\theta}{m})) + \frac{\tau_r}{m}\frac{r}{U}\left(\frac{\partial L_r}{\partial t} + \frac{U}{r}\frac{\partial L_r}{\partial \theta}\right) + \frac{\tau_s}{m}\frac{r}{U}\frac{\partial L_s}{\partial t} - \frac{\mu}{m}\frac{r}{U}\frac{\partial \phi}{\partial t} - \frac{\lambda}{m}\frac{\partial \phi}{\partial \theta} \tag{A4.16}$$

All inertia parameters (including η) must be divided by the number of lobes. In summary, the performance of a compressor in a single-lobed distortion of θ degree extent is exactly equivalent to the performance of the same compressor in an m-lobed distortion of θ/m degree extent if the inertia parameters($\lambda,\mu,\eta,\tau_r,\tau_s$) in the single-lobed case are divided by m in the m-lobed case.

Before proceeding into parametric studies, it was confirmed that the modified version of the original code agreed with analytic calculations for each of the defined diagnostics. Furthermore, calculations could be compared with those made by the original 'error free' code.

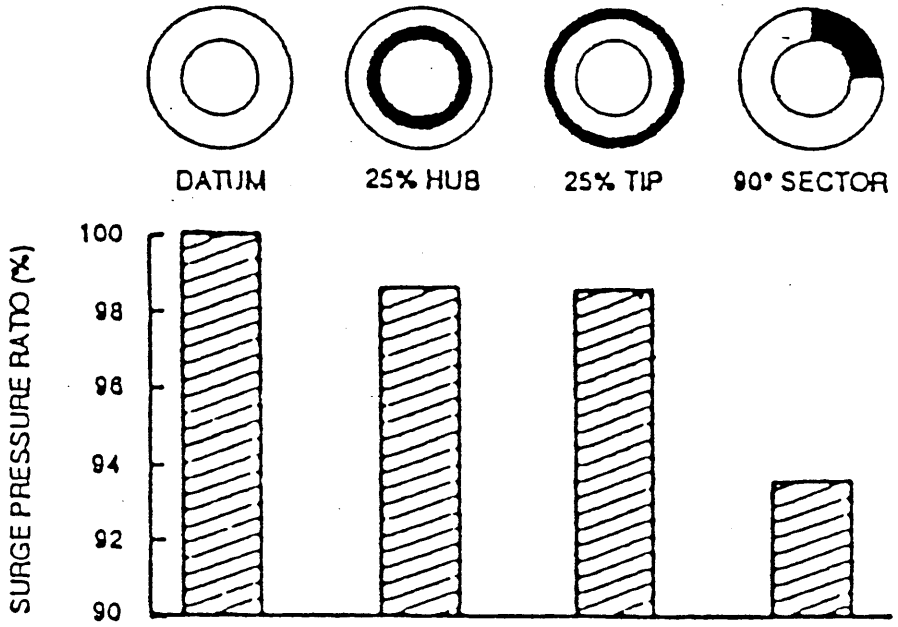

Figure 1.1 Effect of Radial / Circumferential Distortion.

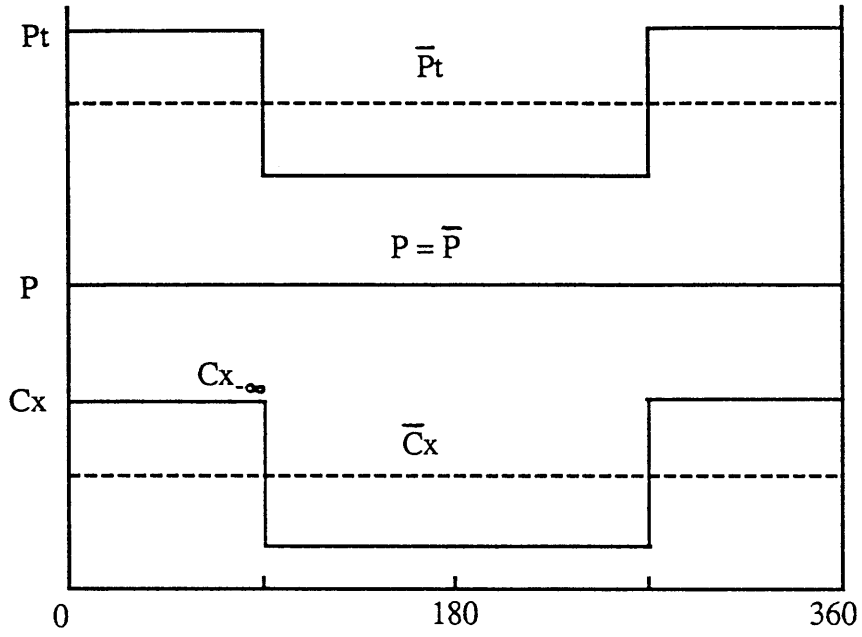

Figure 1.2.a Flow Distortion Far Upstream.

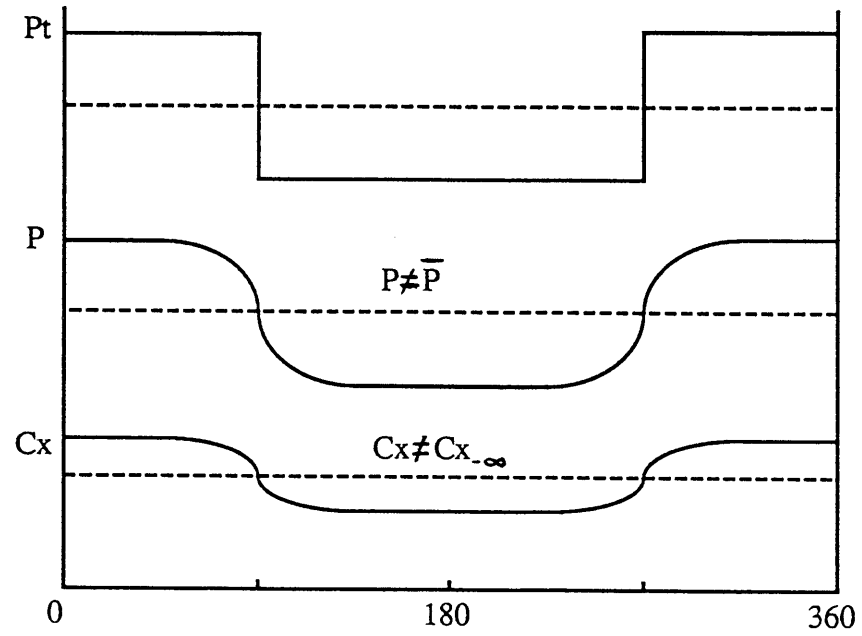

Figure 1.2.b Flow Distortion at Inlet Face of Compressor.

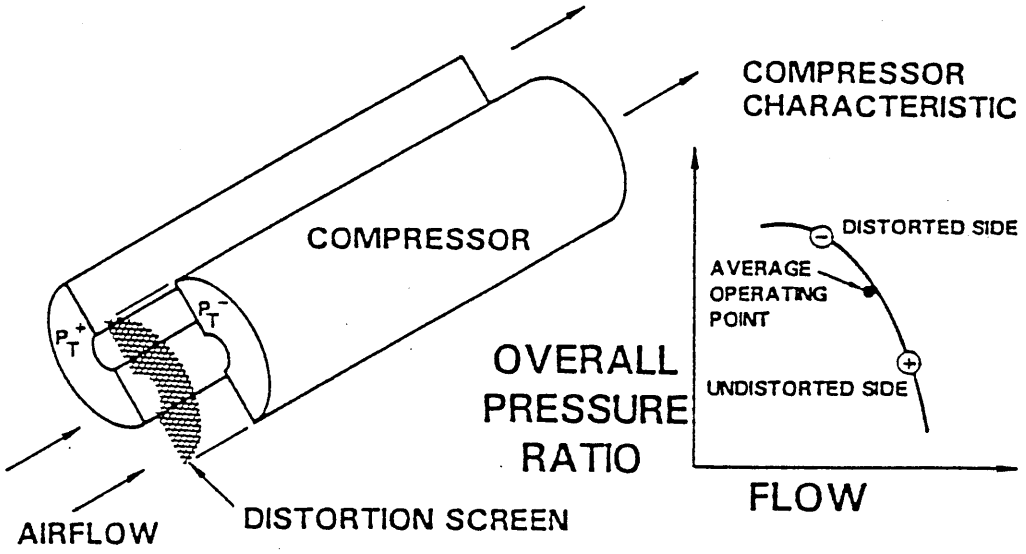

Figure 1.3 Parallel Compressor Theory.

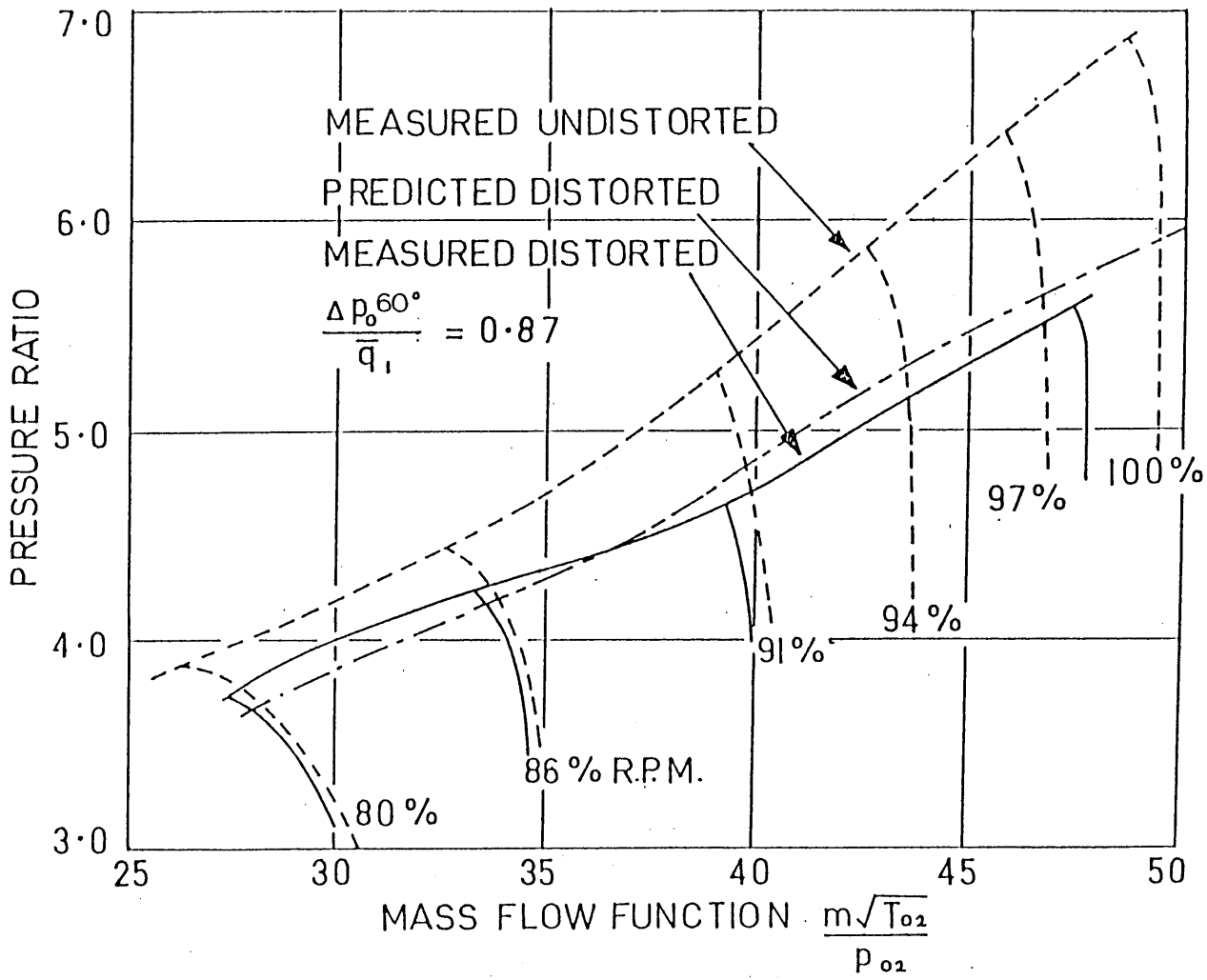

Figure 1.4 Surge Line for Compressor with and without 60 Degree Circumferential Extent Inlet Distortion.

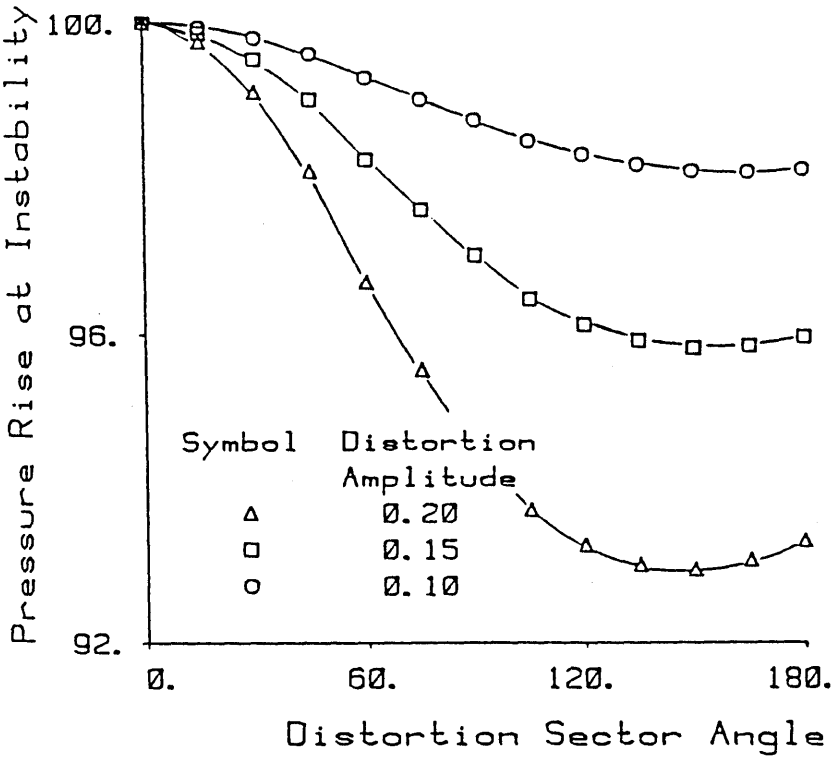

Figure 1.5.a Effect of Distortion Sector Angle on Loss in Stability Margin (theory).

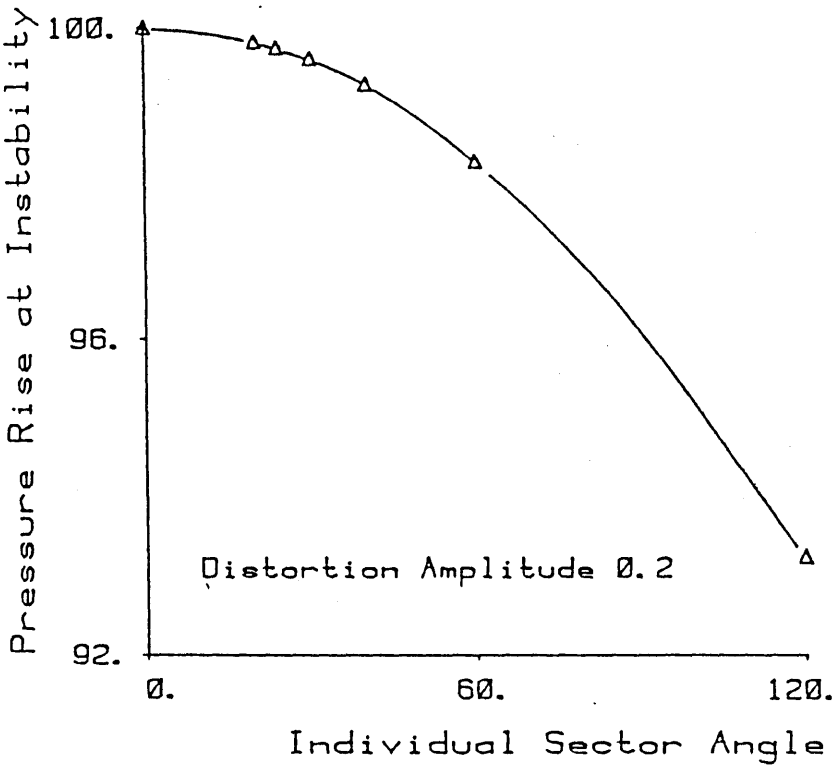

Figure 1.5.b Effect of Individual Sector Angle on Loss in Stability Margin (theory).

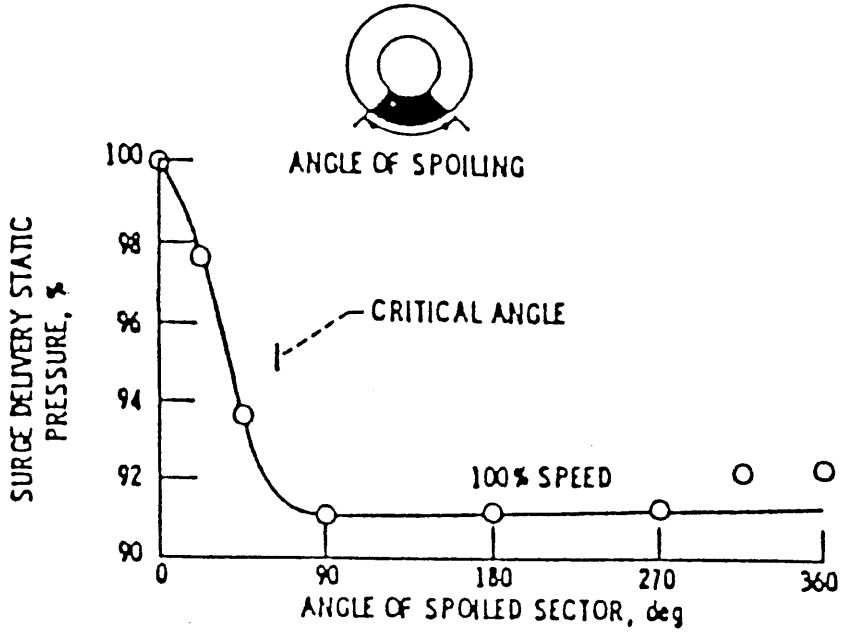

Figure 1.6.a Effect of Distortion Sector Angle on Loss in Stability Margin (experiment).

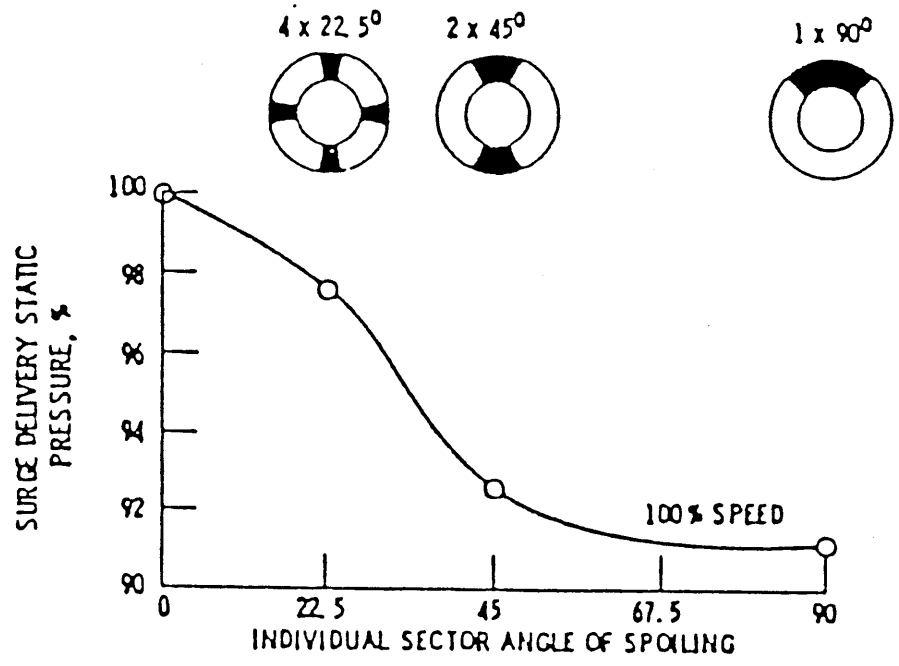

Figure 1.6.b Effect of Individual Sector Angle on Loss in Stability Margin (experiment).

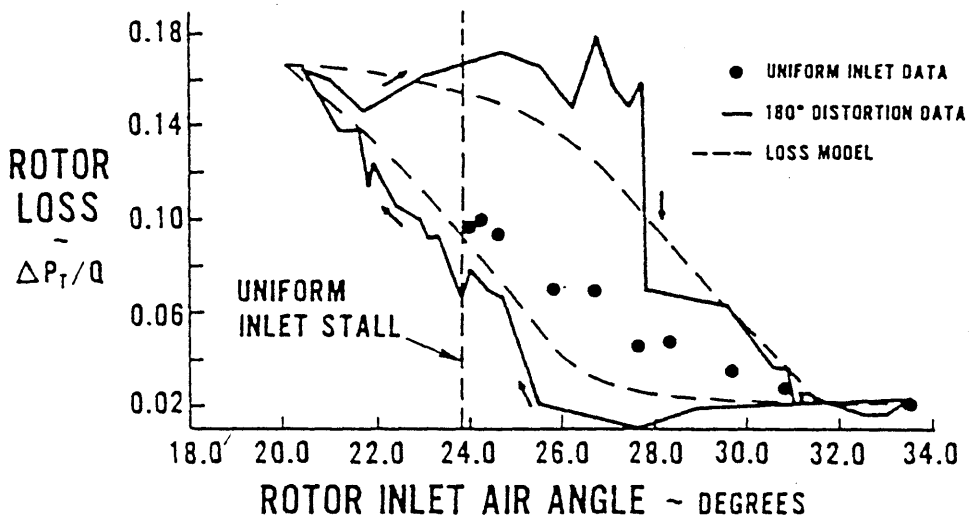

Figure 1.7.a Loss Coefficient as a Function of Incidence.

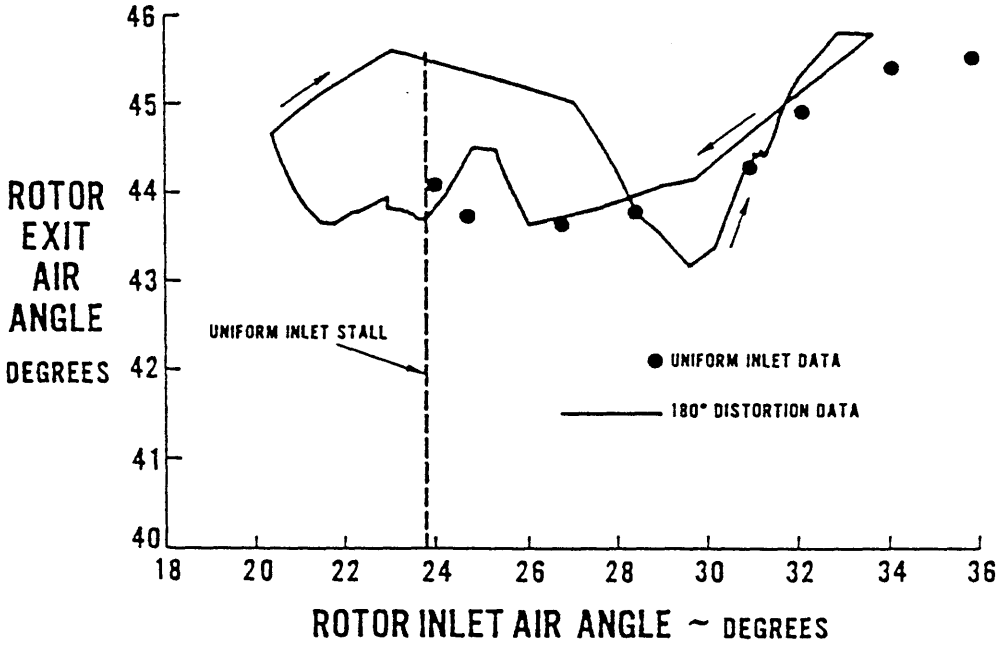

Figure 1.7.b Blade Deviation as a Function of Incidence.

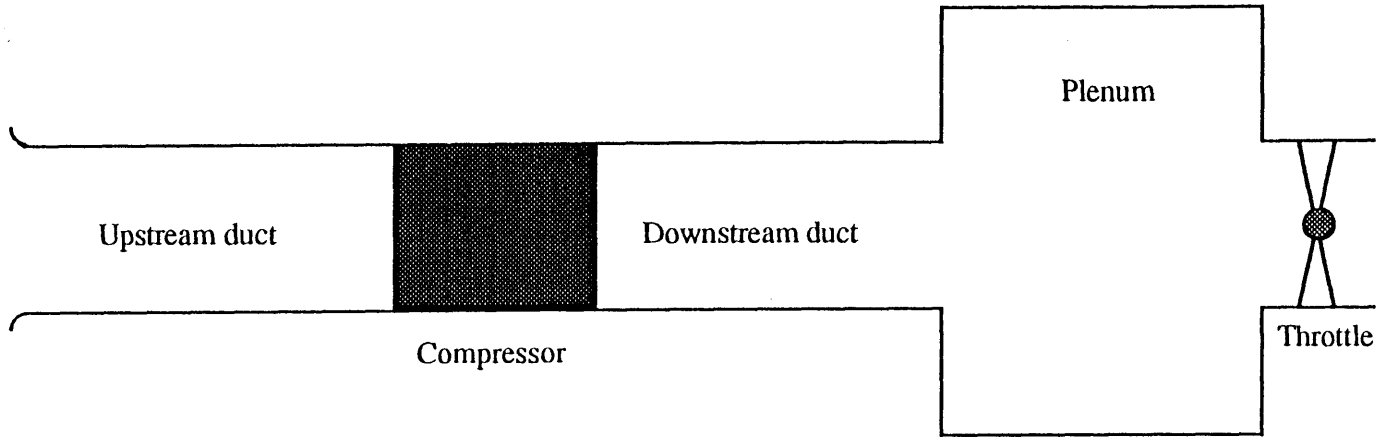

Figure 2.1 Schematic of Compression System Model.

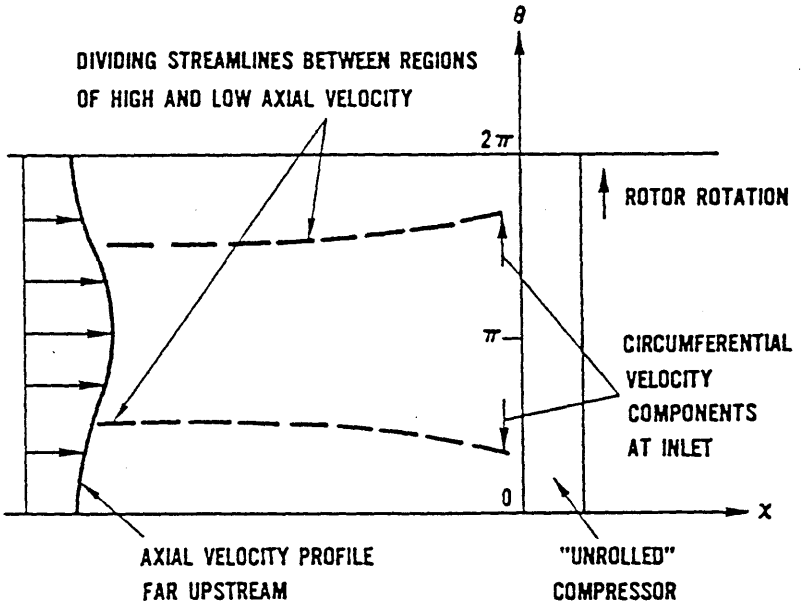

Figure 2.2 Compressor Interaction with Incoming Flow Distortion.

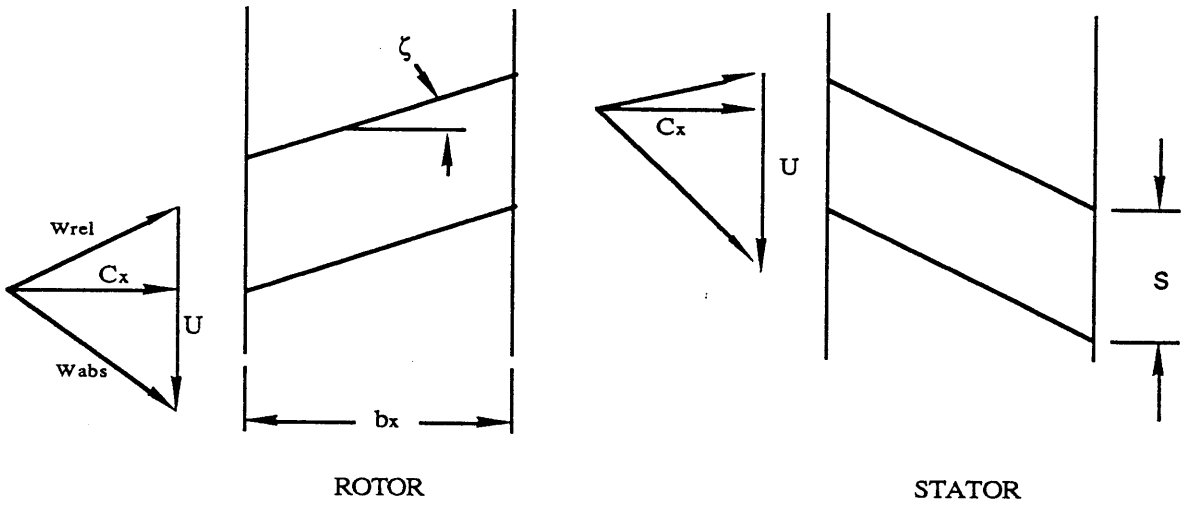

Figure 2.3 Blade Geometry.

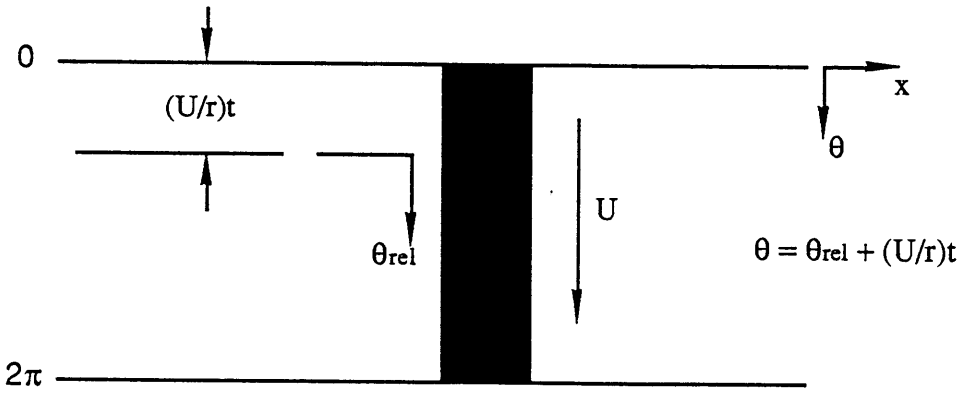

Figure 2.4 Description of Rotor Relative Frame.

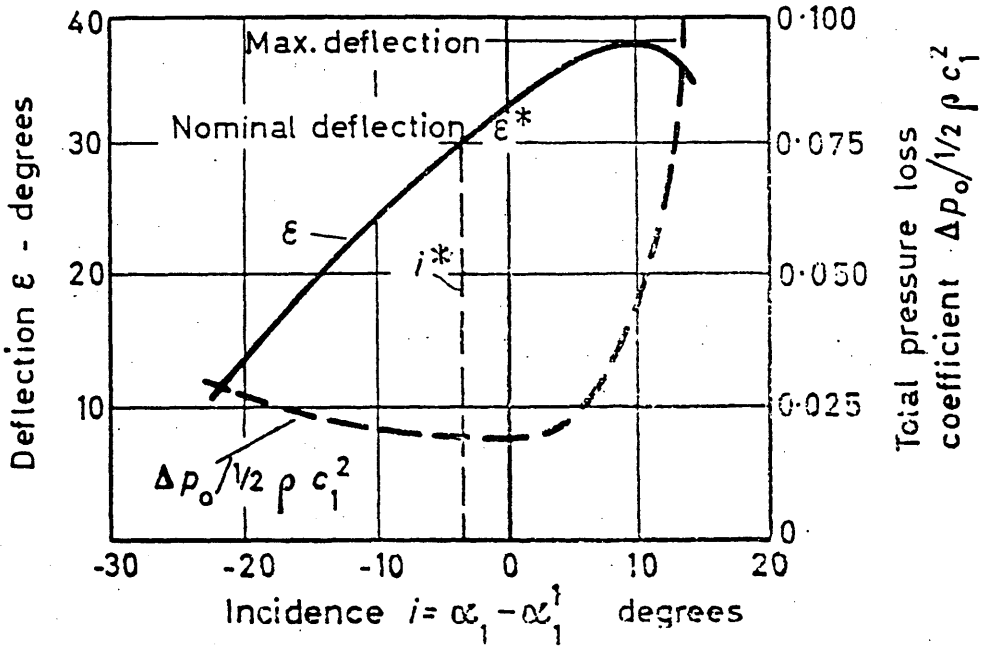

Figure 2.5 Howell's Correlation for Loss Coefficient and Blade Deflection.

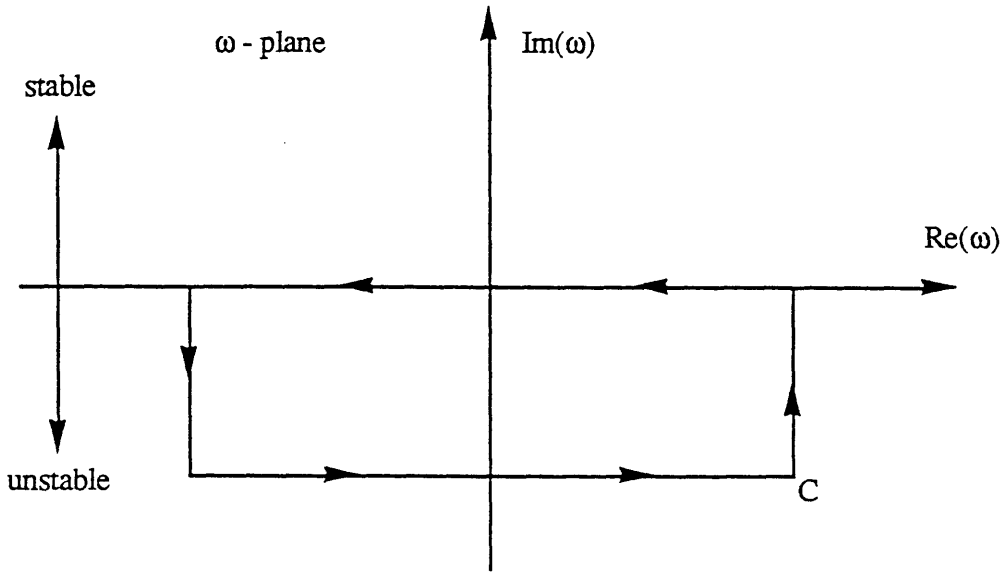

Figure 3.1 $\tilde{\omega}$ - plane.

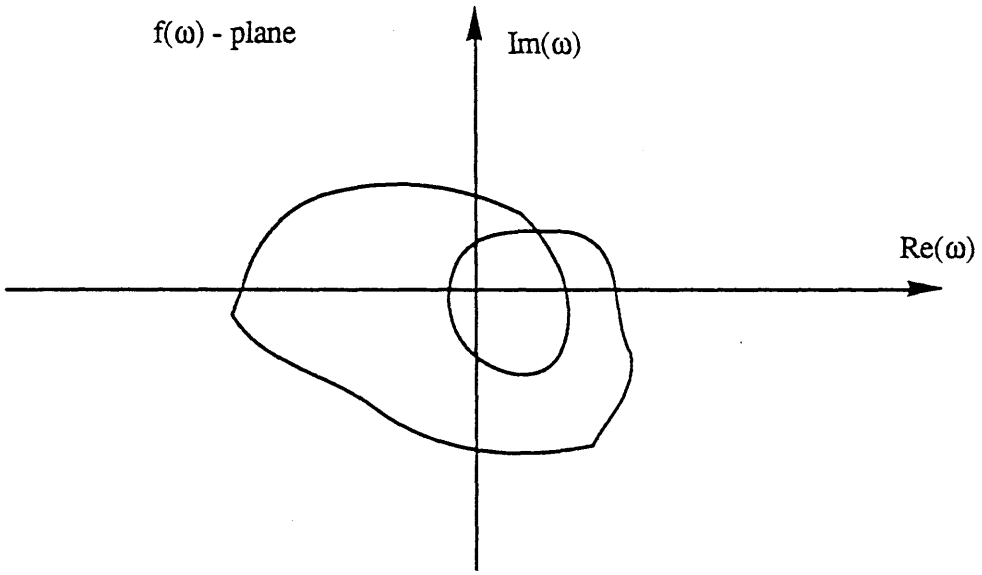

Figure 3.2 f($\tilde{\omega}$) - plane.

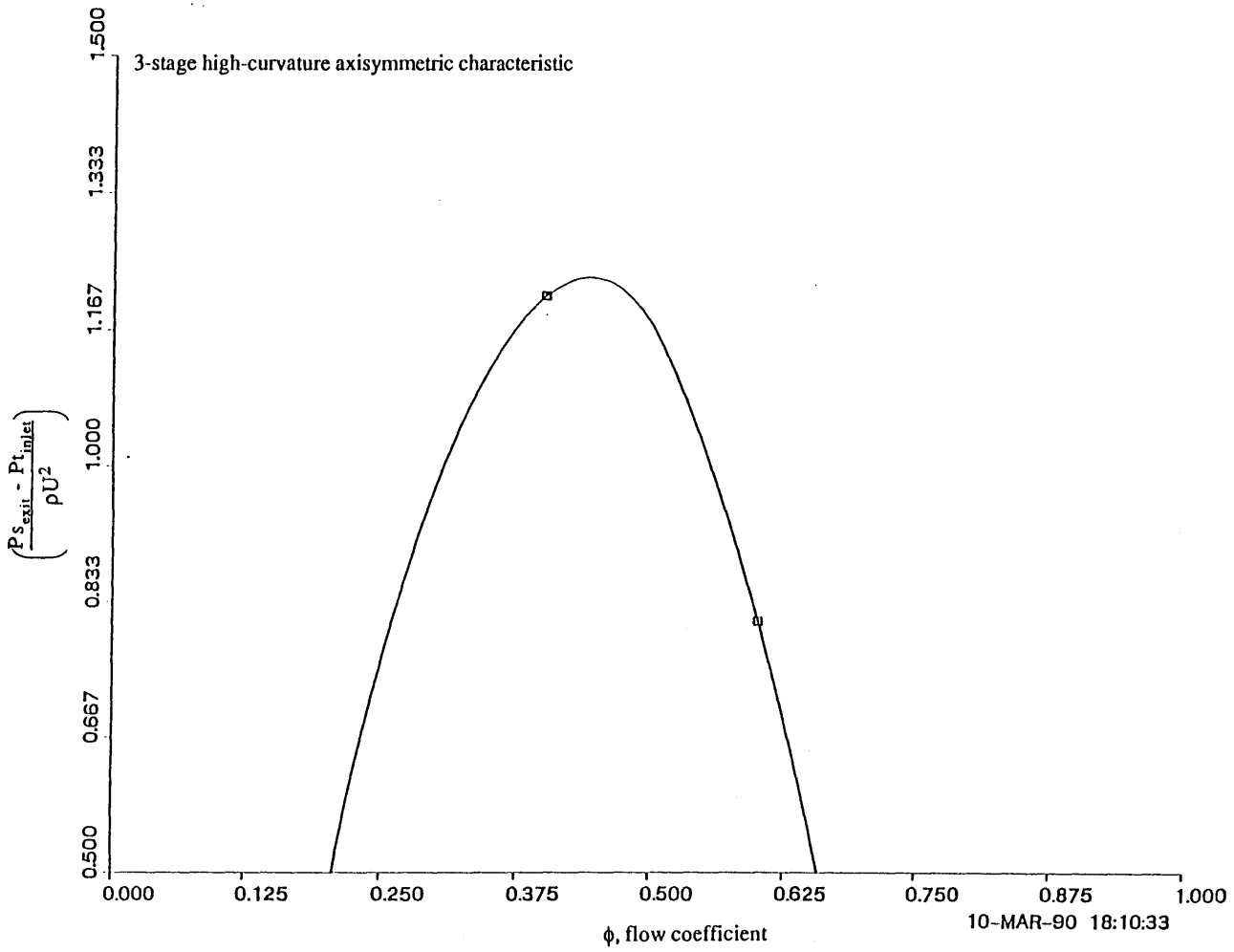

Figure 3.3 Axisymmetric Performance of a 3-Stage High Curvature Compressor.

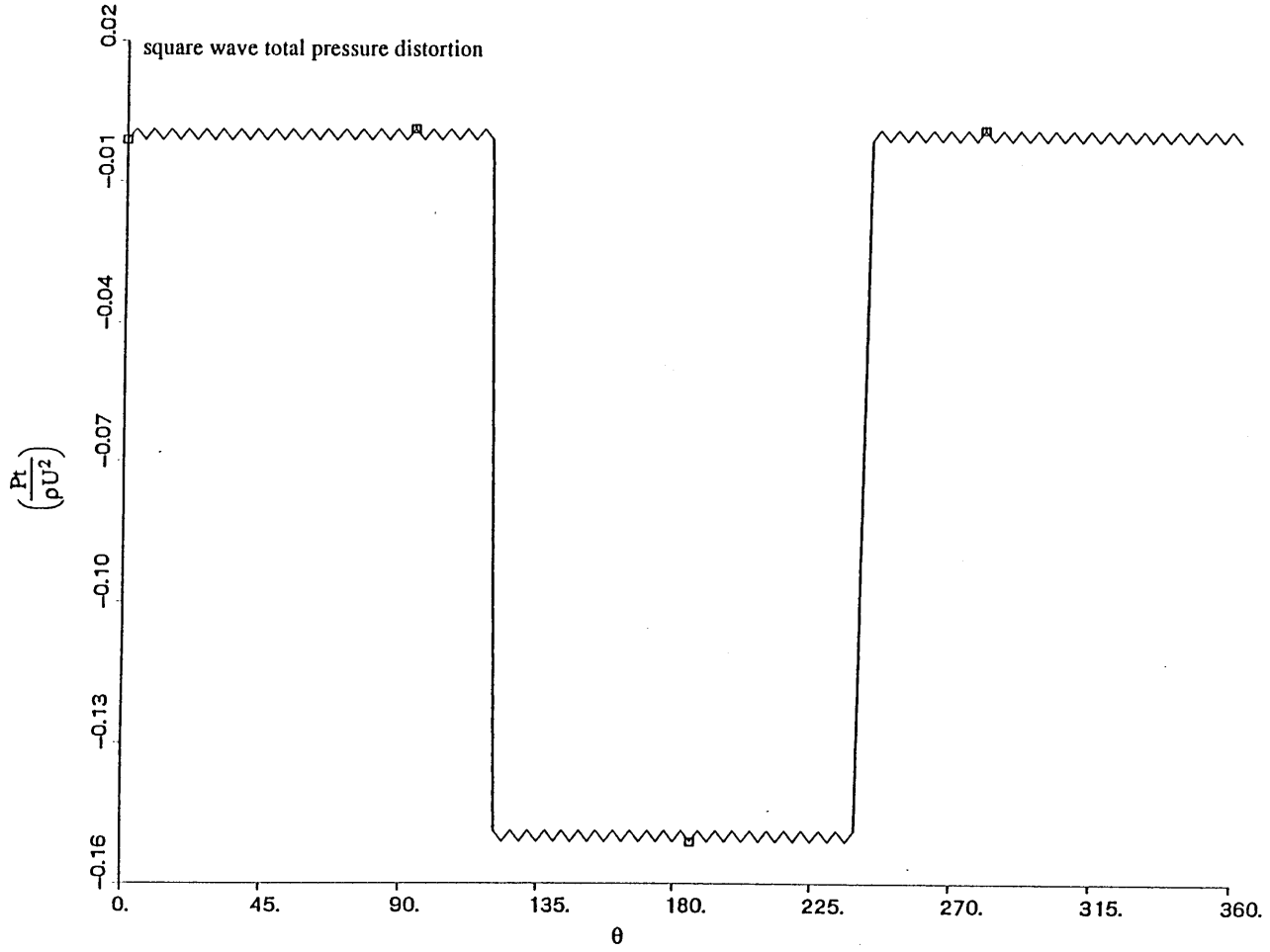

Figure 3.4 Square Wave Total Pressure Distortion.

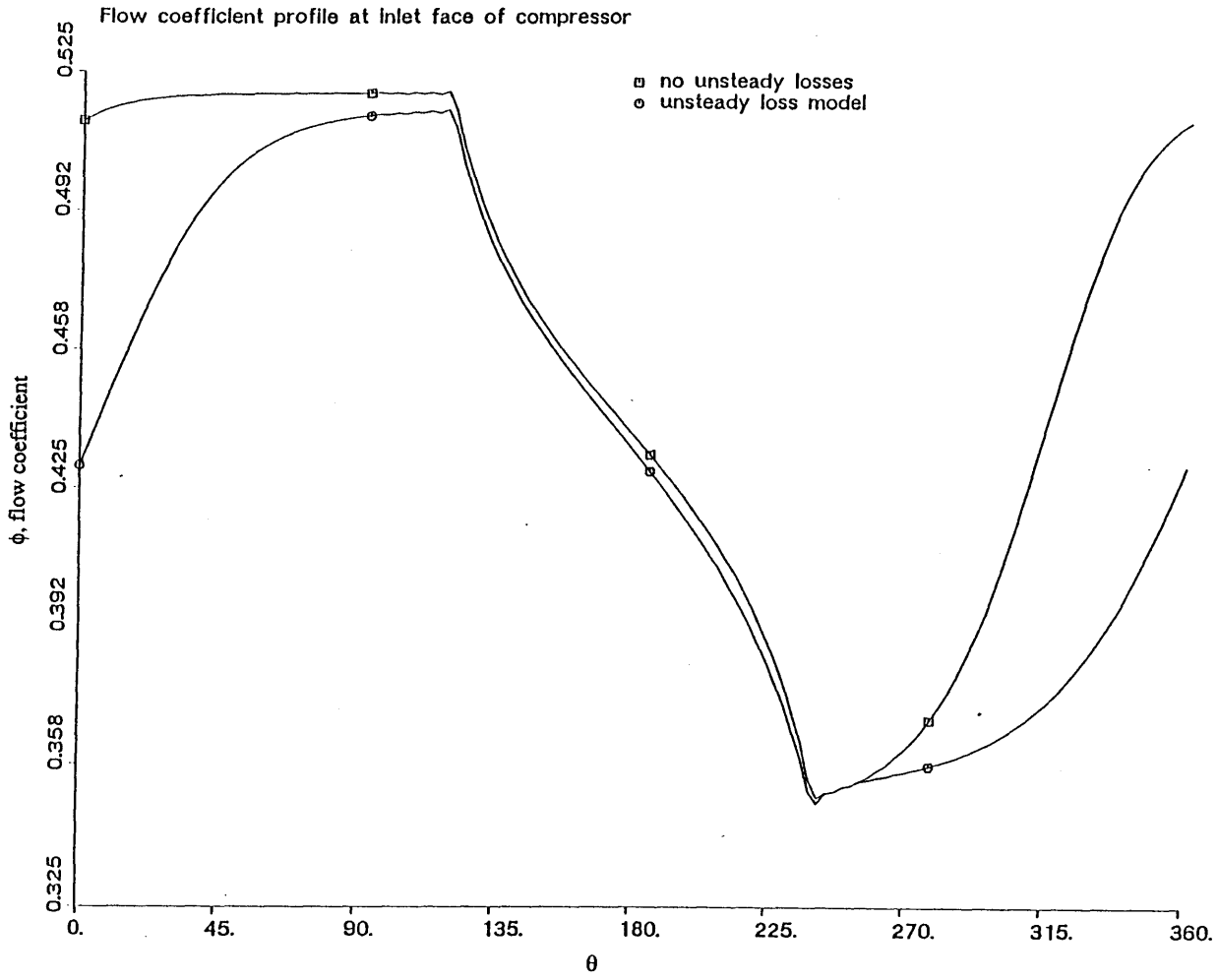

Figure 3.5 Flow Coefficient Profile at Inlet Face to Compressor.

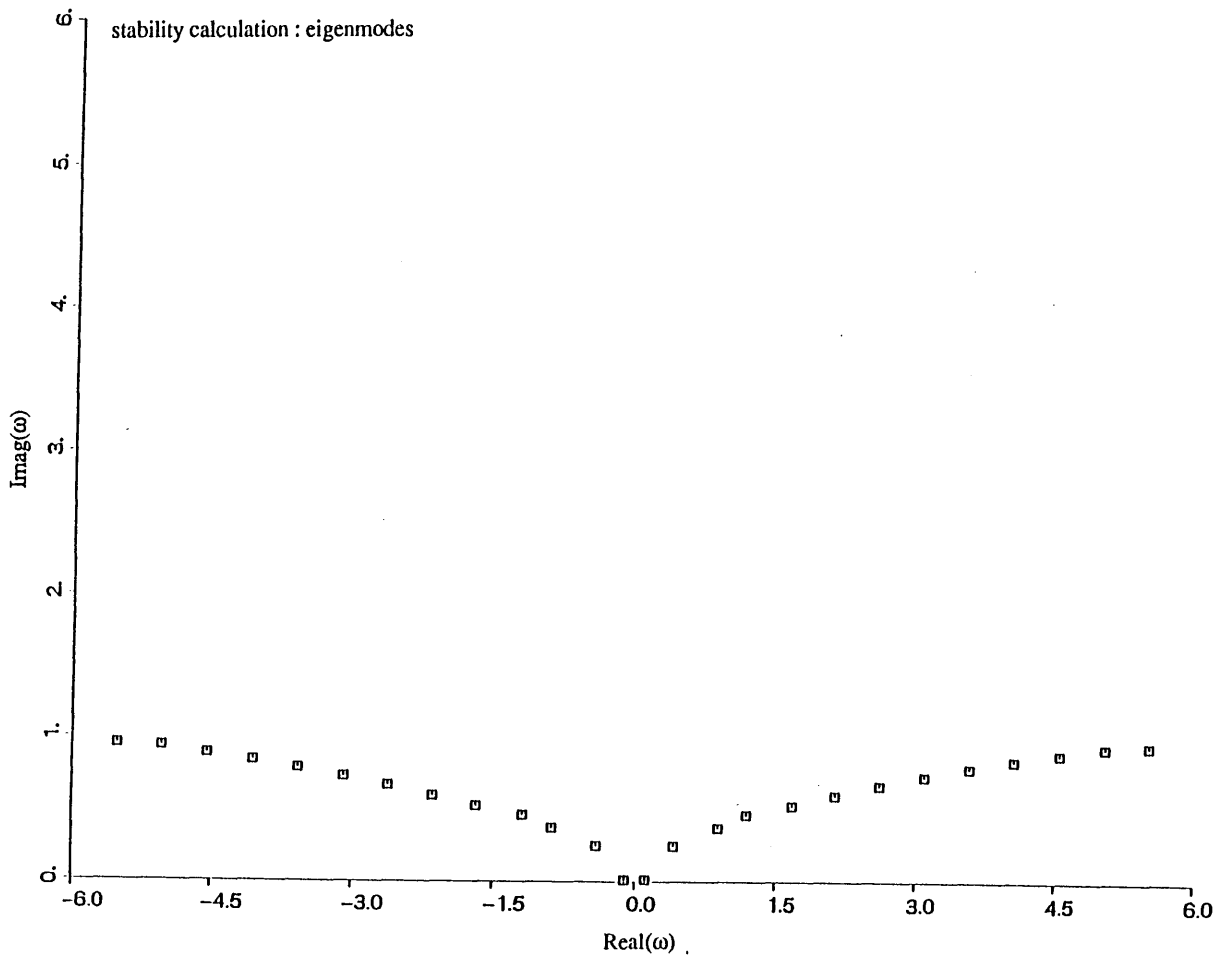

Figure 3.6 Eigenmodes at Neutral Stability.

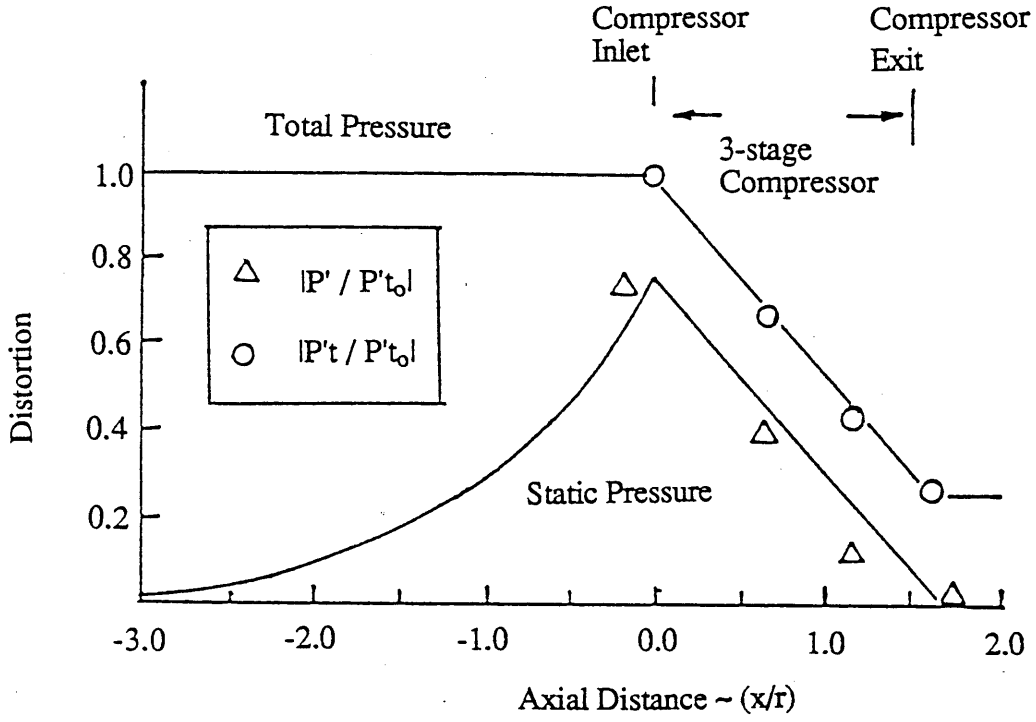

Figure 4.1 Axial Extent of Flowfield Redistribution Upstream of Compressor Inlet.

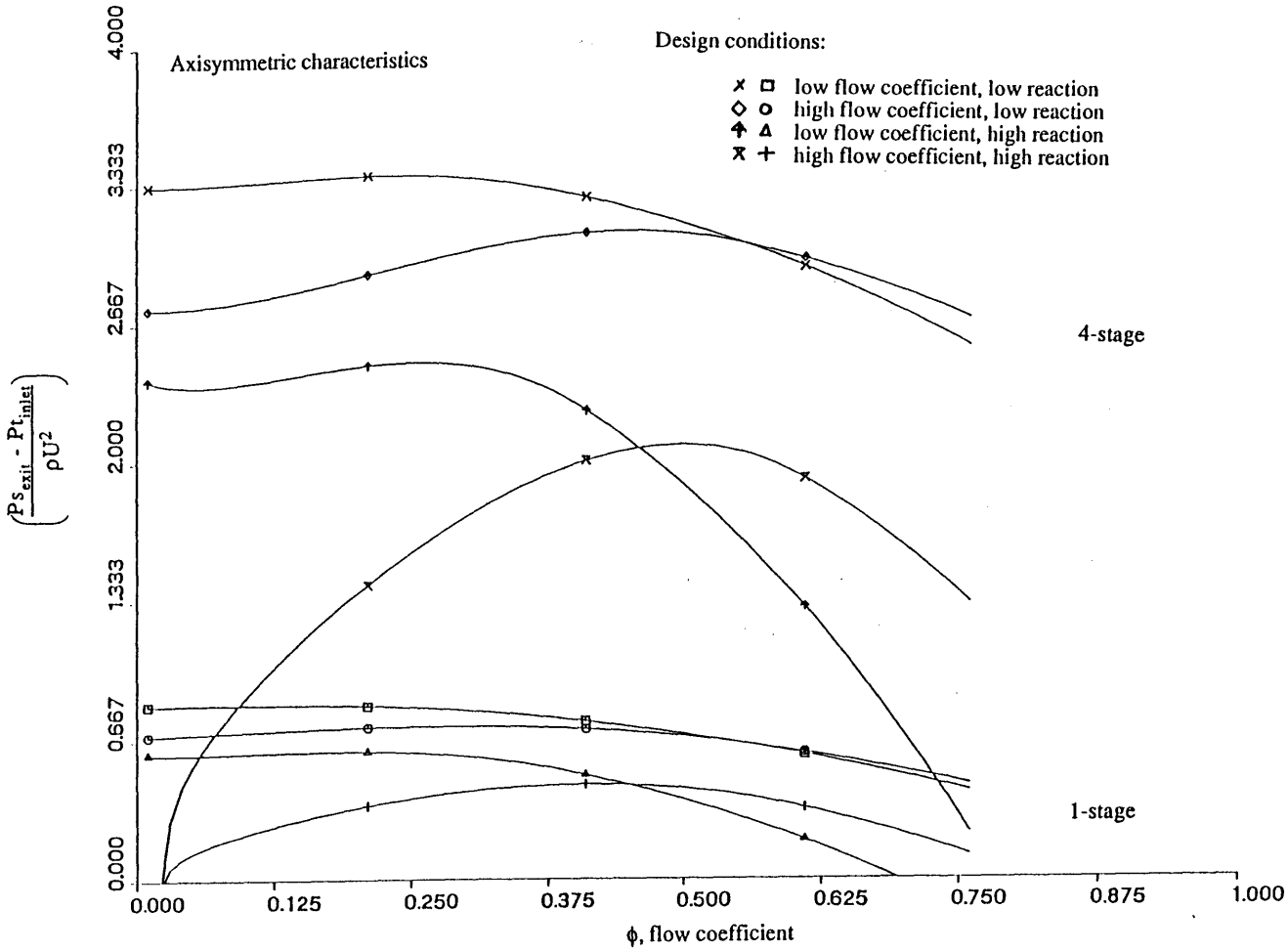

Figure 4.2 Axisymmetric Characteristics for Compressors of Various Design Conditions.

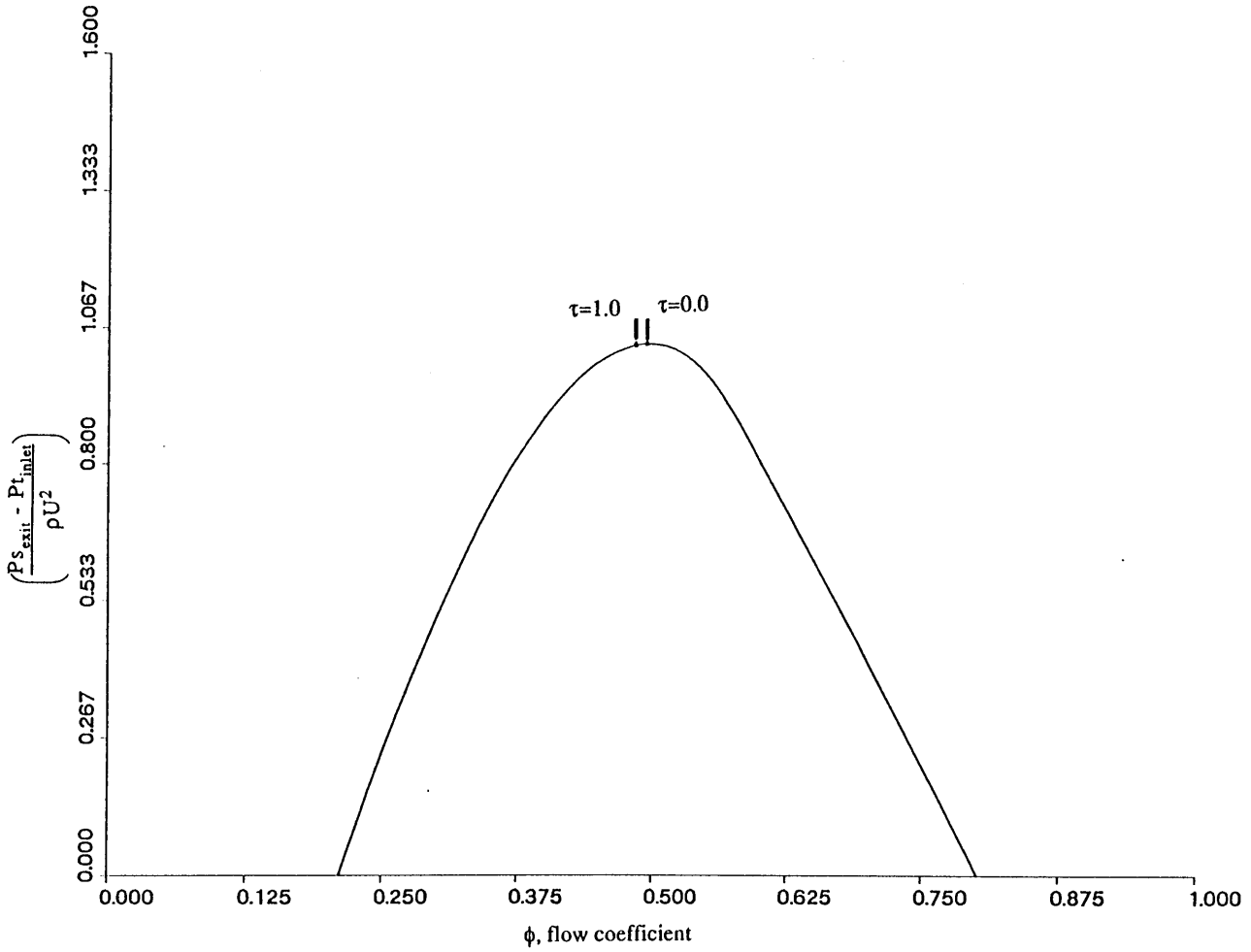

Figure 4.3 Effect of Unsteady Losses on Clean Flow Stability Margin.

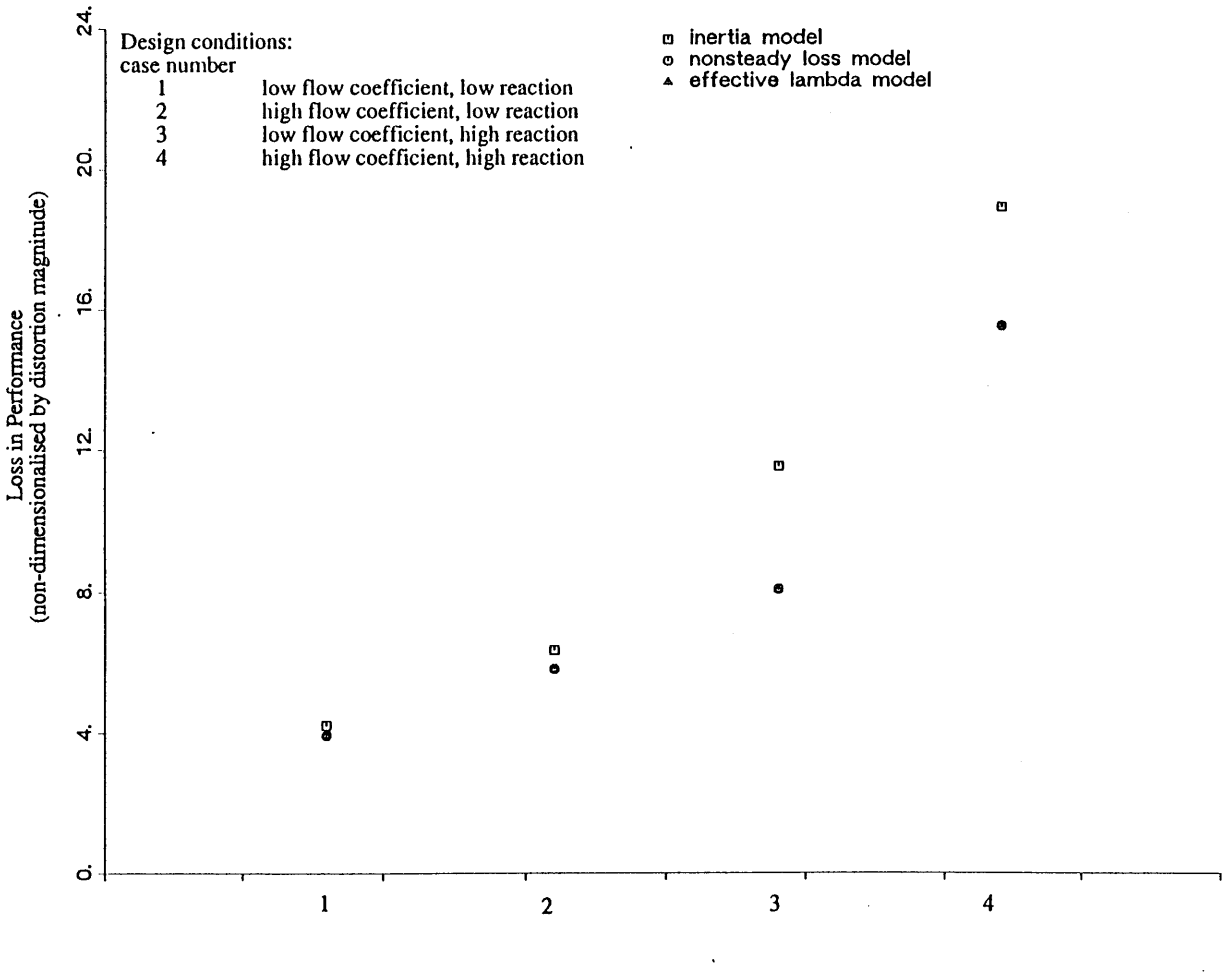

Figure 4.4.a Effect of Unsteady Losses on Stability Prediction for Compressors of Various Design Conditions (single stage).

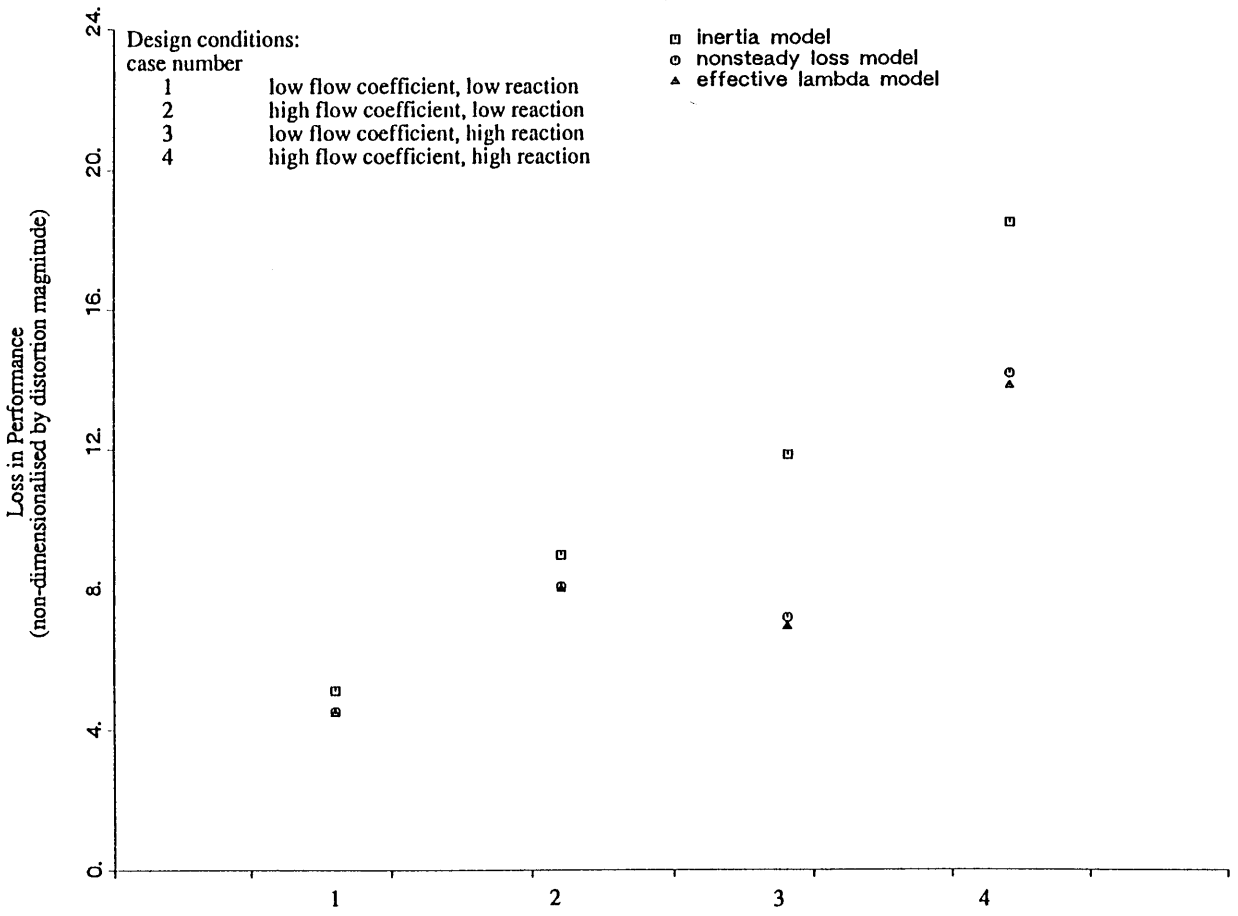

Figure 4.4.b Effect of Unsteady Losses on Stability Prediction for Compressors of Various Design Conditions (4 stage).

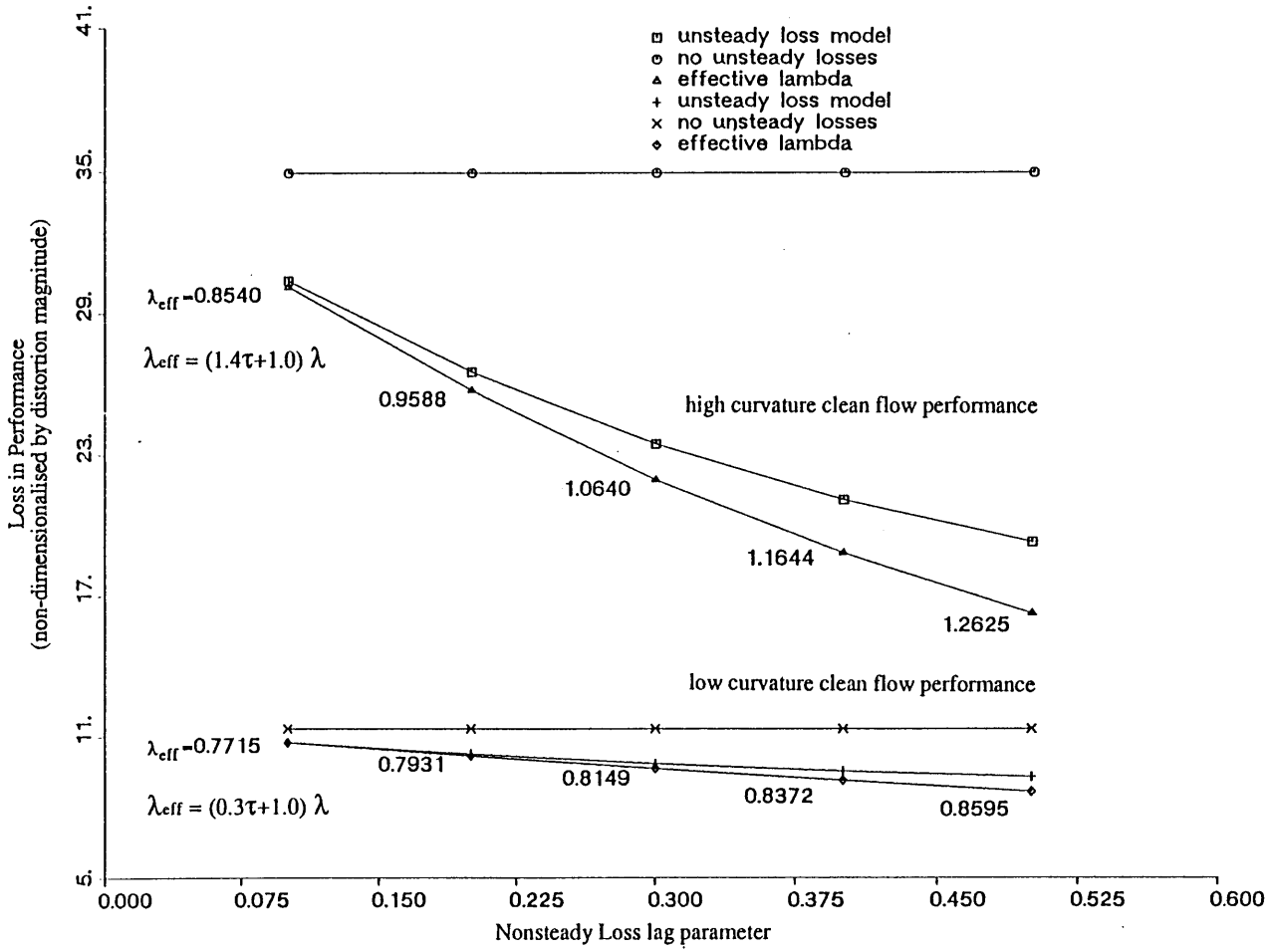

Figure 4.5 Effect of Unsteady Losses on Compressor Performance.

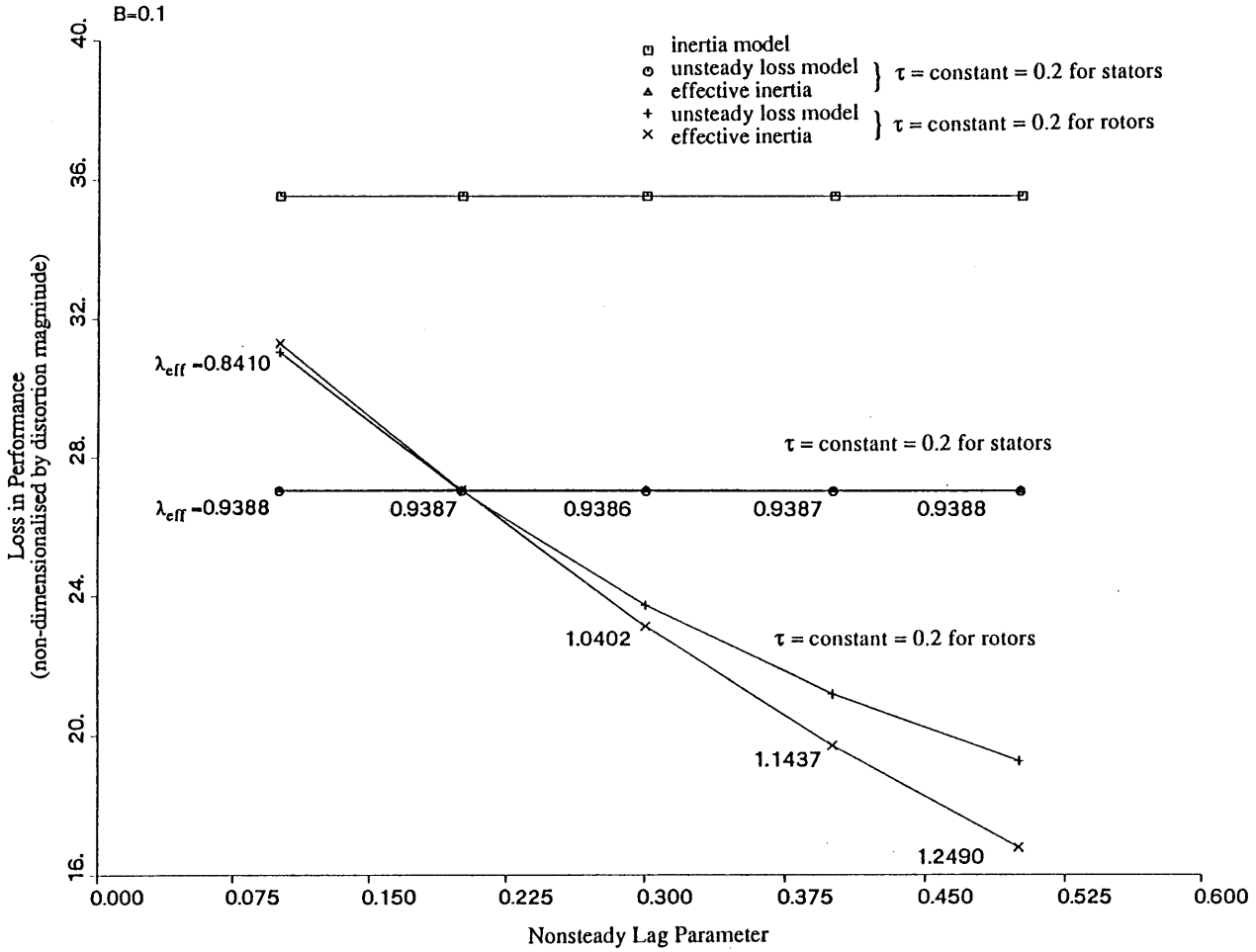

Figure 4.6.a Effect of Unsteady Losses on Rotor Performance versus Stator Performance (B=0.1).

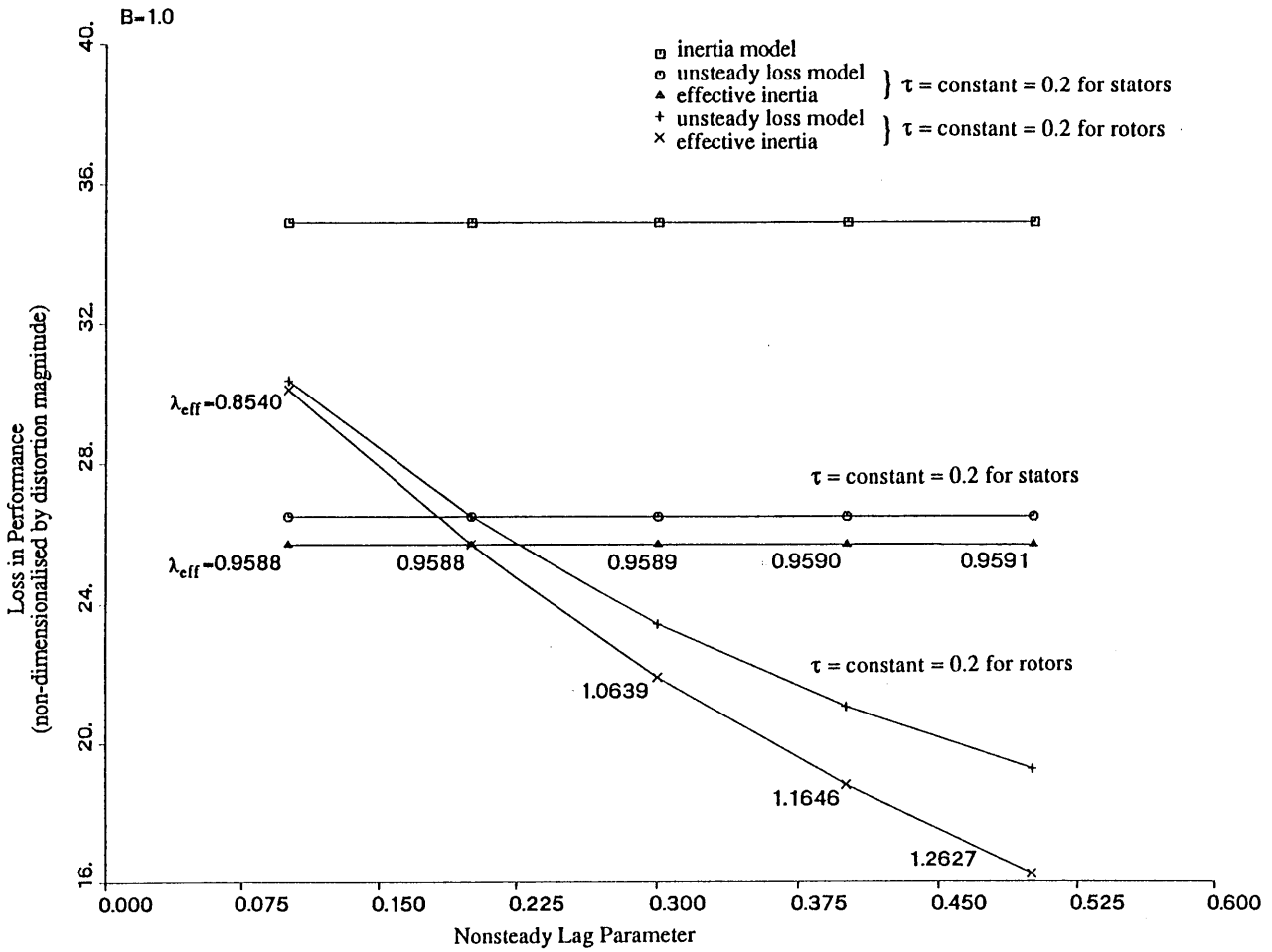

Figure 4.6.b Effect of Unsteady Losses on Rotor Performance versus Stator Performance (B=1.0).

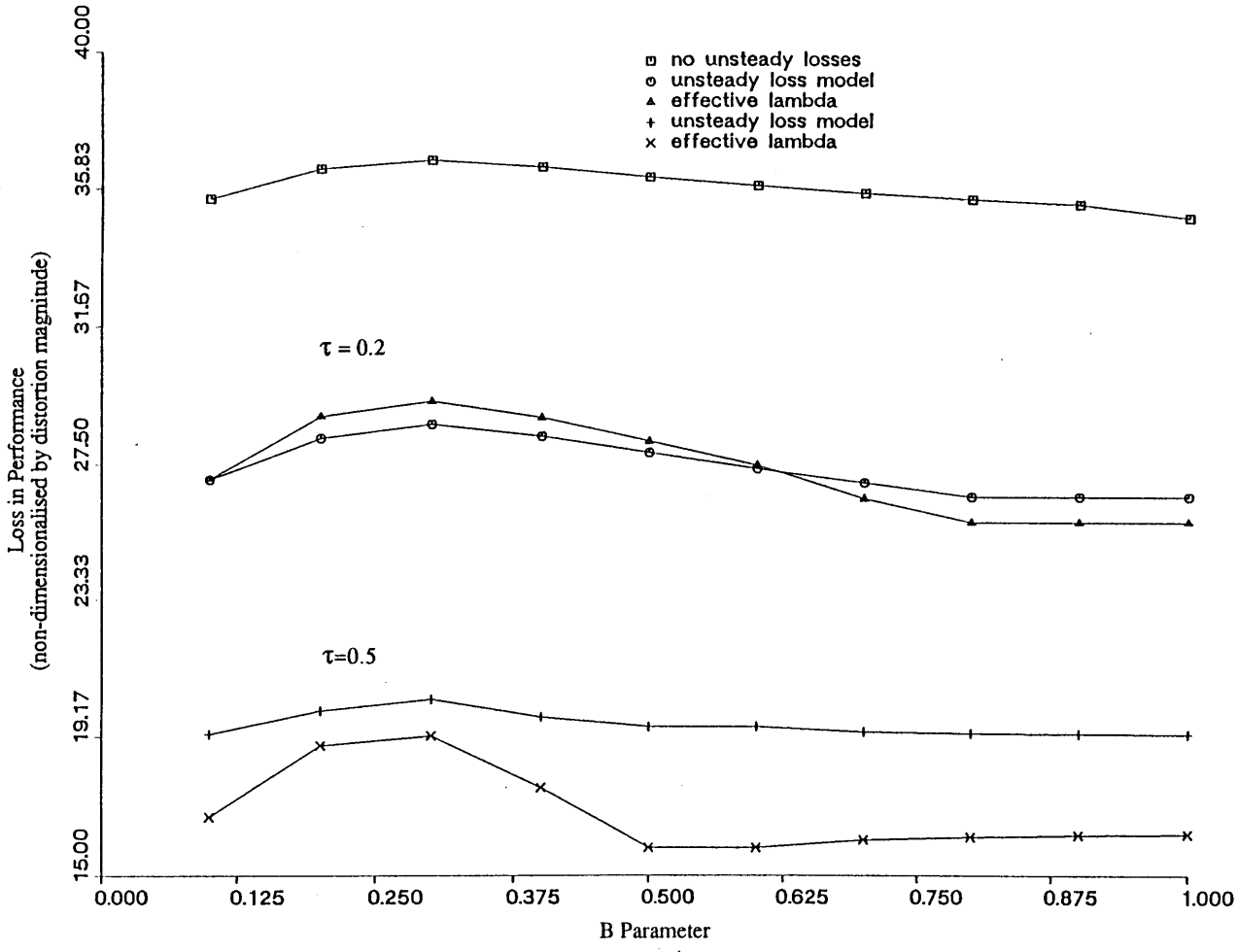

Figure 4.7 Effect of B Parameter on Distorted Performance for a High Curvature Clean Flow Characteristic.

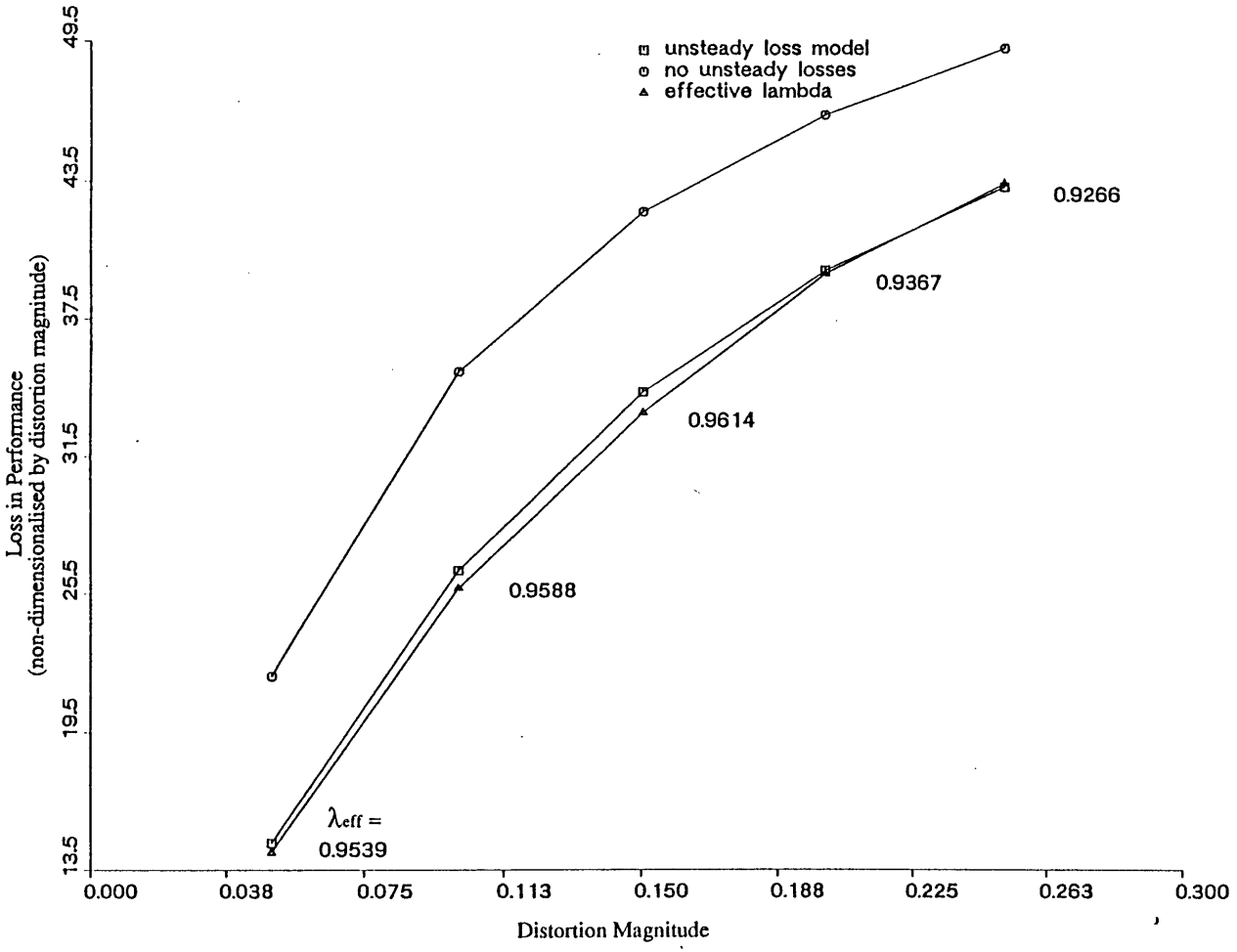

Figure 4.8 Effect of Distortion Magnitude on Various Unsteady Loss Model Predictions (high curvature clean flow characteristic).

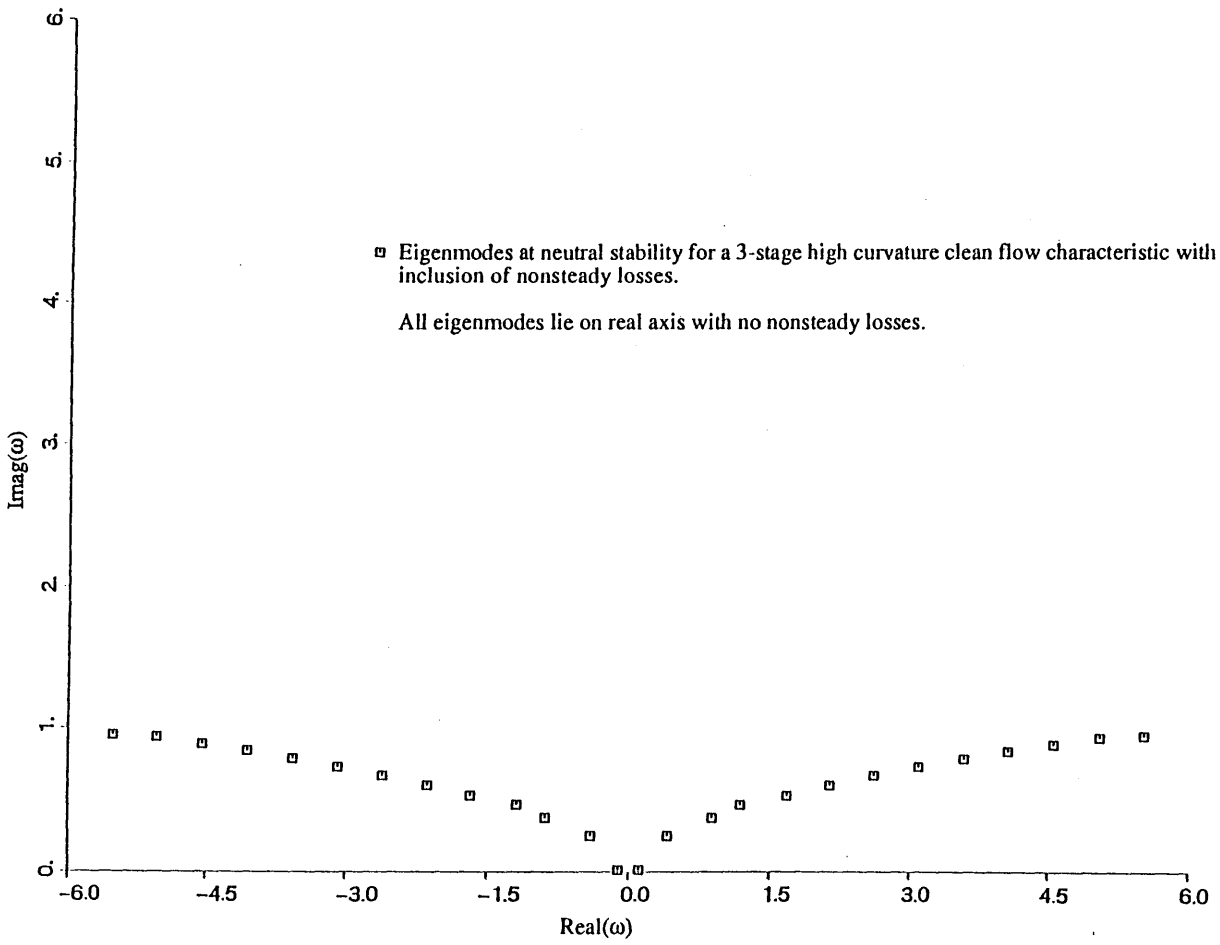

Figure 4.9 Eigenmodes at Neutral Stability with Inclusion of Unsteady Losses.

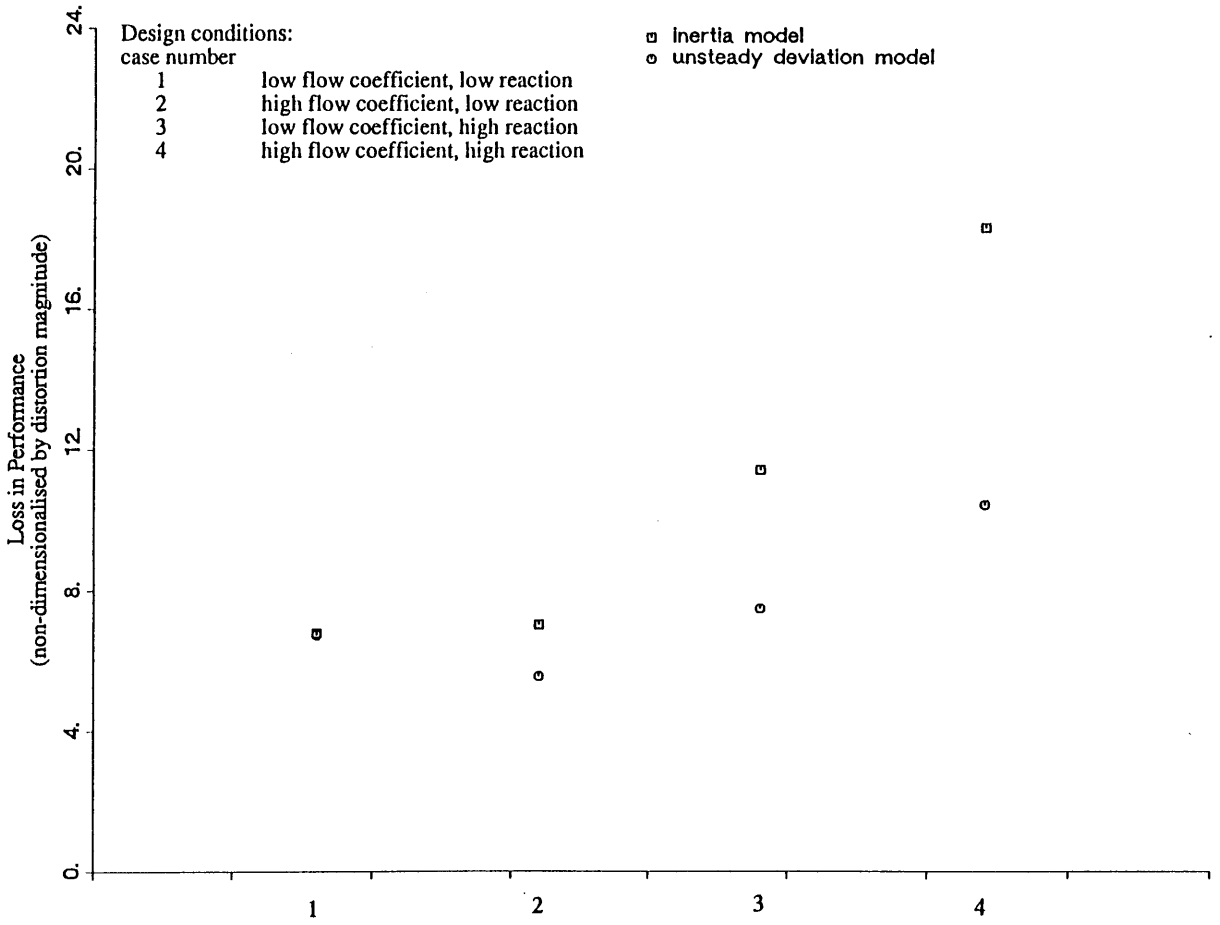

Figure 4.10.a Effect of Unsteady Deviations on Stability Prediction for Compressors of Various Design Conditions (single stage).

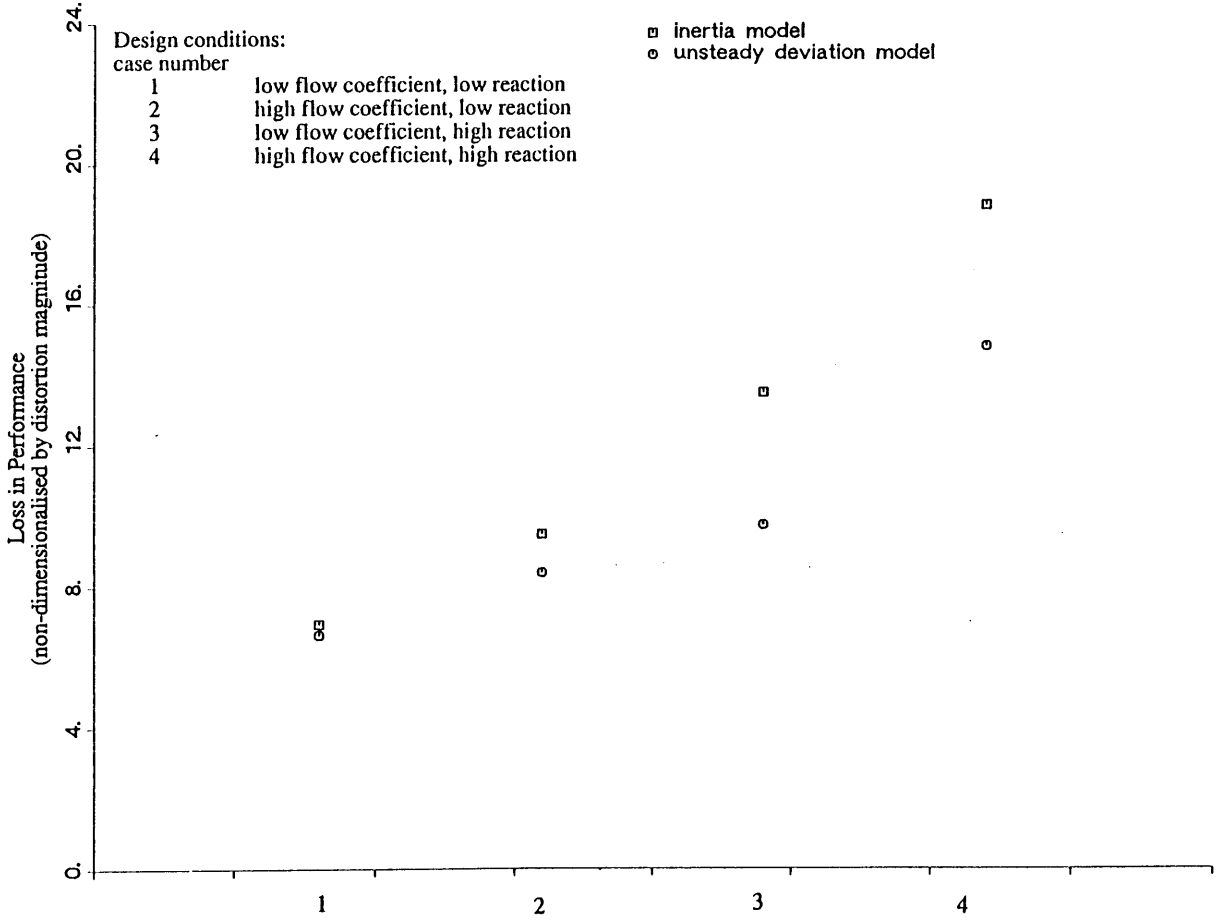

Figure 4.10.b Effect of Unsteady Deviations on Stability Prediction for Compressors of Various Design Conditions (4 stage).

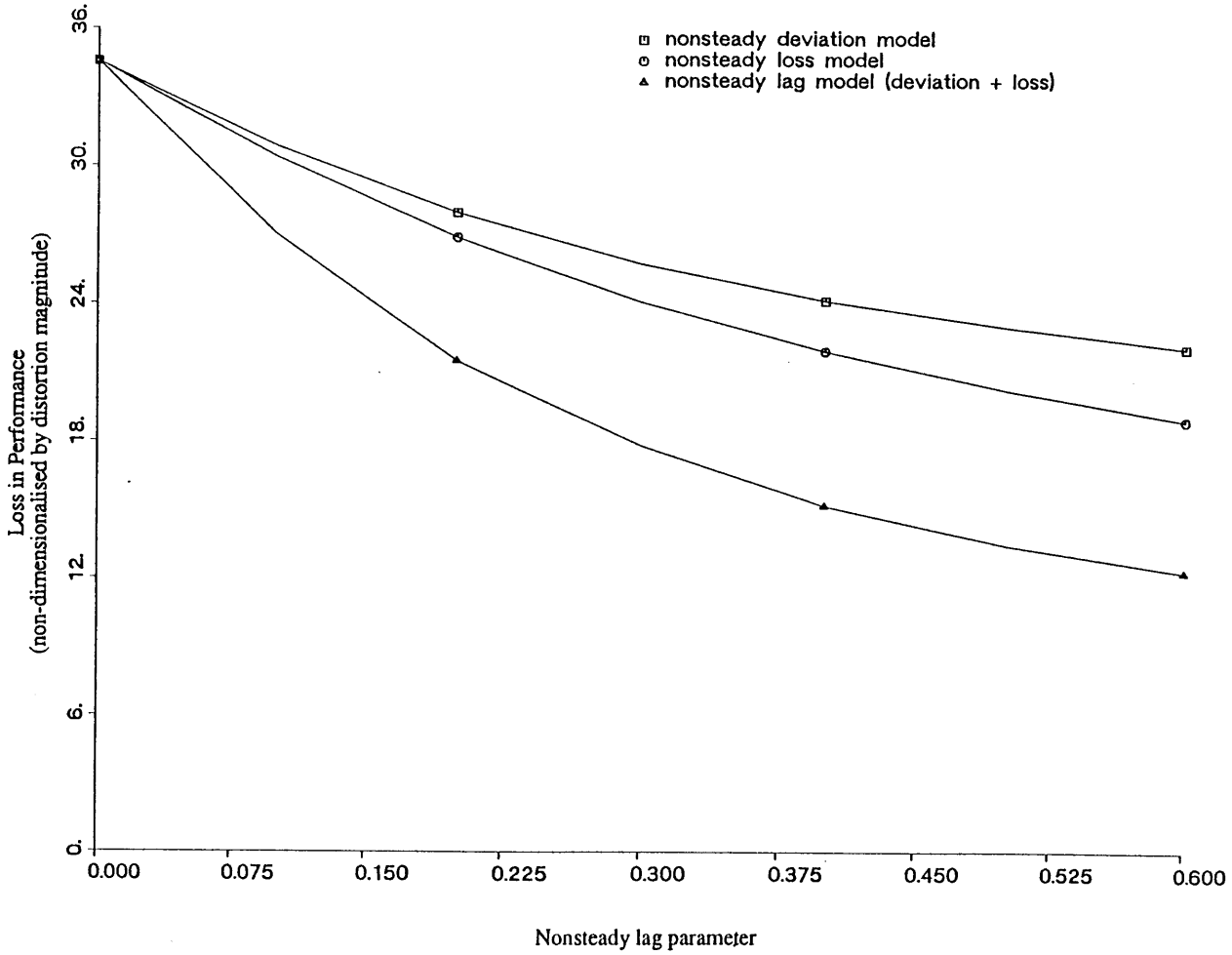

Figure 4.11 Effect of Unsteady Losses and Unsteady Deviations on Compressor Performance.

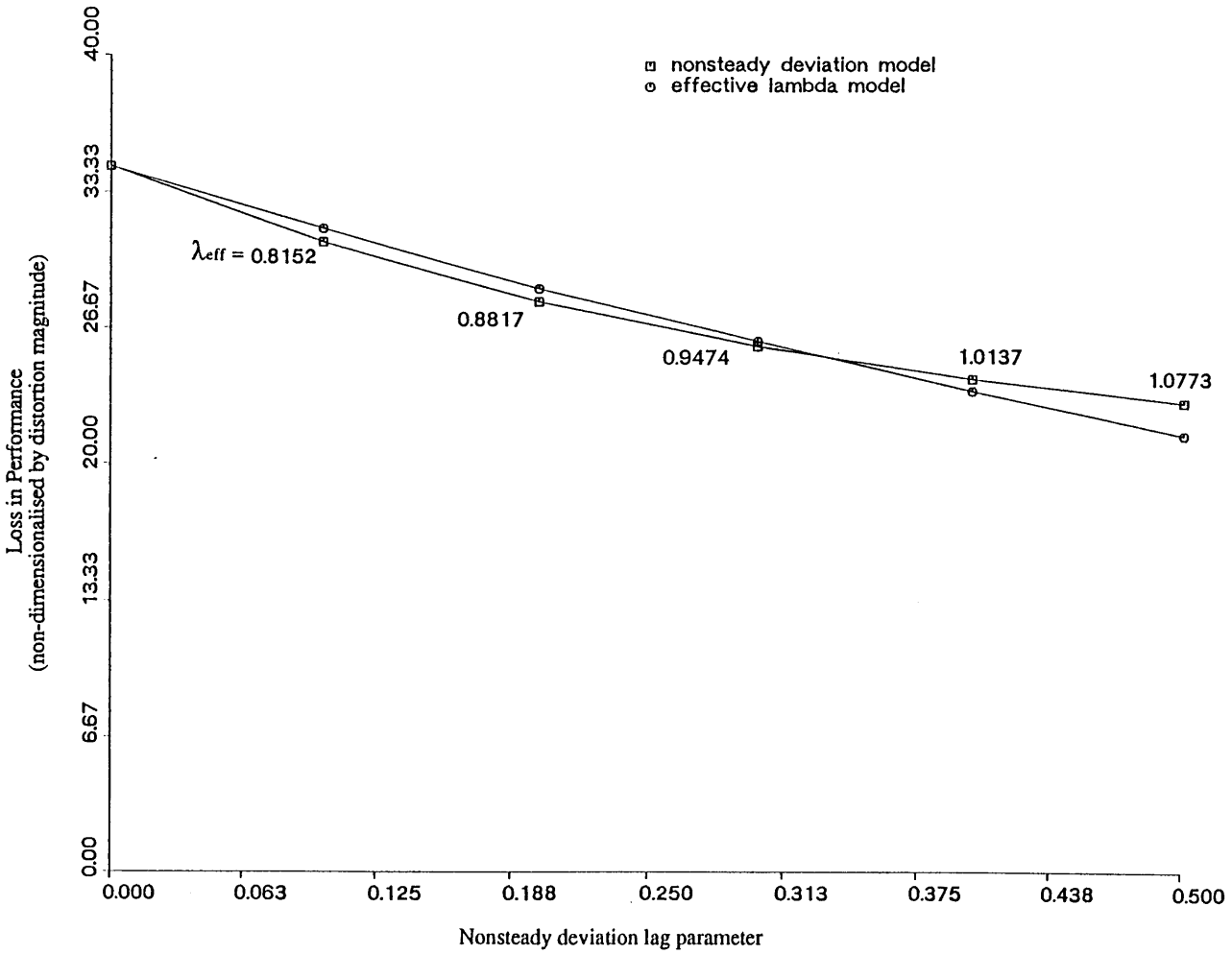

Figure 4.12 Comparison of Improved Unsteady Deviation Model with Simpler Effective Inertia Model.

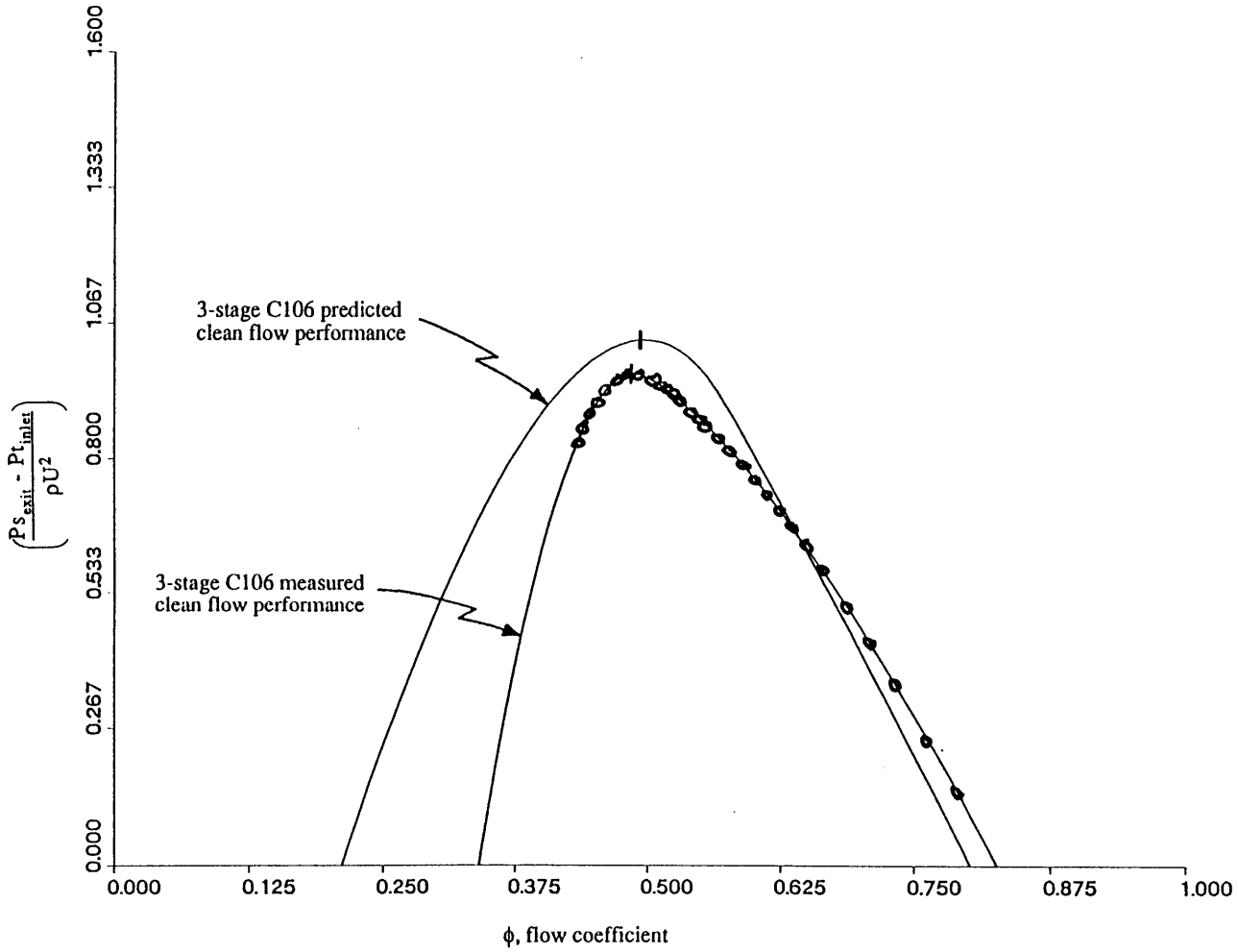

Figure 5.1 Axisymmetric Characteristic for 3-stage C106 Compressor (theory & expt.).

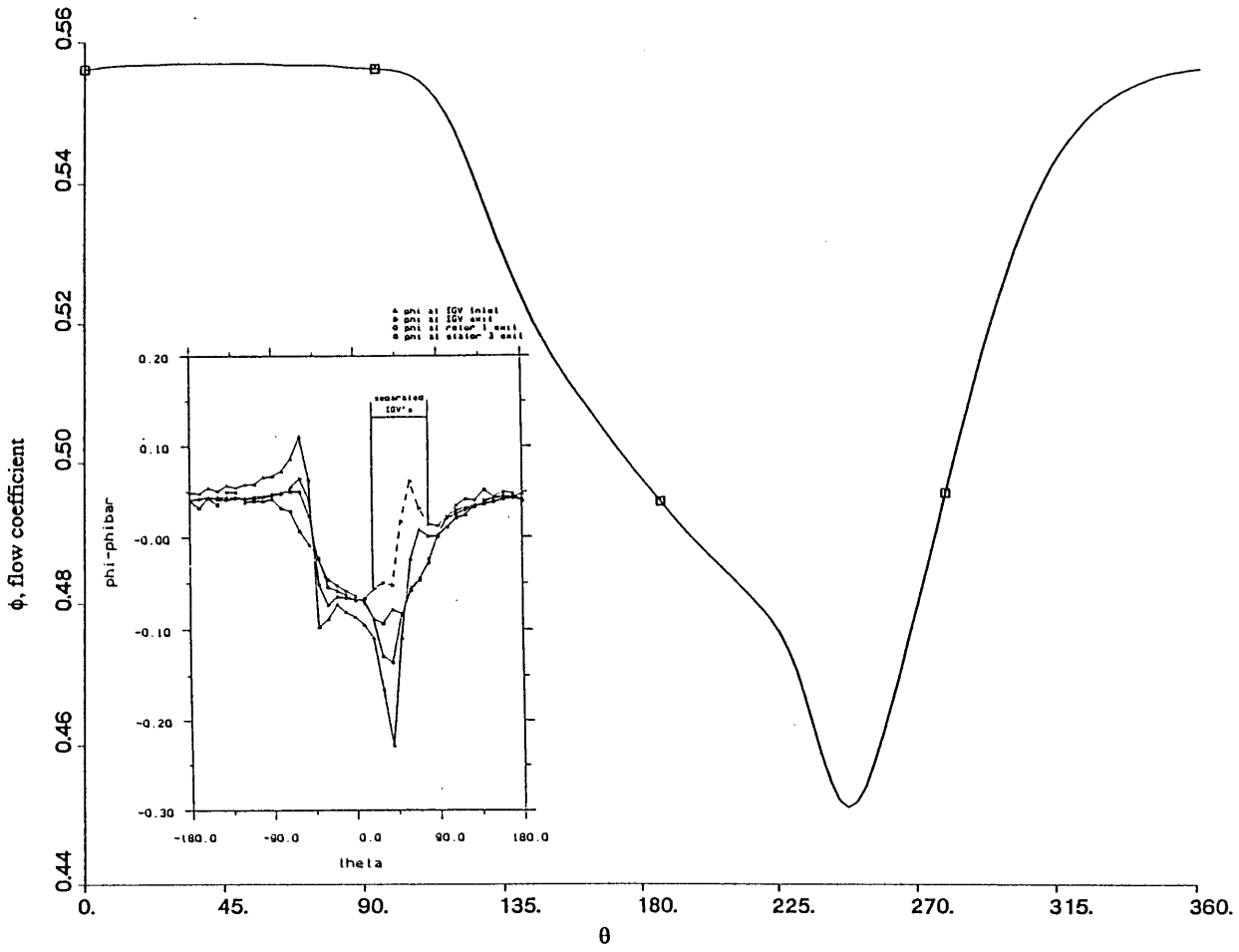

Figure 5.2 Flow Coefficient Profile at Compressor Inlet Face.

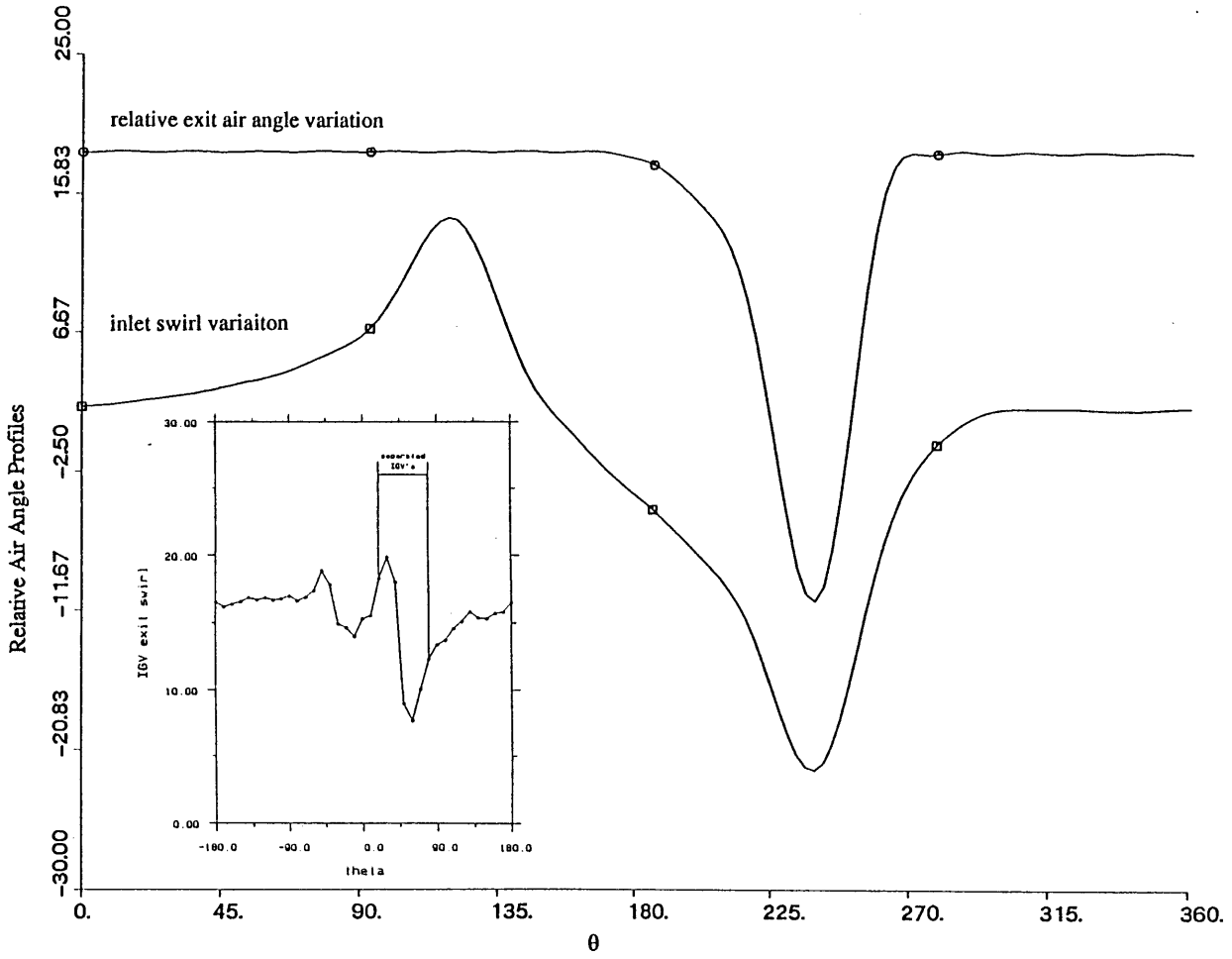

Figure 5.3 IGV Swirl Angle Variation and Deviation Variation.

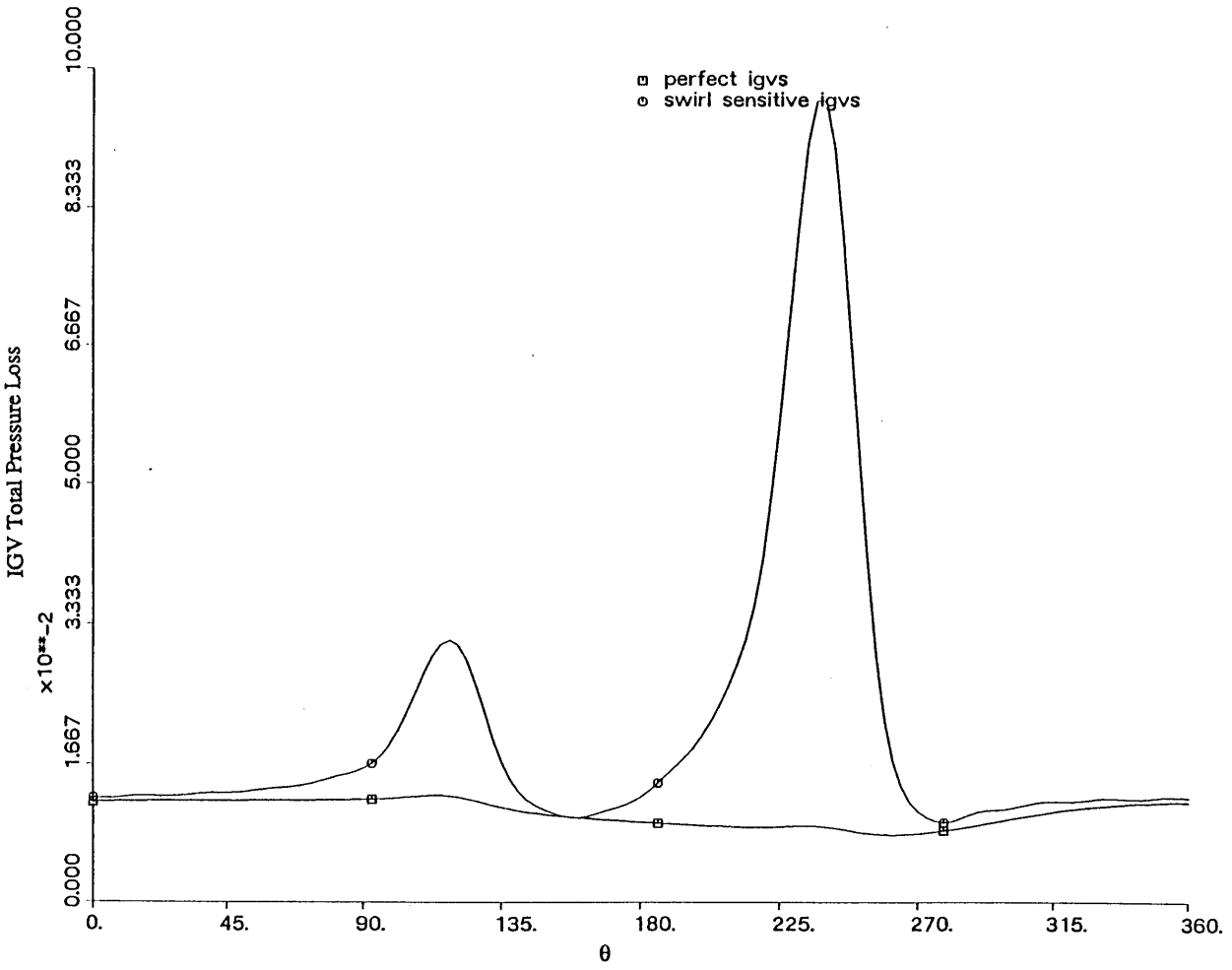

Figure 5.4 IGV Total Pressure Loss Profile.

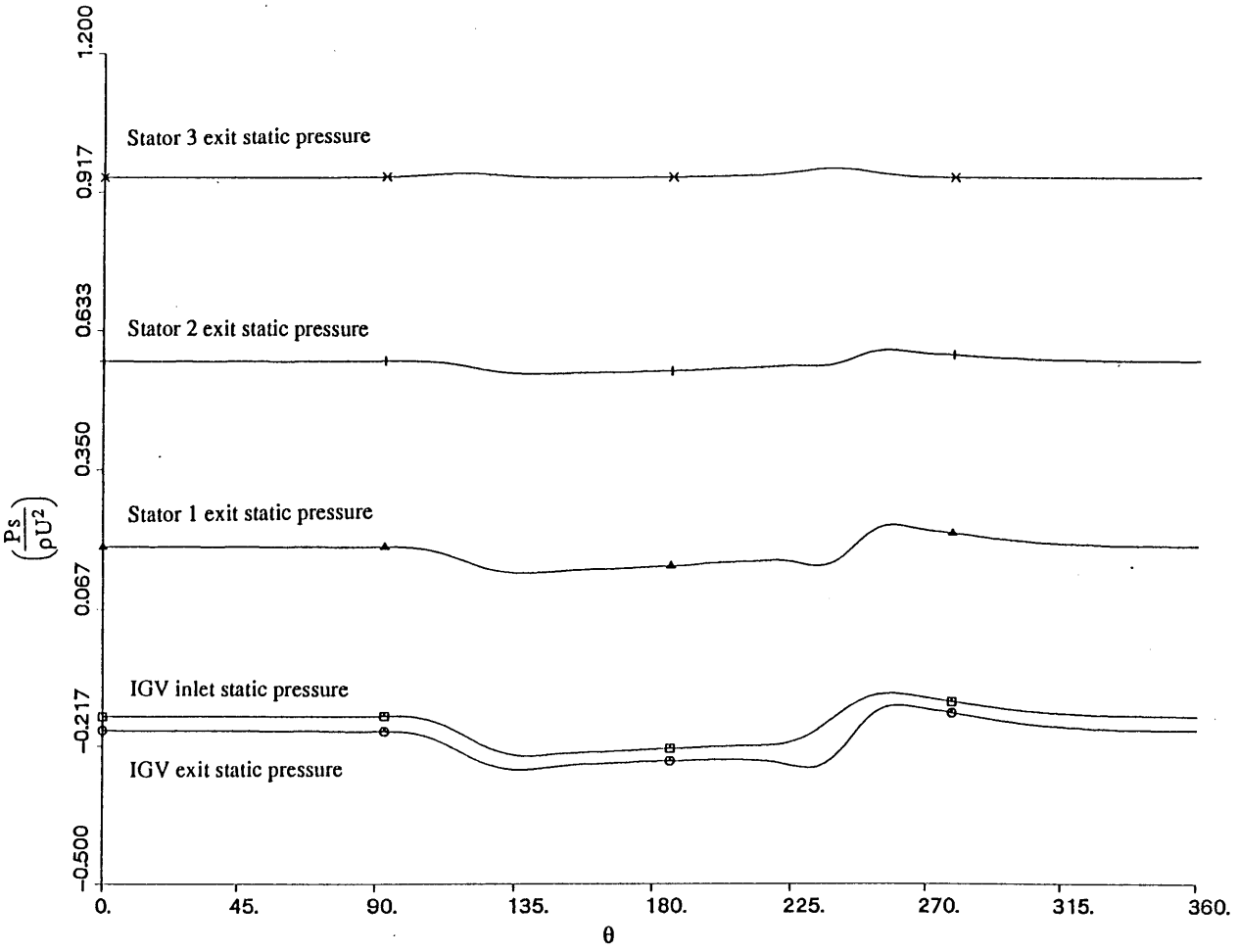

Figure 5.5 IGV Static Pressure Profiles at Various Locations Through the Compressor.

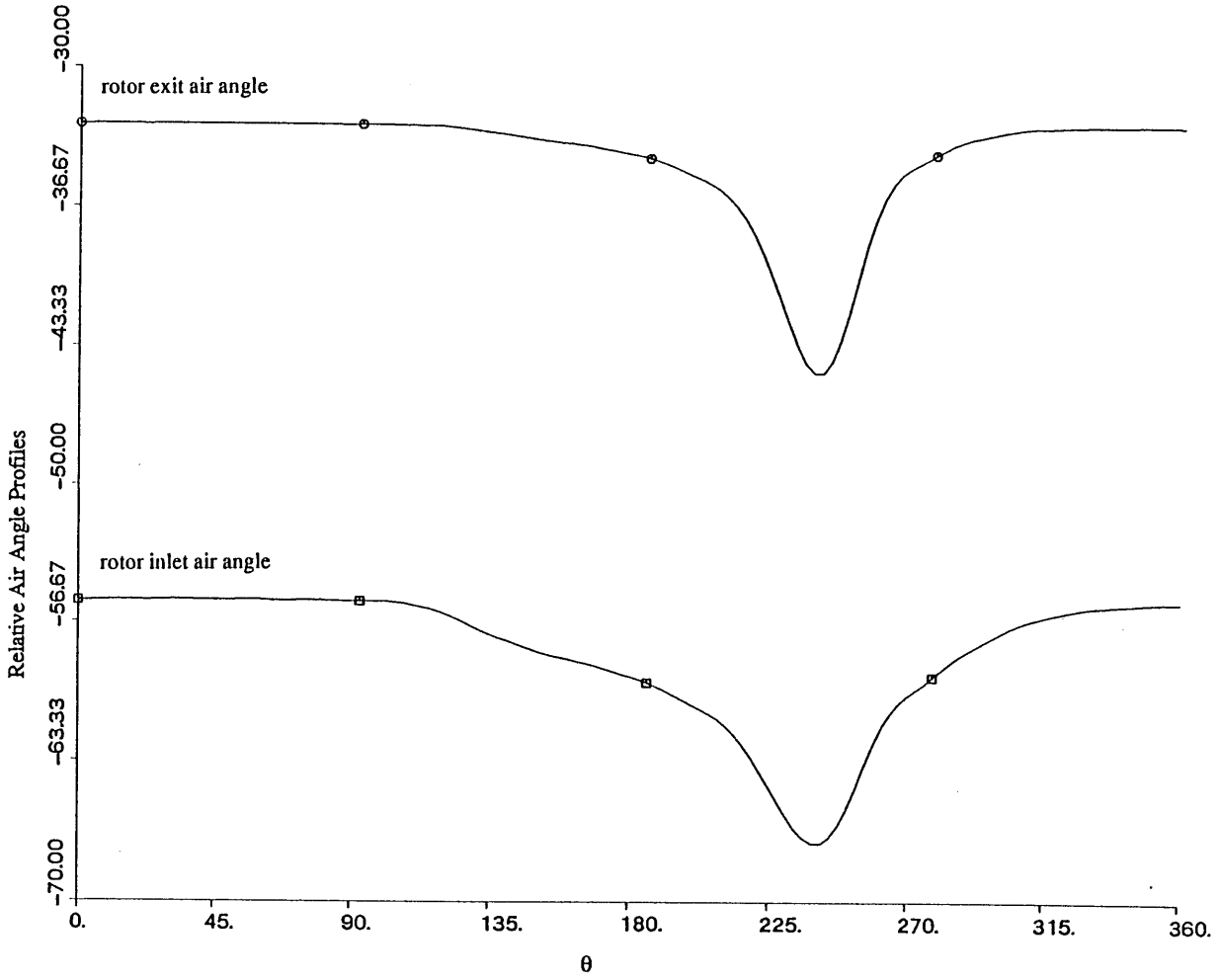

Figure 5.6 Relative Inlet and Exit Air Angle Profiles of First Rotor.

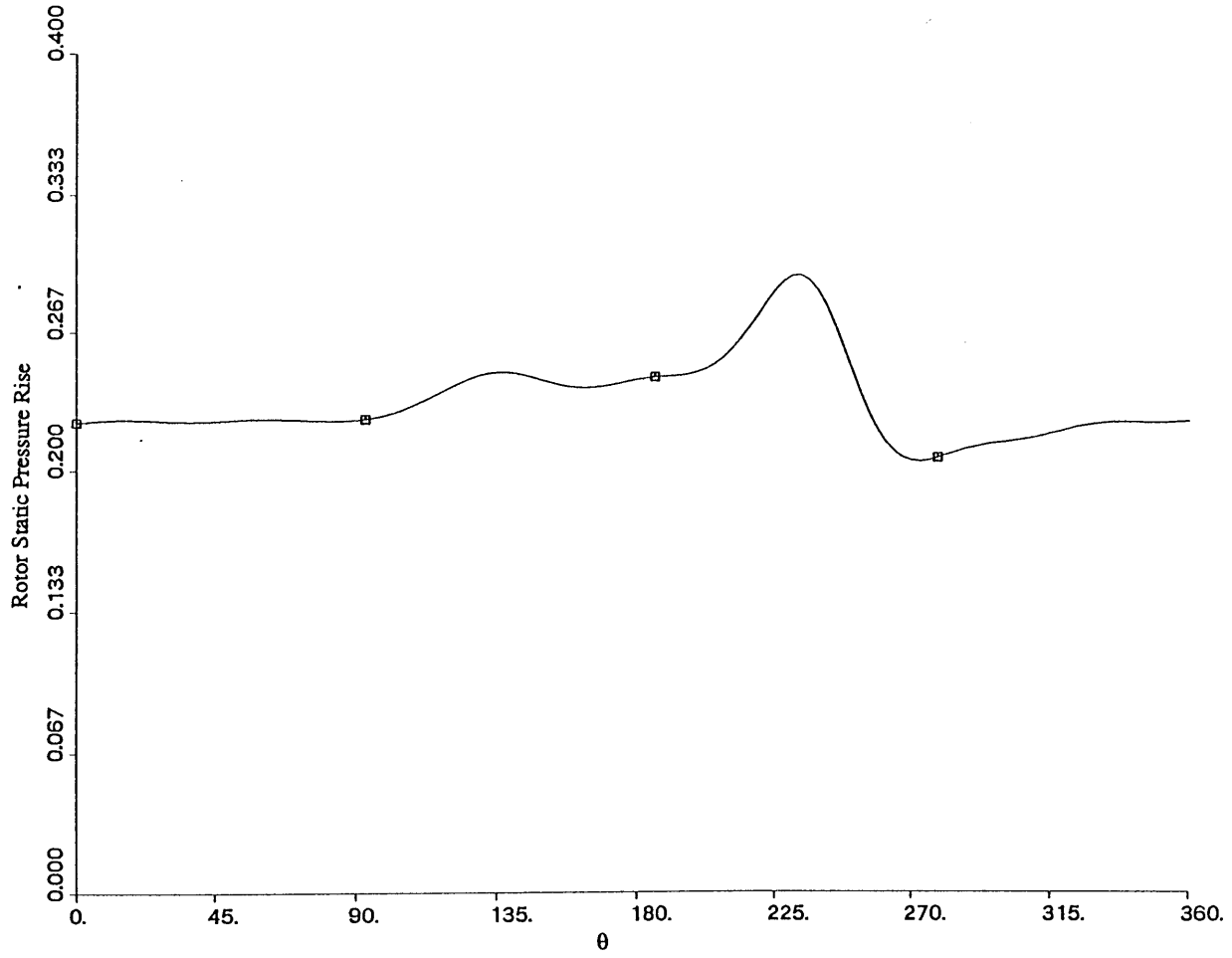

Figure 5.7 First Rotor Static Pressure Rise.

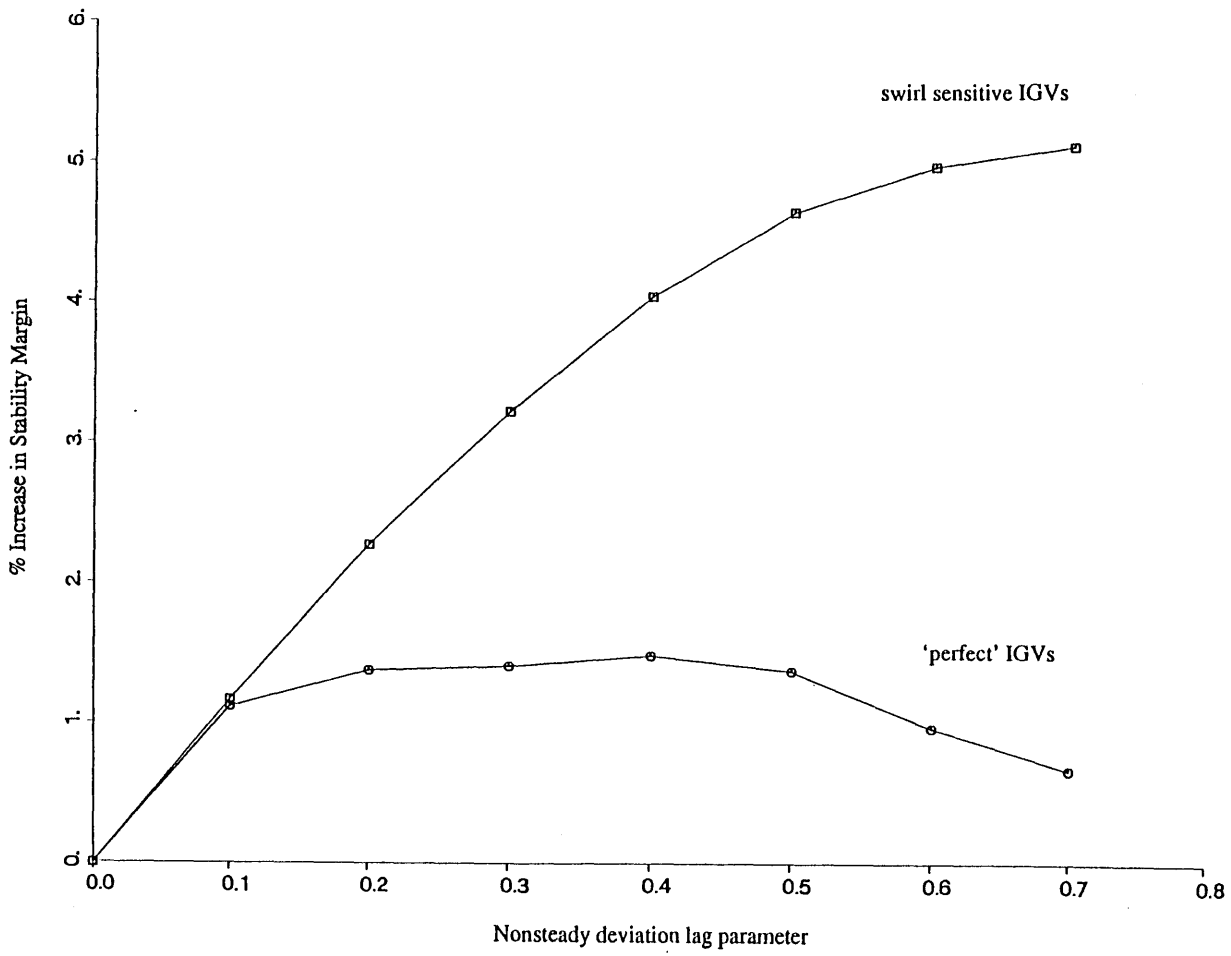

Figure 5.8 Effect of Unsteady Deviations on the Stability Margin of a Swirl Sensitive Compressor (B=1.0).

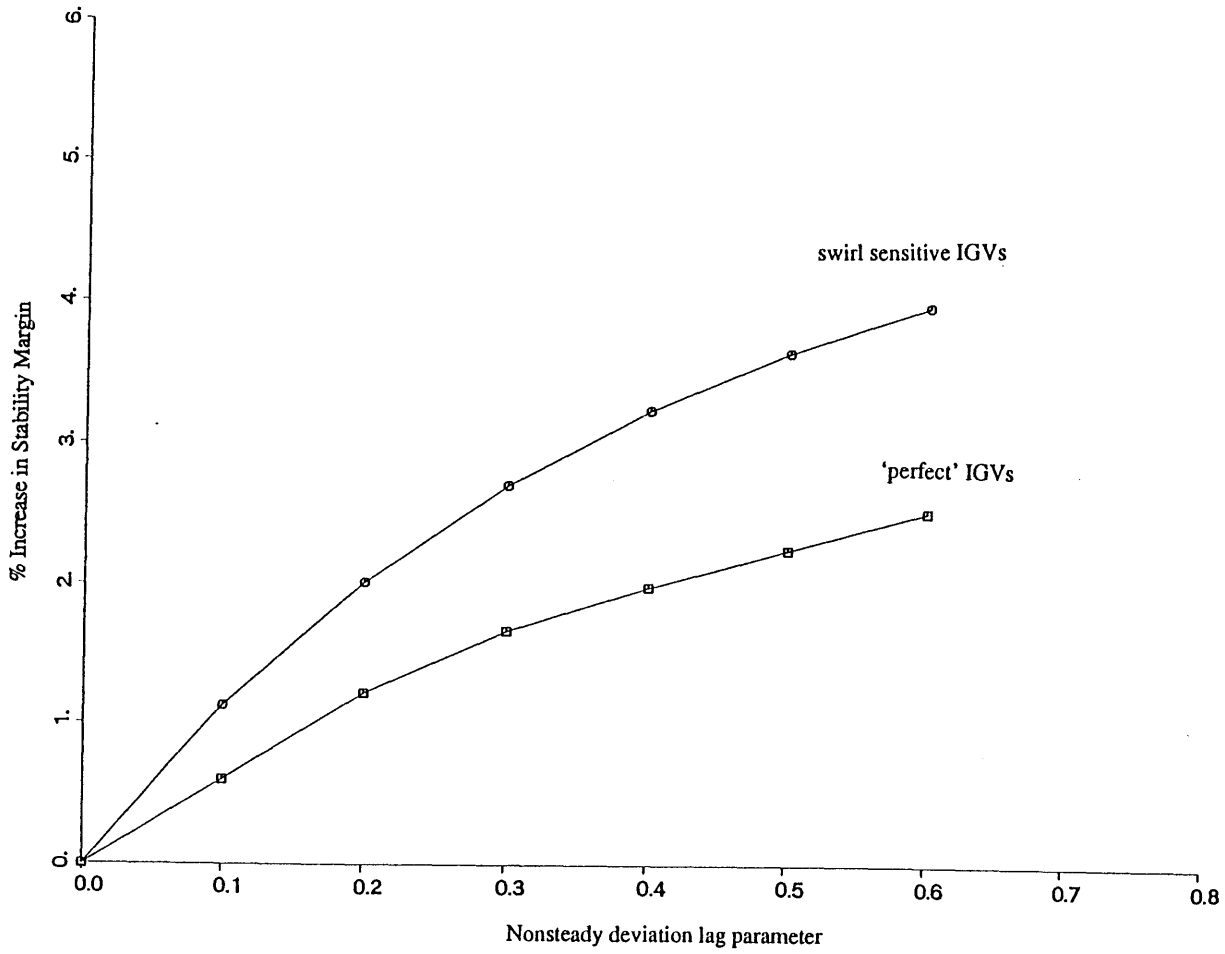

Figure 5.9 Effect of Unsteady Deviations on the Stability Margin of a Swirl Sensitive Compressor (B=0.1).

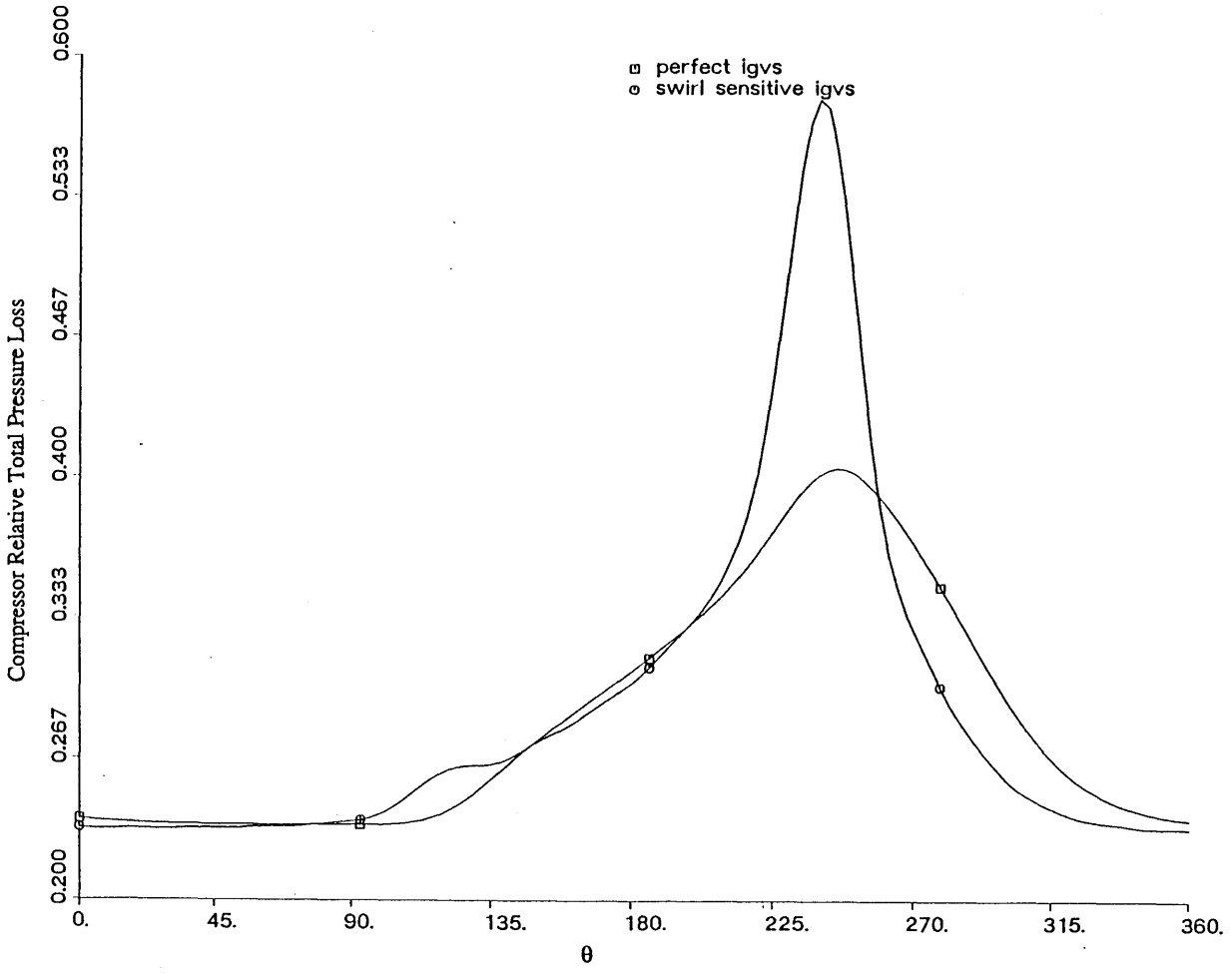

Figure 5.10 Overall Relative Total Pressure Loss through Compressor.

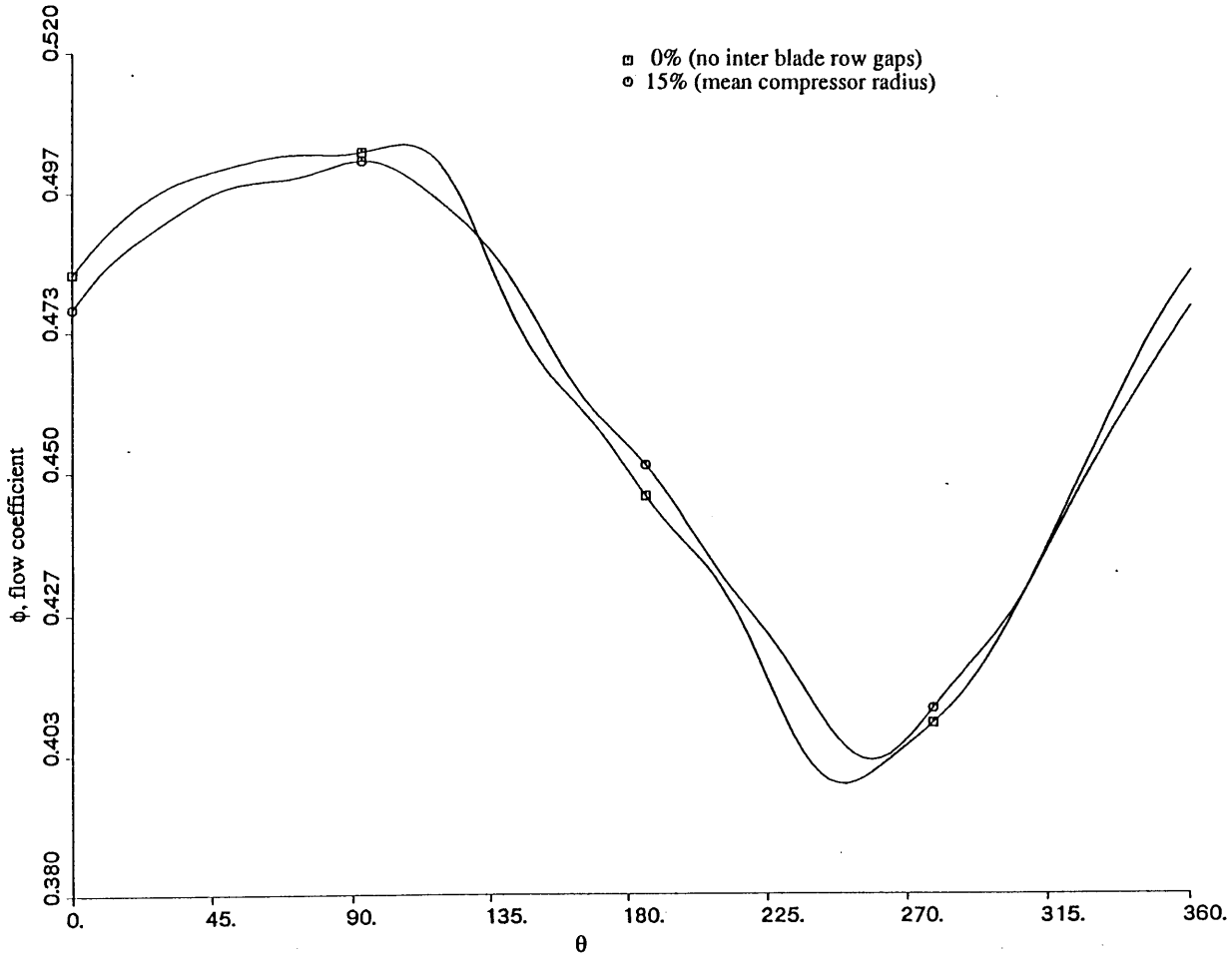

Figure 6.1 Flow Coefficient Profiles at the Compressor Inlet Face for a Single Stage Compressor (w/ and w/o inter blade row gaps).

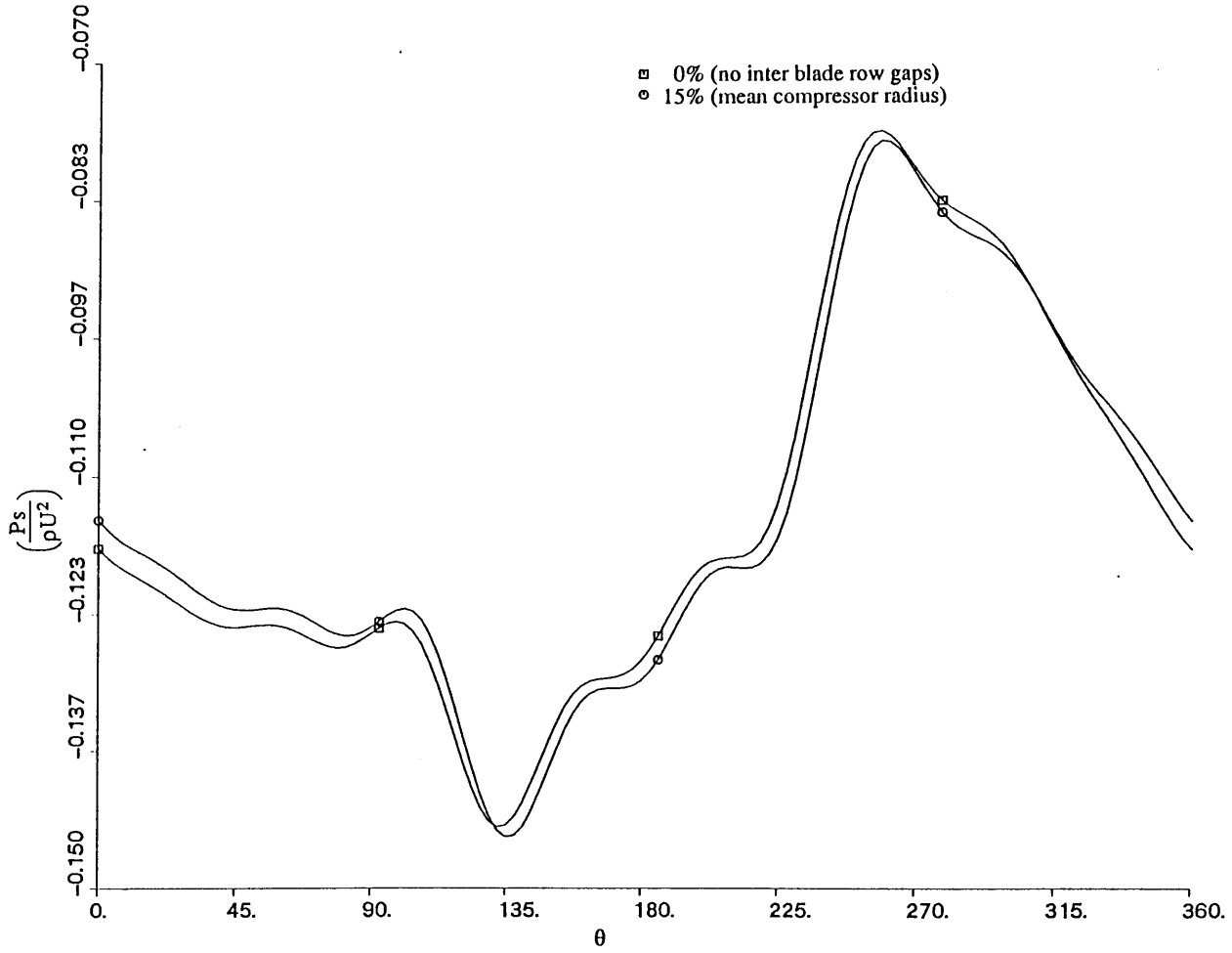

Figure 6.2 Static Pressure Field at the Compressor Inlet.

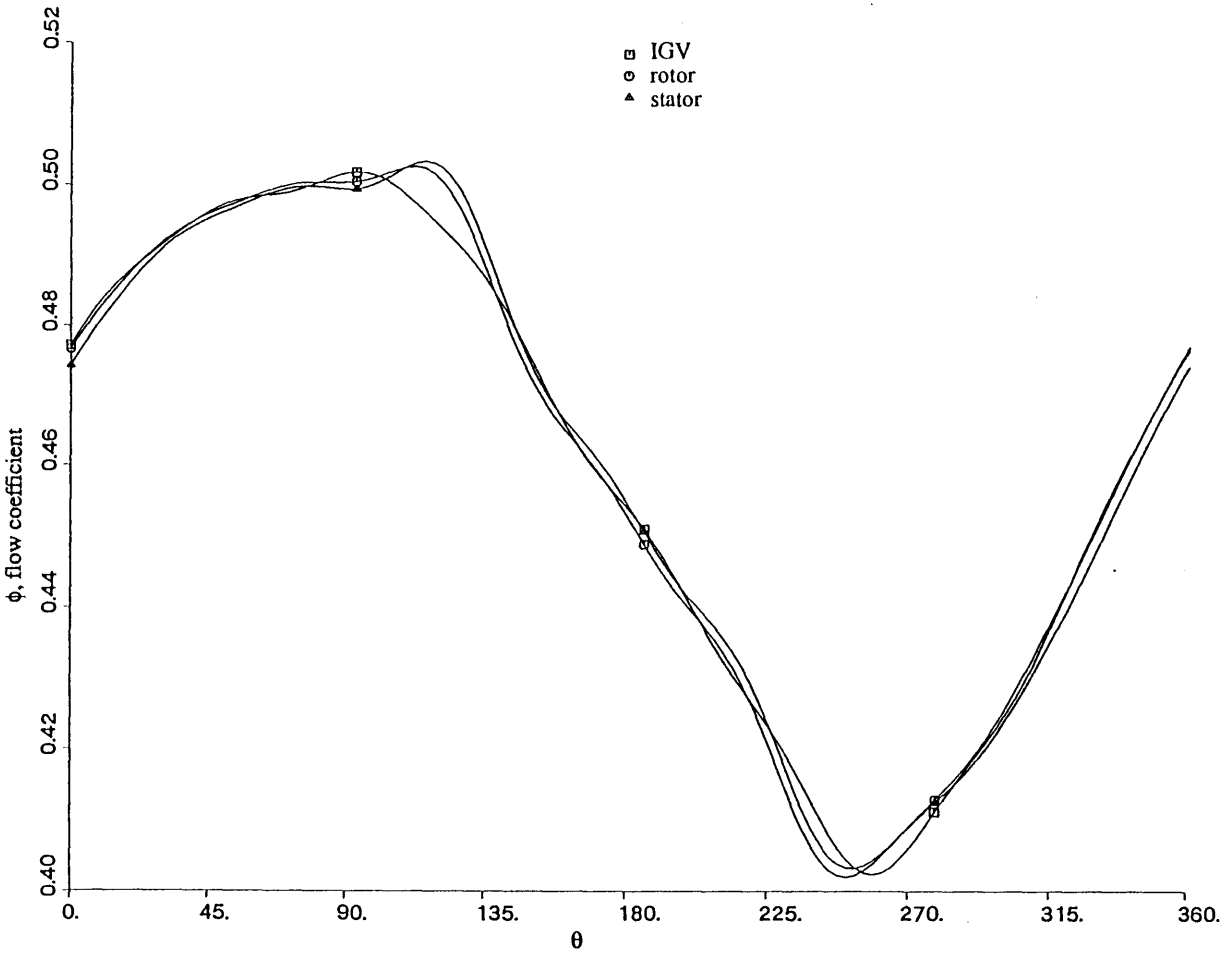

Figure 6.3 Evolution of Flow Coefficient Profile Through a Single Stage Compressor.

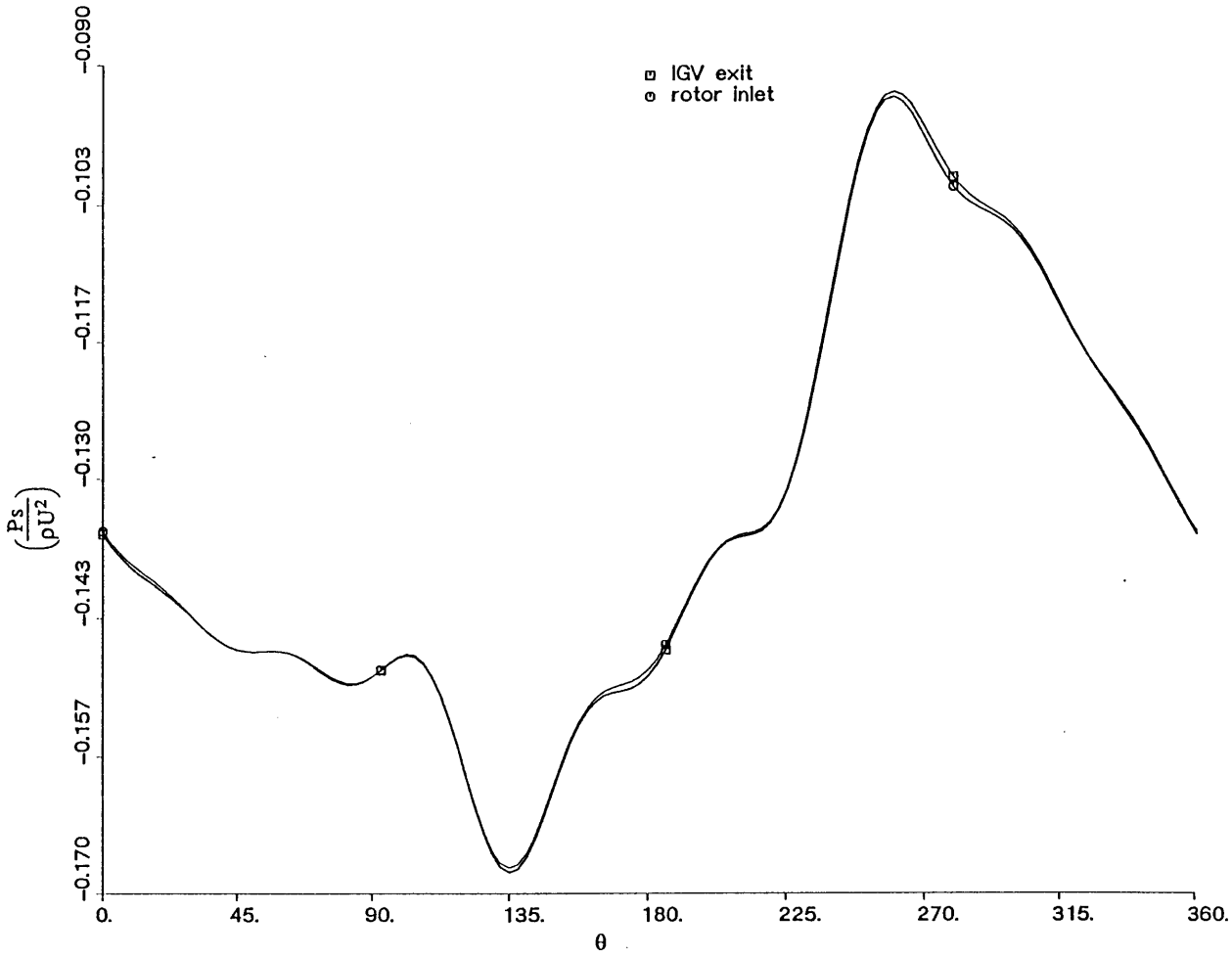

Figure 6.4.b Static Pressure Variation Between Rotor and Stator.

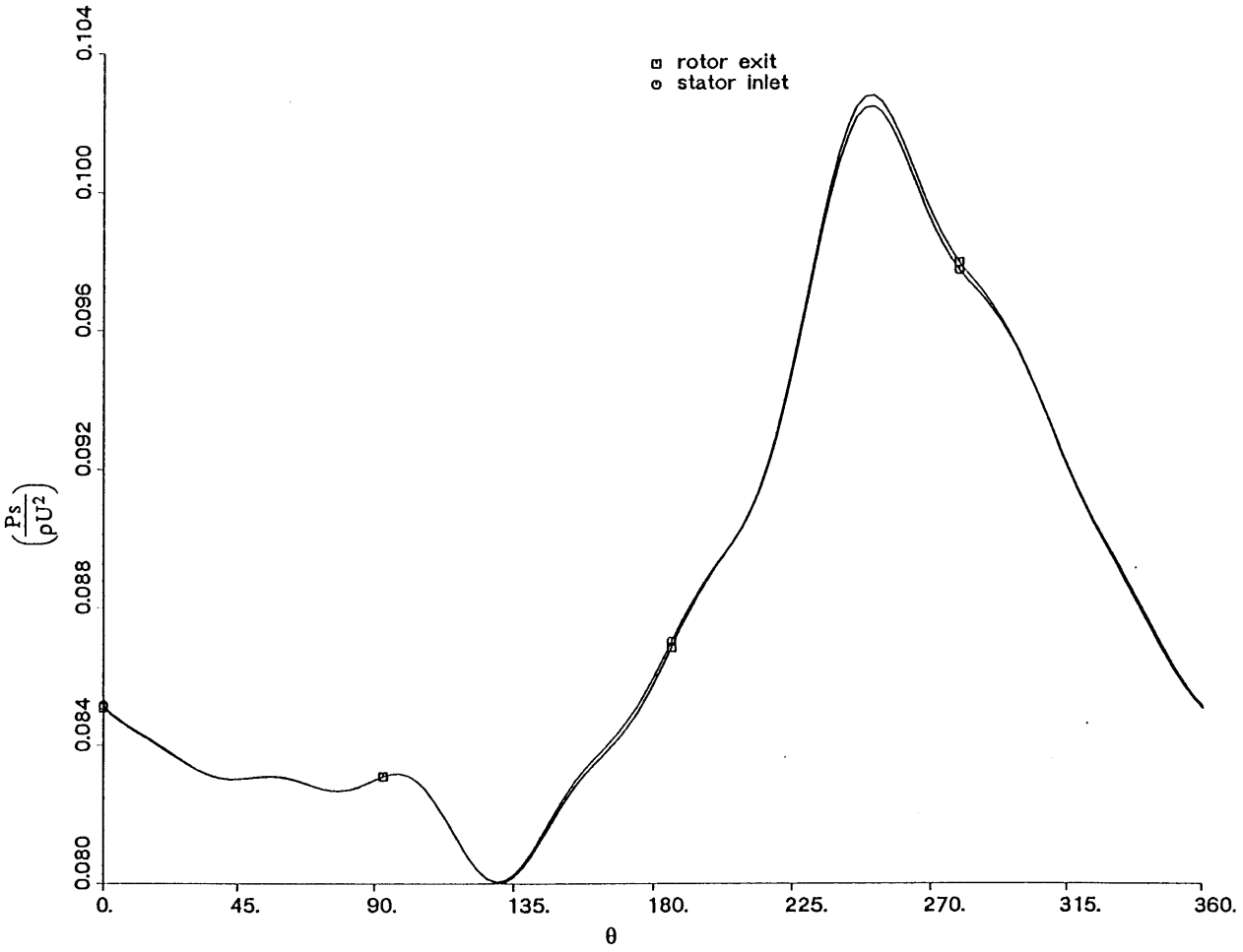

Figure 6.4.a Static Pressure Variation Between IGV and Rotor.

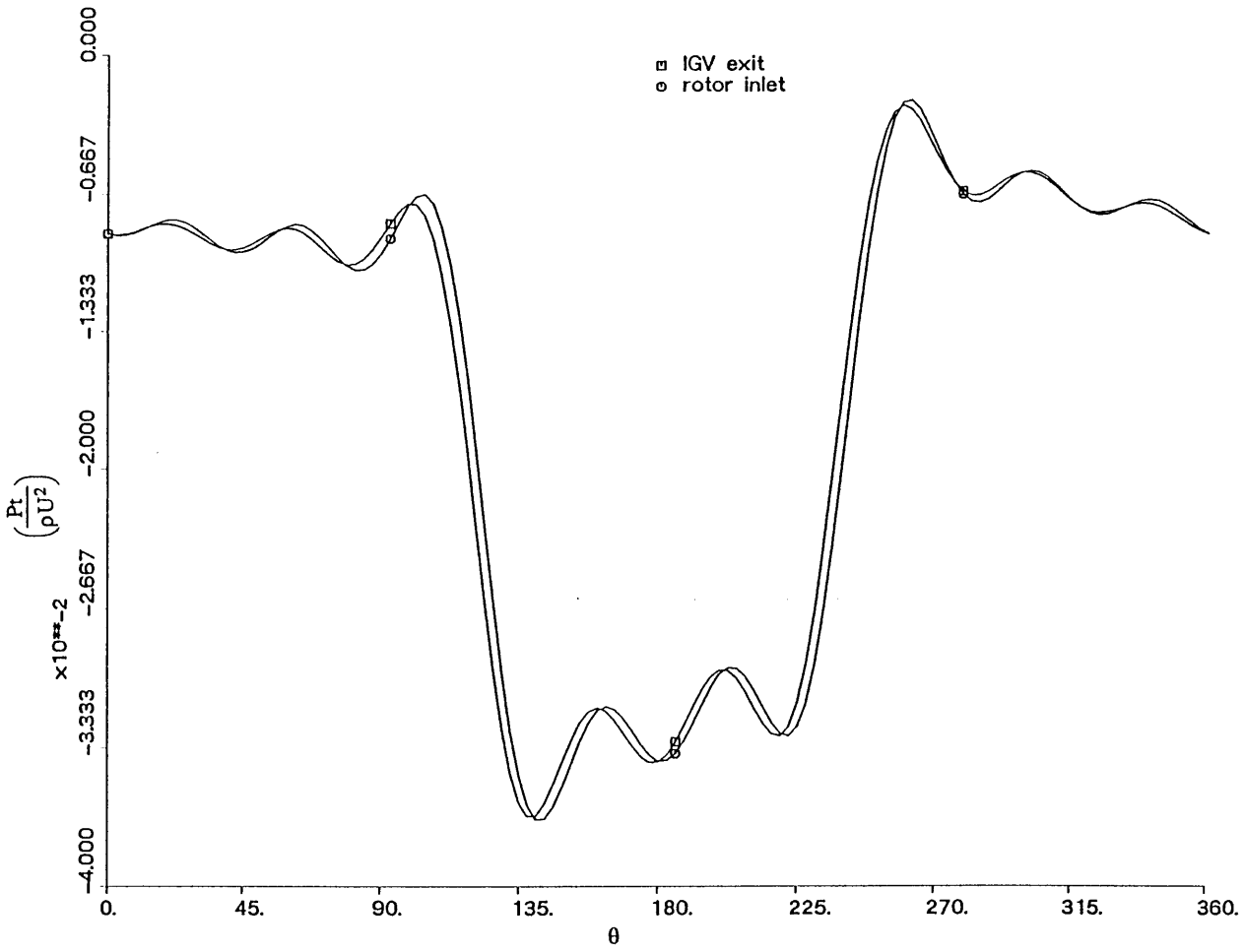

Figure 6.5 Advection of Total Pressure Non-uniformity with Mean Flow between IGV and Rotor.

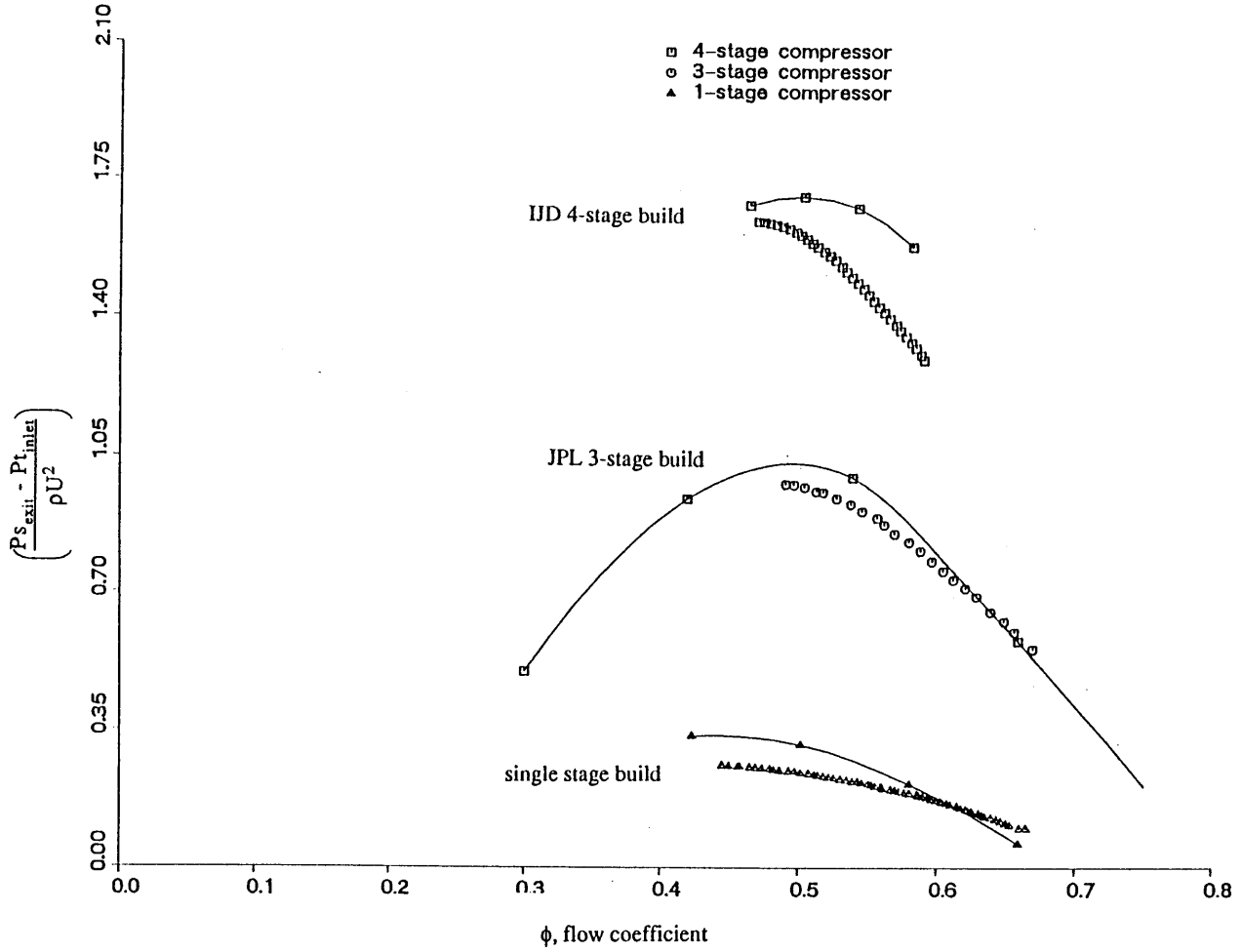

Figure A1.1 Clean Flow Performance of Several Compressors (theory and actual).